2021

# MECHANISMS OF CADMIUM-INDUCED AND EPIDERMAL GROWTH FACTOR RECEPTOR MUTATION-DRIVEN LUNG TUMORIGENESIS

Hsuan-Pei Lin
*University of Kentucky*, ibugogo2657@gmail.com
Author ORCID Identifier:
 https://orcid.org/0000-0003-2938-8785
Digital Object Identifier: https://doi.org/10.13023/etd.2021.356

Right click to open a feedback form in a new tab to let us know how this document benefits you.

STUDENT AGREEMENT:

I represent that my thesis or dissertation and abstract are my original work. Proper attribution has been given to all outside sources. I understand that I am solely responsible for obtaining any needed copyright permissions. I have obtained needed written permission statement(s) from the owner(s) of each third-party copyrighted matter to be included in my work, allowing electronic distribution (if such use is not permitted by the fair use doctrine) which will be submitted to UKnowledge as Additional File.

I hereby grant to The University of Kentucky and its agents the irrevocable, non-exclusive, and royalty-free license to archive and make accessible my work in whole or in part in all forms of media, now or hereafter known. I agree that the document mentioned above may be made available immediately for worldwide access unless an embargo applies.

I retain all other ownership rights to the copyright of my work. I also retain the right to use in future works (such as articles or books) all or part of my work. I understand that I am free to register the copyright to my work.

REVIEW, APPROVAL AND ACCEPTANCE

The document mentioned above has been reviewed and accepted by the student's advisor, on behalf of the advisory committee, and by the Director of Graduate Studies (DGS), on behalf of the program; we verify that this is the final, approved version of the student's thesis including all changes required by the advisory committee. The undersigned agree to abide by the statements above.

<div align="right">

Hsuan-Pei Lin, Student

Dr. Chengfeng Yang, Major Professor

Dr. Isabel Mellon, Director of Graduate Studies

</div>

MECHANISMS OF CADMIUM-INDUCED AND EPIDERMAL GROWTH
FACTOR RECEPTOR MUTATION-DRIVEN LUNG TUMORIGENESIS

---

DISSERTATION

---

A dissertation submitted in partial fulfillment of the
requirements for the degree of Doctor of Philosophy in the
College of Medicine
at the University of Kentucky

By

Hsuan-Pei Lin

Lexington, Kentucky

Co-Directors: Dr. Chengfeng Yang, Professor of Toxicology and Cancer Biology

and         Dr. Zhishan Wang, Assistant Professor of Toxicology and Cancer
Biology

Lexington, Kentucky

2021

ABSTRACT OF DISSERTATION


MECHANISMS OF CADMIUM-INDUCED AND EPIDERMAL GROWTH
FACTOR RECEPTOR MUTATION-DRIVEN LUNG TUMORIGENESIS

Cadmium (Cd) is a ubiquitous pollutant in the environment and a known carcinogen for lung cancer. Cd has been shown to act as a weak mutagen, which suggests that it may exert tumorigenic effect through non-genotoxic ways, such as epigenetic mechanisms. The goal of this project is to investigate the mechanisms of Cd carcinogenesis focusing on the role of lncRNA dysregulations. The Cd-exposed cells formed significantly more colonies in soft agar, displayed cancer stem cell (CSC)-like property and formed tumors in nude mice. Mechanistically, the lncRNA microarray analysis revealed that chronic Cd exposure dysregulates lncRNA expressions. Q-PCR analysis confirmed the significant upregulation of the oncogenic lncRNA DUXAP10 level in Cd-transformed cells. Knockdown of DUXAP10 in Cd-transformed cells significantly reduced their CSC-like property. Further mechanistic studies showed that DUXAP10 activates the Hedgehog pathway to promote Cd-induced CSC-like property. Furthermore, it was determined that chronic Cd exposure upregulates DUXAP10 expression by inducing Pax6 expression.

In addition to oncogenic lncRNA upregulation, Cd exposure was also found to downregulate the expression of a tumor suppressive lncRNA MEG3 in Cd-transformed cells. Meanwhile, the levels of DNMTs in Cd-transformed cells were found significantly elevated. Bisulfite-sequencing study revealed that the differentially methylated region (DMR) upstream of MEG3 is hypermethylated in Cd-transformed cells, indicating that the promoted DNMTs activity contributed to downregulation of MEG3. Stably expressing MEG3 in Cd-transformed cells decreased cell proliferation and induced CSC-like property. Further studies showed that MEG3 inhibits cell transformation by limiting cell proliferation and inducing apoptosis. Mechanistic studies revealed that MEG3 reduced cell proliferation by regulating the levels of cell cycle proteins and induced apoptosis

by inhibiting the level of Bcl-xL. These findings suggest that dysregulations of lncRNAs play important roles in Cd carcinogenesis.

As well as epigenetic dysregulations, we also determined the effect of genetic factor contributing to lung cancer. Enhanced EGFR signaling contributes to 60% of NSCLC cases. However, there is an unmet need to solve acquired resistance to tyrosine kinase inhibitors and low response rate for immunotherapy in lung cancer patients. This study was performed to investigate the role of SOCS3 in EGFR mutation-driven lung cancer and to explore the potential of its regulatory axis as therapeutic target for the development of novel approach. In our transgenic mouse model, overexpression of SOCS3 significantly inhibited tumor formation with mutated EGFR. Further investigation for the underlying mechanism revealed that SOCS3 downregulates YAP protein, which further suppressed Bcl-2 family proteins. External YAP inhibitor was shown to efficiently inhibit the growth of tumor organoids. In vivo studies demonstrated that SOCS3 downregulating YAP leads to less immunosuppressive tumor microenvironment. Lastly, SOCS3 was often found to be silenced in cancers. To mimic this circumstance, the therapeutic efficacy of utilizing external YAP inhibitor combined with anti-PD-L1 was assessed and showed promising outcomes. These results suggest the critical role of SOCS3 as a biomarker for the oncolytic immune environment and provide a novel insight for improving lung cancer immunotherapy.

KEY WORDS: EGFR, cadmium, carcinogenesis, SOCS3, DUXAP10, MEG3

<div style="text-align:right">

_____Hsuan-Pei Lin_____ _
*(Name of Student)*


_____07/12/21_____
*(Date)*

</div>

MECHANISMS OF CADMIUM-INDUCED AND EPIDERMAL GROWTH
FACTOR RECEPTOR MUTATION-DRIVEN LUNG TUMORIGENESIS

By
Hsuan-Pei Lin

_____Dr. Chengfeng Yang_____
Co-Director of Dissertation

_____Dr. Zhishang Wang_____
Co-Director of Dissertation

_____Dr. Isabel Mellon_____
Director of Graduate Studies

_____07/30/2021_____
Date

*To my family*

# ACKNOWLEDGMENTS

I would like to express my sincere gratitude to my advisors, the committee members, our DGS, my coworkers, family and friends. Without your kind support and great help, I would not be able to finish the study.

The following dissertation, while an individual work, benefited from the insights and direction of several people. First, my major advisor, Dr. Chengfeng Yang, and the dissertation co-chair, Dr. Zhishan Wang. Under Dr. Yang's guidance, working with multiple projects provided me great chances to learn from different subjects and to gain different insight. I would also like to thank all the lab members for their great help and support. Next, I wish to thank the committee members for providing instructive comments and evaluations at every stage throughout the PhD study, Dr. Christine F. Brainson, Dr. Jin-Ming Yang, and Dr. Yvonne Fondufe-Mittendorf. Moreover, I would like to thank Dr. Isabel Mellon, the director of graduate studies of the Department of Toxicology and Cancer Biology, for guiding me through this bumpy journey. I could not sail through without Dr. Mellon's help. Lastly, I would like to thank my family and friends. It had been a long journey without much joy. But thank you for always being there.

TABLE OF CONTENTS

# LIST OF TABLES

LIST OF FIGURES

CHAPTER 1. INTRODUCTION

## 1.1.1 Lung cancer

Lung cancer is the leading cause of cancer mortality. Each year, almost a quarter of all cancer patients die from lung cancer in the United States, for both males and females. While most lung cancer cases are determined by tobacco consumption, approximately 10 to 16% of cases are never-smokers. For those never smokers, the risk factors could be poor diet, environmental and occupational exposures to toxicants, and genetic susceptibility (Rivera et al., 2016; Warren et al., 2013; Malhotra et al., 2016). Histologically, around 15% of lung cancer is small cell lung cancer (SCLC), while around 85% of cases are non-small cell lung cancer (NSCLC). Based on the cell types and the location of tumors, NSCLC can be further categorized the following main subtypes: squamous cell carcinoma, adenocarcinoma, and large cell carcinoma. Based on anatomic information (tumor sizes, location, invasion) and the overall survival rate, lung cancer could be categorized to different stages. However, with the advances of medicine in the past several years and considering the complexity of lung cancer itself, the traditional staging system has several limitations. For example, the factors that affect the overall survival rate are not merely the anatomical grade of the tumors, but also the progression of the disease which in fact is quite dynamic and could rely on the medical resources available to the patients (de Sousa et al., 2018). In addition, around 70% of the patients already have metastasis by the time of diagnosis, which add to the difficulty of precise diagnosis and efficient treatment. For better clinical outcome, it is essential to

investigate the underlying mechanisms of tumor initiation and progression for lung cancer. In addition, understanding the driving force of the disease would be beneficial for the establishment novel therapeutic strategies.

## 1.1.2 Genetic alteration of lung cancer

Several genetic alterations have been discovered to associate with lung cancer progression and utilized for prognosis. Patients with *BRAF* mutation is a distinct subpopulation which includes approximately 3.5% of NSCLC cases. *BRAF* mutation has been found responsible for constitutive activation of MAPK/ERK pathway and for the rare cases of axillary lymph node metastasis (Leonetti et al., 2018; McEvoy et al., 2017). *RET* rearrangement is another rare genetic alteration found in lung cancer. Transmembrane protein RET is a receptor tyrosine kinase which stimulate downstream signaling, such as MAPK pathway, PI3K-AKT pathway, and STAT3 pathway. Gain of function mutation results in aberrant activation of the receptor which has been found common in adenocarcinoma (Ju et al., 2012).  The receptor for hepatocyte growth factor, *MET*, is often found overexpression in NSCLC and responsible for tumor migration and invasion, particularly in squamous cell carcinoma (Birchmeier et al., 2003; Go et al., 2010). Unlike these mutations with relatively low incidences, *KRAS* and *EGFR* mutation are the most common genetic changes found in lung cancer. Interestingly, while mutated KRAS often demonstrates poor prognosis, mutations of EGFR at different points could have different biological effects and varied therapeutic outcomes. Furthermore, combined mutations of these

oncogenes could further exacerbate cancer progression and hamper the therapeutic efficacy.

## 1.1.3 Lung cancer therapy targeting EGFR

Conventionally, platinum-based chemotherapy, such as carboplatin and cisplatin, is the standard and the primary method for both SCLC and NSCLC at early stage. Particularly for NSCLC, the five-year survival rate is around 5%. Nonetheless, the response rate usually decreases after a period of time due to acquired resistance to chemotherapy, which results in a median survival time of 8 to 10 months. In addition, the patients with advanced NSCLC would display low response rate or eventually experience relapse (Nagasaka and Gadgeel, 2018; [1]Yang et al., 2019; Rossi and Di Maio, 2016). Hence, there is an urgent need for more effective therapy (da Cunha Santos et al., 2010).

Targeted therapy has been under extensive study and achieved significance advance by targeting the molecules involved in the signaling pathways which regulates the growth of cancer cells, such as PI3K/mTOR pathway, STAT pathway, and MAPK/ERK pathway. Upstream of these internal pathways, transmembrane protein epidermal growth factor receptor (EGFR) activates these signaling transduction upon receiving external cues for cell growth. The *EGFR* gene is located on the chromosome 7p11.2, encoding 28 exons and 27 intron for the 170 kDa transmembrane protein (Yarden and Sliwkowski, 2001). Structurally, EGFR contains an extracellular ligand binding domain, a short a-helix transmembrane domain, and the cytoplasmic domain.

The cytoplasmic portion contains two distinct regions: the tyrosine kinase domain, and the C-terminal which is critical for the receptor autophosphorylation and the subsequent signal transduction. Upon binding of its ligands, homodimerization of EGFR monomer or heterodimerization with other HER family members (HER2, HER3, HER4) initiates the signaling cascade to activate its downstream pathways (Wells, 1999). So far, there have been seven EGFR ligands identified: epidermal growth factor (EGF), transforming growth factor-alpha (TGFA), amphiregulin (AREG), epiregulin (EREG), betacellulin (BTC), heparin-binding epidermal growth factor-like growth factor (HBEGF), and epigen (EPGN) (Singh et al., 2016). Though all binds to EGFR, the biological responses induced by these different ligands are different, given each of these ligands display different binding affinity with EGFR and the rest of the HER family (Macdonald-Obermann et al., 2014).

External stimulation activates EGFR to induce corresponding biological effects, such as cell proliferation and anti-apoptosis. Under normal circumstances, EGFR activity remains dormant and is regulated by various mechanisms, such as phosphorylation, ubiquitination, and methylation, to prevent excessive activation (Hsu et al., 2011; Nguyen et al., 2013). In cancers, dysregulated EGFR signaling has been shown to be oncogenic, through mechanisms such as amplified *EGFR* copy number, or enhanced EGFR protein expression, or genetic activating mutations at the kinase loop (Bethune et al., 2010). Among those, targeted therapy is often found hampered due to EGFR mutations.

## 1.1.4 Effects of EGFR mutation subtypes on therapy

The most commonly found EGFR mutations are the deletion at the exon 19 and the point mutation L858R at the exon 21. Exon 19 deletion contains roughly 45~47% of total EGFR mutation cases, whereas the point mutation L858R accounts for 40~41% of total, and left around 10~12% of rare mutations. For exon 19 deletion, more than 10 subtypes have been identified, with mostly the deletion of E746-A750. For the rare mutations, around one third of the cases are the exon 20 insertion or the point mutation G719X at the exon 18 (Kobayashi et al., 2016; Harrison et al., 2020). Identified these EGFR mutations is crucial for diagnosis and prognosis, given the fact that patients' response to tyrosine kinase inhibitors (TKIs) could be highly variable due the altered interaction between the compound and the EGFR mutant. For example, several studies have been shown that the exon 19 deletion and L858R at the exon 21 granted sensitivity to TKI and displayed prolonged overall survival rates. Moreover, some have shown that exon 19 deletion leads to higher response rate to TKI gefitinib and erlotinib, compared to L858R (Sun et al., 2011; Choi et al., 2018; Jackman et al., 2006; Hong et al., 2019). However, the patients with those rare mutations usually display varied sensitivity to different types of TKIs. For example, point mutations G719X and E709K at exon 18, exon 18 deletion, exon 19 insertion, S768I at exon 20, and L861Q at exon 21 favored the therapy with afatinib but showed moderate response to gefitinib or erlotinib (Castellanos et al., 2017).

However, even displaying high response rate to TKI at the beginning, acquired resistance to the treatment is almost inevitable after a period of time.

The known mechanisms of the acquired resistance include secondary EGFR mutation (e.g., T790M, C797X), acquired MAPK/PI3K mutation, cell cycle-related gene mutations, oncogene amplification (such as *MET*, *BRAF*) and fusion of oncoproteins (such as *CCDC6-RET*, *EML4-ALK*). As the acquired resistances often further complicate the therapeutic regimen, EGFR T790M at the exon 20 occurs in the majority of cases and often found to limit therapeutic efficacy (Yun et al., 2008). The third generation TKI, Osimertinib which is an irreversible EGFR inhibitor displays variable response targeting T790M (Suda et al., 2009; Leonetti et al., 2019). Much effort thus has been made to investigate combination therapy to improve efficacy, such as combining targeted therapy, chemotherapy, and immunotherapy. Nonetheless, T790M has also been shown to elevate the expression of PD-L1 which could result in immune escape (Peng et al., 2019). Studying the underlying mechanism of the resistance would be beneficial for innovating effective lung cancer therapy.

In addition to genetic alterations, epigenetic dysregulation is also a risk factor contributing lung cancer progression. Following, we would cover epigenetic dysregulations induced by a lung cancer carcinogen.

1.2.1 Cadmium – lung cancer carcinogen

Cadmium (Cd) is a transient heavy metal and a natural element which is usually found in small amounts in air, water, and soil. However, due to its widely used in industries such as pigments production, batteries manufacturing, metal

coating, and plastics production, Cd contamination has become a public health concern in the United States and worldwide. The major routes of Cd exposure for general population could be cigarette smoke, consumption of Cd-contaminated water and food, and occupational exposure. Studies of Cd toxicity have long been established, and mostly has been shown oncolytic. Since the 90s, Cd has been listed as group I carcinogen by International Agency for Research on Cancer (IARC). With the property of long biological half-life, accumulated Cd in human bodies has become a critical health concern. While Cd is a known carcinogen for lung cancer, its toxic effects have also been observed in other organs such as breast, renal, liver, pancreas, prostate, and immune system. Nonetheless, the mechanisms of its carcinogenesis remain to be defined.

## 1.2.2 Cd toxicity for prostate cancer

In the study of Cd-induced prostate benign prostatic hyperplasia cell transformation, Cd exposure led to increased expression of androgen receptor (AR), estrogen receptor (ER), and prostate-specific antigen (PSA), as well as matrix metalloproteinase 2 and 9 which are critical for the migration and invasion (Prajapati et al., 2020). Besides disrupting endocrine system, it has been reported that Cd exposure benefits cell survival through stimulating the expressions of autophagy protein Pla8, pro-survival protein Bcl-2, and NFκB (Pal et al., 2017; Kolluru et al., 2017). Mechanistically, Cd has been shown to activate signaling of ERK pathway and PI3K/AKT pathway in malignant prostate cells (Dasgupta et al., 2020; Kulkarni et al., 2020). Androgen receptor signaling and PI3K signaling have been demonstrated the two important signaling pathways for

the growth and survival of prostate cancer cells (Lamb et al., 2011; Kaarbø et al., 2010). These studies revealed the oncolytic activity of Cd in prostate. However, the underlying mechanisms of Cd promoting these pathways would need further study.

1.2.3 Cd toxicity for liver & pancreatic cancer

Liver is another organ vulnerable to environmental toxicants such as Cd. While many studies regarding Cd hepatoxicity focused on short term, high concentration of Cd causing DNA damage, rarely has the evidence been presented to show the mechanism of Cd carcinogenesis for hepatocellular carcinoma (Skipper et al., 2016; Ikediobi et al, 2004). It has been shown that hepatocytes respond to Cd-induced oxidative stress by increasing the levels of nuclear factor erythroid 2-related factor 2 (Nrf2) and heme oxygenase-1 (OH-1) (He et al., 2008; Lawal et al., 2015). However, Qu et al. described that chronic exposure to Cd only induced oxidative stress at the early stage of cell transformation. Sustained Cd treatment eventually increased the liver cell tolerance to reactive oxygen species (ROS). They further demonstrated that the induced cell transformation by Cd was due to the overexpression of oncogenes such as cMyc and c-jun, as well as transcription factor AP-1 and NFκB (Qu et al., 2005). In addition to liver, pancreas is another digestive organ which is vulnerable to Cd toxicity, though the hypothesis of Cd causes pancreatic cancer seems plausible (Schwarz and Reis, 2000). Earlier evidence suggests that Cd causes excessive DNA synthesis and increases cAMP level in rats (Kacew et al., 1976). It was also reported that acute Cd exposure induces oxidative stress and

8

aberrant activity of caspase (Djordjevic et al., 2019). Interestingly, Wallace et al. proposed that other than oxidative stress, Cd meditates mitochondrial toxicity in pancreatic cancerous cells (Wallace et al., 2019). With scarce evidence presented, further investigation would be needed to delineate the mechanism of Cd carcinogenetic effects for pancreatic cancer.

## 1.2.4 Cd toxicity for kidney cancer

Nephrotoxicity of Cd has also been widely discussed as a health concern, as kidney is one of the major targets for Cd accumulation. Like what has been found in liver cells, acute toxicity induced by Cd overloading involves generation of ROS which further escalates oxidative stress and causes cellular injury. However, for long term exposure to low dose of Cd, oxidative stress plays minor role for the carcinogenesis. In a mouse model, it was found that Cd led to increased expression of cyclin D1 and c-Myc, suggesting potentially disrupted cell cycle. Furthermore, Cd challenge also promoted Wnt/β-catenin pathway, evidenced by increased levels of Wnt ligands and the receptor Frizzled in the mouse kidney cells. The upregulated Wnt/β-catenin signaling was further found associated with increase of epithelial mesenchymal transition (EMT) markers such as Twist and fibronectin (Chakraborty et al., 2010). In renal cancer cells, Cd was found to promote cell migration and invasion, which were associated with the upregulation of N-cadherin and vimentin and downregulation of E-cadherin. The enhanced EMT here was due to the activation of cAMP/PKA-COX2 signaling with prostaglandin E2 (PGE2) positive feedback loop (Shi et al., 2021).

## 1.2.5 Cd toxicity for breast cancer

Studies of Cd toxic effects on breast cancer progression have long been established, though whether Cd is a driving force for the development of breast cancer has not been determined (Aquino et al., 2012). While initiation of tumorigenesis of breast cancer could be hormone-dependent or hormone-independent, Cd has been found to mimic the action of estrogen on estrogen receptor to induce the downstream response and promote the growth of cancer cells (Garcia-Morales et al., 1994; Sun et al., 2007). Though rarely addressed, Cd has also been proposed to stimulate the cancer stem cell population in breast cancer, identified by stem cell markers such CD44, CD24, CD133, and ALDH1. Mechanistically, the authors discovered enhanced Ras/Raf/MEK/ERK signaling in the Cd-treated breast cancer cells (Ju et al., 2017). In addition to the enhanced cell proliferation, studies have also revealed that Cd promotes the phenotype of migration and invasion. Cd exposure could increase the expression of TGFB Induced Factor Homeobox 1 (TGIF), matrix metalloproteinase-2 (MMP2), matrix metalloproteinase-9 (MMP9), and integrins, as well as enhanced β-catenin signaling in breast cancer cells (Wei et al., 2017; Wang et al., 2019[1]). As the evidence above well explained the mechanisms of Cd-enhanced migratory and invasive phenotypes, Liang et al. further discovered that Cd might promote metastasis through down-regulating ACSS2/ATG5 axis mediated autophagy (Liang et al., 2021). However, these studies have used cancer cell models to describe Cd-induced malignancy. It still remains unclear whether Cd initiates breast cancer development and more studies would be needed.

## 1.2.6 Cd toxicity for lung cancer

Cd is a well-known lung cancer carcinogen. To general population, the exposure routes could be cigarette smoke or Cd-contaminated food/water. To occupational workers in the industries such as mining or battery manufacturing, the impact of Cd toxicity is profound and has been widely discussed ('t Mannetje et al., 2011; Chen et al., 2016). Several studies examined the toxic effects of Cd in lung cancer cells. Similar to the studies mentioned above in the breast cancer part, it has been found that Cd also exerts estrogen-like activity and activate MAPK/ERK pathway in the lung cancer cells (Huff et al., 2016; Zhai et al., 2019). Meanwhile, Cd also induced the expression of TGIF which plays a crucial role migration and invasion (Wang et al., 2019[2]). In lung adenocarcinoma cells (A549), Cd promoted enhanced cell proliferation and inflammatory response which was indicated by the increase of IL-1$\beta$, IL-6, and TNF-$\alpha$ (Kundu et al., 2011). The underlying mechanism of such inflammatory response might be due to the generation of ROS, suggested by the study described below (Wang et al., 2018). In addition to the cancer cell lines utilized, many studies have showed that Cd exposure leads to cell malignant transformation (Person et al., 2013; Wang et al., 2018; Cao et al., 2020). In the model of human lung epithelial cell (HPL-1D) transformed by Cd, enhanced cell proliferation and upregulation of vimentin and metalloproteinases were observed (Person et al., 2013). Human bronchial epithelial cell line (BEAS-2B) is another common cell line utilized for the study of Cd-induced cell transformation. Cao et al. reported that MAPK signaling pathway was highly activated in the BEAS-2B cells exposed to Cd. Wang et al. presented

that the challenge of Cd to the BEAS-2B cells stimulated pro-inflammatory response, in which the generation of ROS played the major role to create an inflammatory microenvironment. Interestingly, these two studies observed different aspect of apoptotic response upon the Cd toxicity. The results of Cao et al. revealed that Cd exposure led to ROS accumulation and increased apoptosis, as well as downregulated Bcl-2 and upregulated Bax and cleaved caspase-3 (Cao et al., 2020). On the other hand, the data of Wang et al. showed that the generated ROS contributed to cell transformation, in which upregulated Bcl-2 and Bcl-xL, along with apoptosis resistance was observed (Wang et al., 2018). Comparing these two studies, the Cd exposure time and dosage were different, which might explain the inconsistent outcomes. These studies are good examples to demonstrate the complexity of Cd toxicity and suggest that to investigate the mechanisms of Cd carcinogenesis, multi-dimensional factors should be thoroughly considered.

1.2.7 Cd toxicity for embryogenesis and the immune system

Though the mechanism of Cd carcinogenesis remains inconclusive, Cd seems to exert the oncolytic effects in a tissue-dependent context, with targeting cell type-specific signaling pathways. Furthermore, Cd has been demonstrated to impact embryogenesis and organ development. In a prostate model, Cd exposure has been shown to deregulate the expressions of development related genes, including EYA2, KPNA7, and PITX2 (Kolluru et al., 2019). This study suggests potential role of developmental signaling pathways involved in Cd carcinogenesis. In addition, several studies have revealed that Cd interferes with

the immune system. Cd has been shown to increase the level of metallothionein in human lymphocytes and monocytes (Sone and Kimura, 1988). Metallothionein is an important protein against metal toxicity and oxidative stress, however, it has also been shown to associate with the expression of VEGF-A and stabilization of HIF-1$\alpha$ (Kim et al., 2008; Kojima et al., 2008; Wierzowiecka et al., 2016). A study of Palazon et al. reported the inverse correlation between the HIF-1$\alpha$-VEGF-A axis and CD8^{+} T cell infiltration (Palazon et al., 2017). Although the role of metallothionein in carcinogenesis has not been determined, these studies suggest a potential oncogenic role of metallothionein (Cherian et al., 2003; Bizoń et al., 2017). It further hints that Cd induced metallothionein expression in the immune cells could lead to malignant outcomes. Another study regarding Cd-induced dysregulation in the immune system is that chronic Cd exposure resulted in abnormal production of interferon-gamma (IFN-$\gamma$) and interleukin 10 (IL-10) by various T cell subgroups (Turley et al., 2019). Though there is no direct evidence showing positive correlation between Cd-induced disrupted immune system and Cd oncolytic effects, malfunctioning immune system has been shown to favor tumor progression. Hence, it would be beneficial to include the study of Cd toxicity to the immune system for investigating Cd carcinogenesis in general.

While most metals have been shown genotoxic, Cd, however, has been speculated to exert carcinogenic function through non-genotoxic ways such as epigenetic modifications. It has been shown that unless at high concentration, Cd usually does not cause genetic toxicity and has been seen as a weak mutagen.

The most studies of Cd oncolytic toxicity have been focused on epigenetic modifications.

1.2.8 Cd caused DNA & histone modifications

Aberrant DNA methylation is a commonly found epigenetic dysregulation associated with Cd oncolytic effects. In the liver of the mice exposed to Cd at high dose (40 mg/kg) for two weeks, promoter of protease-activate receptor-4 (PAR-4) was found demethylated, which contributed to deregulation of MAPK pathway and PI3K-Akt pathway. While PAR-4 exerts tissue-specific functions, further experiments would be needed to explore the downstream affected targets in the liver (Ren et al., 2021). In general, PAR-4 creates a local environment which is prone to inflammatory (Heuberger et al., 2019). The finding echoes what has been discussed above that Cd exposure induces inflammatory response in breast cancer and lung cancer. In hepatocarcinoma cell HepG2 and breast cancer cell MCF-7, Cd exposure at 1 $\mu$M induced global DNA methylation due to decreased expression of DNA methyltransferases (DNMTs), which further led to demethylated promoters and increased expressions of protein arginine methyltransferase 5 (PRMT5) and enhancer of Zeste homolog 2 (EZH2). The upregulation of PRMT5 and EZH2 resulted in globally increased levels of H3K27me3, H4R3me2s, and symmetric dimethylarginine (SDMA) which is a pro-inflammatory agent (Ghosh et al., 2019). Nonetheless, there were studies which observed increased levels of DNMTs under the stress of Cd. In the study of Yuan et al., rats exposed to Cd for 8 to 12 weeks demonstrated enhanced lymphocyte proliferation. The followed up in vitro study identified upregulated DNMT1 and

DNMT3B in human lymphoblast cells which were exposed to Cd for 3 months. The induced DNMTs caused remarkably decrease of tumor suppressor p16 (Yuan et al., 2013). In addition to p16, p14 and RASSF1A were also found inactivated in melanoma and Cd transformed human prostate cells (Benbrahim-Tallaa et al., 2007; Venza et al., 2015). While the role of Cd in the expression of DNMTs seems polarized, Takiguchi et al. found that the expression of DNMTs under Cd stress could be dynamic. In the rat liver cells which were exposed to Cd for 1 week, DNMT activity was dramatically decreased for nearly 40% and genomic hypomethylation was observed. However, prolonged exposure (10 weeks) not only induced cell malignant phenotypes, but also significantly increased DNMTs activity and thus genomic hypermethylation (Takiguchi et al., 2003). Histone modification is another epigenetic mechanism and has been described in Cd associated cell transformation. Under both acute and chronic Cd exposure (5 $\mu$M for 48 h; 2 $\mu$M for 20 weeks), BEAS-2B cells displayed global increased levels of H3K4me3 and H3K9me2. Meanwhile, the activities of H3K4 and H3K9 demethylases KDM5A and KDM3A were found inhibited, while the protein levels of the two demethylases were not significantly affected (Xiao et al., 2015). The authors claimed that Cd might directly bind to these proteins to inhibit their activities, but further experiments would be needed to address this.

Non-coding RNAs dysregulation is another often discussed epigenetic modification in the studied of Cd carcinogenesis. A microRNA (miRNA) is a small single strand non-coding RNA containing around 22 nucleotides. A long non-coding RNA (lncRNA), on the other hand, is the one with more than 200

nucleotides. Both types of non-coding RNAs could interact with DNA, RNA, or protein to exert various biological functions, such as RNA silencing and post-transcriptional modification. Both miRNA and lncRNA have been reported to involve in Cd carcinogenesis.

1.2.9 Cd-induced miRNA dysregulation

Cd exposure in the cells could result into either downregulation of tumor-suppressive miRNA or upregulation of oncogenic miRNA. In bladder cancer patients, Cd concentration in the blood has been found strongly associated with the level of miR-21 (Awadalla et al., 2020). MiR-21-21 has been demonstrated to play critical roles in diseases such as cancer and cardiovascular diseases. Specifically, miR-21 regulates several immune response and developmental process (Kumarswamy et al., 2011). Cd-induced miR-21 might be a potential regulatory axis to explain Cd-induced inflammation. In rat ovarian granulosa cells with high concentration of Cd exposure (20 $\mu$M), miR-204-5p reduced the level of Bcl-2, which led to apoptosis (Zhong et al., 2020). Similarly, Sun et al. reported that acute exposure to Cd largely reduced Bcl-2 level due to another miRNA, miR-92a-2-5p which was promoted by Cd-induced c-Myc. (Sun et al., 2021). These results suggest that Cd could regulate Bcl-2 level through different sets of miRNA network. In human bronchial epithelial cells (16HBE) transformed by chronic Cd exposure, miR-27b-3p was found significantly upregulated and regulates multiple target mRNAs, such as ADAMTS10 and CCM2 (Liu et al., 2015). ADAMTS10 is a member of disintegrin and metalloproteinases which was critical during embryo development (Somerville et al., 2004). CCM2 is a scaffold

protein involved in various signaling pathway such as MAPK pathway (Fisher et al., 2014). MiR-27b-3p has been shown to promote migration and invasion in colorectal cancer ([2]Yang et al., 2019). In addition, Tanwar et al. also reported that acute Cd exposure stimulates the level of miR-30, which results in enhanced expression of Snail in BEAS-2B cells (Tanwar et al., 2019). The results suggest that Cd might promote metastatic characteristics through upregulation of the miRNA.

1.2.10 Cd-induced lncRNA dysregulation

LncRNAs, one of the non-coding RNA subgroups, have been often found interacting with miRNAs or proteins to modulate downstream response. In Cd carcinogenesis, the discovered lncRNA activities include DNA-damage response, apoptosis/ferroptosis control, cell proliferation, and invasion. In prostate cancer patients, serum Cd concentration was found positively correlation to tumor-node-metastasis. Further study demonstrated a lncRNA, OIP5-AS1, promotes cancer progression and ferroptosis resistance through regulating the level of oncoprotein SLC7A11. SLC7A11 has been shown overexpressed in KRAS-mutated lung adenocarcinoma with major function of protecting cells from oxidative stress (Hu et al., 2019). The expression of SLC7A11 is regulated by miR-128-3p. LncRNA OIP5-AS1 functions as a sponge for miR-128-3p, which facilitate the expression of SLC7A11 (Zhang et al., 2021). In contrast to the endogenous competing mechanism described above, another mechanism has been brought up, that lncRNA binding to miRNA to promote its stability upon the stress of Cd. Gao et al. described that lncRNA MT1DP which is induced by Cd in hepatocytes binds to

miR-365 to repress the level of nuclear factor erythroid 2-related factor 2 (Nrf2) and promote cell death (Gao et al., 2018). In addition to apoptosis/ferroptosis regulation, Cd-induced lncRNA also involves in compromised DNA repair system. A study from Zhou et al. revealed that inhibiting lncRNA-ENST00000446135 rescued the expression of a set of DNA repair-related genes, including DDB1/2, MSH2, OGG1, ERCC1, XRC1, and BARD1 (Zhou et al., 2020). Moreover, in Cd transformed 16HBE, Cd has also been shown to upregulate the level of oncogenic lncRNA MALAT1 which regulates cell proliferation, migration, invasion, as well as apoptosis (Huang et al., 2017).

1.2.11 epitranscriptomic modification

Lastly, epitranscriptomic regulation is a relatively novel mechanism found to be involved in Cd carcinogenesis. Briefly, epitranscriptome studies biochemical modifications on RNAs that affect gene expression (e.g., mRNA stability). Among the various types of epitrancriptomic regulations reported, $m^6A$ modification is the most common one. There has been a study demonstrating that $m^6A$ modification on lncRNA MALAT1 could stabilize the lncRNA or facilitate its binding to target proteins (He et al., 2020). In pancreatic $\beta$ cells that treated with Cd, aberrant $m^6A$ modification was portrayed in lncRNAs including MALAT1 and lncRNA PVT1, along with the affected levels of $m^6A$ "writer" – methyltransferase-like 3 (METTL3) and the "eraser" – fat mass and obesity-associated protein (FTO), suggesting that epitranscriptomic dysregulation could play an important role in Cd carcinogenesis (Qu et al., 2021).

Together, Cd toxic effects could be varied in different cell types and could be dependent on the exposure dosage and time. Acute exposure to Cd at high concentration, the rapidly built-up oxidative stress or Cd-induced mitochondrial toxicity could result in programmed cell death. However, several responses could be evoked to facilitate cell survival, such induction of Bcl-2 or autophagic related protein expression. Meanwhile, the estrogen-like action of Cd could also promote the cell survival and proliferation pathways such as MAPK.ERK pathway. In addition to become tolerant to Cd toxicity, sustained Cd exposure brings in other modifications which further allow the cells to adopt more malignant phenotypes, including enhanced migration and invasion. Furthermore, as Cd mostly exerts oncolytic functions through non-genotoxic ways, we could see the intertwined epigenetic modifications, including DNA methylation, histone modification, and non-coding RNA dysregulation. These intricated modifications further link to another level of regulation – epitranscriptomics. To delineate the underlying mechanism of Cd carcinogenesis, it is important to identify the dominant signaling pathways in the specific type of cells. And it is essential to investigate different networks of each epigenetic modifications.

CHAPTER 2. LONG NON-CODING RNA *DUXAP10* ACTIVATES THE

HEDGEHOG PATHWAY TO PROMOTE CHRONIC CADMIUM EXPOSURE-

INDUCED CANCER STEM CELL-LIKE PROPERTY AND TUMORIGENESIS

## 2.1 ABSTRACT

Cadmium (Cd) is a ubiquitously present pollutant in the environment and a known carcinogen for lung cancer. However, the mechanism of Cd carcinogenesis remains to be clearly defined. Cd has been shown to act as a weak mutagen, which suggests that it may exert tumorigenic effect through non-genotoxic ways, such as epigenetic mechanisms. Long non-coding RNAs (LncRNAs) refer to RNA molecules that are longer than 200 nucleotides in length but lack protein coding capacities. Regulation of gene expression by lncRNAs is considered as one of important epigenetic mechanisms. The goal of this study is to investigate the mechanism of cadmium carcinogenesis focusing on the role lncRNA dysregulations. Cadmium-induced malignant transformation of human bronchial epithelia BEAS-2B cells was accomplished by 9 month of low dose Cd (CdCl$_2$, 2.5 μM) exposure. The Cd-exposed cells formed significantly more colonies in soft agar, displayed cancer stem cell (CSC)-like property and formed tumors in nude mice. Mechanistically, chronic low dose Cd exposure did not cause significant genotoxic effects. However, the lncRNA microarray analysis revealed that chronic low dose Cd exposure dysregulates lncRNA expressions. Further Q-PCR analysis confirmed the significant up-regulation of the oncogenic lncRNA *DUXAP10* level in Cd-transformed cells. Moreover, siRNA knockdown of *DUXAP10* expression in

Cd-transformed cells significantly reduced their CSC-like property. Further mechanistic studies showed that *DUXAP10* activates the Hedgehog pathway to promote Cd-induced CSC-like property. Furthermore, it was determined that chronic low dose Cd exposure up-regulates *DUXAP10* expression by inducing Pax6 expression. In summary, these findings suggest that the lncRNA *DUXAP10* up-regulation may play an important role in Cd carcinogenesis.

Key words: cadmium; cancer stem cell-like property; long non-coding RNA; *DUXAP10*; Hedgehog pathway; Pax6.


## 2.2 INTRODUCTION

Cadmium (Cd) is a naturally occurring toxic metal. It has been widely used in industries for productions of, for example, batteries, cell phones, and computer circuit boards. Hence, occupational exposure is the major route for the first-line workers during these manufacturing process. Several studies have revealed elevated levels of Cd contamination in the workers' blood and urine (Akerstrom et al., 2013; Baloch et al., 2020). For the general population, the exposure routes could be Cd-contaminated water or food or tobacco smoke. With long biological half-life of 15-20 years, toxicity of Cd is considered cumulative and poses a great health risk. Cd is listed as a class I carcinogen by International Agency for Research on Cancer (IARC). It is a known carcinogen for lung cancer (Huff et al., 2007). Many studies have also reported its association with other types of cancer, including breast cancer (Wei et al., 2018; Song et al., 2015), liver cancer (Xiao et

21

al., 2015; Ali et al., 2015), prostate cancer (Achanzar et al., 2001; Golovine et al., 2010; Dasgupta et al., 2020), melanoma (Venza et al., 2015), and lymphoma (Yuan et al., 2013). However, the exact carcinogenic mechanism of Cd remains unclear.

Cd has only minor or barely genotoxicity, especially at low dose, and has been considered a weak mutagen (Misra et al., 1998; Waalkes, 2000). It has been proposed that Cd exerts its oncogenic effect more likely through epigenetic non-genotoxic ways. Regulations of gene expression by non-coding RNAs such as microRNAs and long non-coding RNAs (lncRNAs) are considered as important epigenetic mechanisms (Wang et al., 2021; Zhang et al., 2019; Dykes et al., 2017; Humphries et al., 2016; Mercer et al., 2013). LncRNAs refer to RNA molecules that are longer than 200 nucleotides in length but lack protein coding capacities. Studies have shown that lncRNA dysregulations are critically involved in cancer initiation and progression (Chi et al., 2019; Li et al., 2016). While emerging evidence suggests that lncRNA dysregulations may play important roles in environmental carcinogenesis (Wang et al., 2021), how Cd exposure dysregulates lncRNA expression and whether lncRNA dysregulations play a role in Cd carcinogenesis remain largely unknown.

Although the mortality rate of lung cancer has dropped since 2017 due to improved treatment, lung cancer remains the leading cause of cancer death to both males and females in the US (Siegel et al., 2020; Siegel et al., 2021). Lung cancer cells can metastasize at early stage even before it can be detected, which complicates the prognosis, diagnosis, and the therapy. Eventually the hindered

therapeutic efficiency leads to low overall survival rate of lung cancer patients (Cheng et al., 2021; Cui et al. 2021.; Rudin et al., 2021). The presence of cancer stem cells (CSCs) has been considered the driven force for such metastasis and tumor relapse after the therapy (Perona et al., 2011). Critical properties of this distinct population, including self-renewal, drug resistance, and multilineage differentiation, make it difficult to be eliminated in the therapy. Previously others and our studies have reported hexavalent chromium [Cr (VI)]- induced CSC-like properties and the related mechanic studies in human bronchial epithelial cells (Dai et al., 2017; Wang et al., 2018; Wang et al., 2019; Clementino et al., 2020; Li et al., 2021). However, it is unknown whether and how chronic low dose Cd exposure is capable of inducing CSC-like property. In the present study, human bronchial epithelial cells (BEAS-2B) were exposed to Cd at a low dose for nine months, mimicking chronic exposure of heavy metal to humans. The goal of this study is to investigate the mechanism of Cd carcinogenesis focusing on the role of lncRNA dysregulations.

## 2.3 MATERIALS AND METHODS

### 2.3.1 Cell culture and chemical treatments

Immortalized human bronchial epithelial BEAS-2B cell line was purchased from America Type Culture Collection (ATCC, Manassas, VA). BEAS-2B cells were cultured in Dulbecco's Modified Eagle Medium (DMEM) (Thermo Fisher, MA)

supplemented with 5% fetal bovine serum (FBS) and 1% Penicillin-Streptomycin (P/S).

### 2.3.2 Cell transformation by chronic exposure of cadmium ($CdCl_2$)

BEAS-2B cells were first treated with different doses of $CdCl_2$ (2.5, 5, and 10 $\mu$M) (Sigma-Aldrich) for 24 h and observed the morphology under the microscope to determine the cytotoxic effect of Cd. It was found that 5 and 10 $\mu$M of $CdCl_2$ had toxic effects on the viability and proliferation of BEAS-2B cells, while 2.5 $\mu$M of $CdCl_2$ had no obvious cytotoxic effects. This dose was then chosen for chronic cell transformation experiment following our published protocol (Wang et al., 2011). Briefly, BEAS-2B cells were continuously exposed to a vehicle control ($H_2O$) or 2.5 $\mu$M of $CdCl_2$. When reaching about 80-90% confluence after exposure, cells were sub-cultured. Cd was freshly added to cells each time after overnight cell attachment. Soft agar colony formation assay was performed after every 4-week Cd exposure to assess cell transformation. This process was repeated for 38 weeks.

### 2.3.3 Microarray analysis

Total RNA was extracted from passage-paired BEAS-2B control and Cd-transformed cell pellets by TRIzol reagents according to the manufacturer's protocol (Invitrogen, CA). The RNA samples were then sent to Arraystar Inc.

(Rockville, MD) for microarray analysis. The array raw data was further analyzed by Arraystar Inc. and the microarray raw data was deposited to the National Center for Biotechnology Information (NCBI)'s data repository (Access ID: GSE175472).

### 2.3.4 Soft agar colony formation assay

The soft agar colony formation assay was carried out in 60 mm cell culture dishes for each group as previously described (Yang et al., 2005). Briefly, cultured cells were collected by trypsinization and suspended in DMEM containing 10% FBS at density of 0.25 x $10^4$ cells/mL. Normal melting point agarose (4 mL of 0.6% agarose in DMEM containing 10% FBS) was placed into each 60 mm cell culture dish as the bottom layer. After solidification, 4 mL of cell mixture consisting of 2 mL of cell suspension and 2 mL of 0.8% low melting point agarose in DMEM containing 10% FBS were poured over the bottom layer agarose. After solidification of the upper layer, 3 mL of DMEM containing 10% FBS was added, and dishes were incubated at 37℃ in cell incubator with 5% $CO_2$. After 4-week incubation, colonies formed in the agarose dishes were stained with 0.003% crystal violet, photographed and counted.

### 2.3.5 Suspension culture spheroid formation assay

The spheroid formation assay was performed following the published protocol (Dontu et al., 2003) with minor modifications. Briefly, single cells were plated in ultra-low attachment 24-well culture plates (Corning, NY) at a density of 2 x $10^3$

cells per well suspended in serum-free DMEM containing human recombinant basic fibroblast growth factor (bFGF, 20 ng/mL) (R&D, Minneapolis, MN), human recombinant epidermal growth factor (EGF, 20 ng/mL) (R&D, Minneapolis, MN), B27 (Invitrogen, Carlsbad, CA) and heparin (4 $\mu$g/mL, Sigma-Aldrich). Plates were incubated at 37℃ in cell incubator with 5% $CO_2$. Spheres > 50 $\mu$m were viewed, photographed and counted under a phase-contrast microscope after 10-day culture.

## 2.3.6 Nude mouse xenograft tumorigenesis study

Passage-matched control and Cd-transformed cells (1.5 x $10^6$ cells in 0.1 mL of 1:1 growth factor-reduced Matrigel and serum-free DMEM) were injected subcutaneously into the right flank of female nude mice (Nu/Nu, Charles River laboratories, ten mice in each group). Animals were maintained under specific pathogen-free conditions, and animal protocols were reviewed and approved by the University of Kentucky Institutional Animal Care and Use Committee. All mice were euthanized 12 weeks after injection, and the xenograft tumors were harvested and photographed.

## 2.3.7 Western blot analysis

Cells were lysed using lysis buffer following our published protocol (Yang et al., 2006; Wang et al., 2014). The cell lysates were then applied to the bicinchoninic acid assay (Bio-rad) to determine protein concentration, followed by SDS-

polyacrylamide gel electrophoresis (PAGE) (20-30 µg of protein/lane). The separated proteins were then transferred to polyvinylidene fluoride membrane (PVDF, Millipore, MA). Five percent milk in PBS was applied for the blocking step before primary antibody incubation. The following primary antibodies were used: anti-KLF4, anti-KLF5, anti-Nanog, anti-GLI1, anti-SHH, anti-PTCH1, anti-PTCH2, anti-Pax6 (Cell Signaling Technology, Beverly, MA) (dilution 1:1000); anti-phospho-histone H2A.X (Ser139) ($\gamma$H2AX) (dilution 1:1000), and anti-$\beta$-actin (Millipore Sigma, St. Louis, MO) (dilution 1:8000). After overnight primary antibody incubation at 4 °C, the membranes were washed and then incubated with HRP-conjugated antibodies for 1 h at room temperature. Images were developed by Amersham Imager 680 (GE Healthcare Life Sciences, MA).

### 2.3.8 Kaplan-Meier plotter survival analysis

The Kaplan-Meier potter (KM plotter, http://kmplot.com/analysis/) was utilized to analyze the correlation between levels of Pax6/*DUXAP10* and overall survival (OS)/recurrence-free survival (RFS) in 1144 lung cancer patients.

### 2.3.9 Flow cytometry analysis of CD133+ cells

Cells were detached from the culture dishes with Versene solution (Gibco). After centrifugation, cells were re-suspended in DMEM with 2% FBS and 1% PS. 0.25 µg of PE-anti CD 133 (Promini-1) (Biolegend, CA) was added to the cells. After 40 minutes of incubation, cells were washed and stained with DAPI for viability.

Fluorescence-activated cell sorting was carried out by the flow cytometer BD LSR II (Becton Dickinson). Raw data was analyzed by using Flowjo software (Becton Dickinson).

### 2.3.10 Quantitative PCR

Total RNA extraction was performed by TRIzol reagent following the manufacturer's instruction (Invitrogen, CA). Quality and Quantity of extracted RNA was determined by NanoDrop™ spectrophotometer (Thermo Fisher, MA) before applying to TaqMan gene expression assays. Quantitative PCR was performed by ABI QuantStudio 3 qPCR System (Applied Biosystems). The $2^{-\Delta\Delta}$ ct analysis method was utilized to quantify relative RNA expression levels of each gene, with human 18S RNA as the internal control.

### 2.3.11 Immunofluorescence (IF) staining of cultured cells

Cells were seeded on cover-glass placed in 6-well plates and cultured for 48 h (including the inhibitor treatment or RNA interference) before the antibody staining. For the staining process, cells were first washed and fixed with 4% paraformaldehyde for 20 min at room temperature. Permeabilization was performed by the use of 1% Triton X-100 in PBS and incubated for 1.5 min at room temperature, followed by blocking with 3% bovine serum albumin (BSA) for 30 min. The primary antibodies, phospho-histone H2A.X (Ser139) ($\gamma$H2AX) (Santa Cruz) and GLI1 (Cell Signaling Technology), were diluted in PBS with 1% BSA at a ratio

of 1:200. Following the primary antibody incubation for overnight at 4°C, cells were washed before the secondary antibody incubation (Alexa 546 goat anti-mouse/rabbit IgG, 1:300, Invitrogen). After 1 h of incubation at room temperature, cells were washed again and stained with nuclear 4'6-diamidino-2-phenylinodole (DAPI) for 10 min before mounting. IF staining pictures taken under a Nikon fluorescent microscope are presented as the overlaid images of $\gamma$H2AX, GLI1 staining in red fluorescence with nuclear 4'6-diamidino-2-phenylinodole (DAPI) staining in blue fluorescence. The image overlaid was done using Nikon NIS-Elements software.

### 2.3.12 Chromatin immunoprecipitation (ChIP) -qPCR assay

The ChIP-qPCR assay was utilized to detect the abundance of transcription factor Pax6 in the promoter region of *DUXAP10*. The ChIP assay was performed by using the Pierce$^{TM}$ Agarose ChIP kit (Thermo Scientific) following the manufacturer's protocol. Briefly, cells were cross-linked with 1% formaldehyde, followed by Micrococcal Nuclease digestion. The fragmented DNA were applied to immunoprecipitation with 5 $\mu$g of anti-Pax6 antibody (#sc-32766, Santa Cruz) per reaction. The ChIP DNA was then examined by qPCR for the enrichment of the target protein at the promoter region of interest. The Percent Input Method was adopted to present the ChIP-qPCR results.

## 2.3.13 RNA interference by transient transfection

Cells were seeded in 6-well plates or 60 mm dishes (Corning) 24 h before transfection in DMEM supplemented with 5% FBS and 1% P/S. Before transfection, the culture medium was refreshed with serum-free DMEM. siRNA was then transfected using Lipofectamine 3000 (Invitrogen) according to the manufacturer's protocol. Four hours after, equal volume of DMEM with 10% FBS and 1% P/S was added to the plates/dishes. The cells would be ready for further analysis in 48 h.

## 2.3.14 Plasmid construction

The sequence of *DUXAP10* was submitted to GenScript Biotech (NJ, USA) for the synthesis and subcloning of *DUXAP10* into the vector pBluescript II SK(+). The *DUXAP10* anti-sense (*DUXAP10*-AS) fragment was the PCR product using the *DUXAP10* plasmid as the template. The amplified *DUXAP10*-AS was digested with restriction enzymes KpnI and XhoI (BioLabs, New England) and then subcloned into vector pBluescript II SK(+). Both plasmids bearing sense and anti-sense *DUXAP10* were introduced into competent cells DH5$\alpha$, followed by plasmid extraction using ZymoPURE$^{TM}$ II Plasmid Midiprep Kit (Zymo Research). The extracted plasmids from DH5$\alpha$-*DUXAP10* –sense and –antisense strains were evaluated by restriction enzyme PstI (BioLabs, New England) before proceeding to RNA pulldown assay.

## 2.3.15 RNA pulldown assay

The plasmids pBluescript-*DUXAP10* and pBluescript-*DUXAP10*-AS were linearized by restriction enzyme EcoRI-HF (BioLabs, New England), followed by in vitro transcription for synthesis of biotinylated RNA and RNA pulldown described in the study of Feng et al., 2014. In brief, four μg of linearized plasmids were added to the mixture of 10X Biotin mix (Roche), T7 RNA polymerase (Promega), 5X Transcription buffer (Promega), and DNAse/RNase-free water, incubated at 37°C for 3 h, and proceeded to DNase I digestion at 37°C for 15 min. Biotinylated RNA was purified using G-50 Sephadex Columns (Roche). RNA pulldown was then carried out by incubating 20 μg of the biotinylated RNA with total protein lysates from Cd-T cells on a rotator at 4°C for 1 h, followed by repeated washing and centrifugation steps. Finally, the precipitated protein-beads complexes were resuspended with protein loading buffer and boiled for 10 min. After centrifugation, the supernatant containing the pulled-down proteins were applied to Western blot analysis.

## 2.3.16 Statistical analysis

The statistical analyses for the significance of differences in presented numerical data (mean ± SD) were carried out by testing different treatment effects using two-tailed t-tests for comparison of two data sets. A *p*-value of < 0.05 was considered statistically significant.

2.4 RESULTS

2.4.1 Chronic low dose of Cd exposure induces CSC-like property and tumorigenesis

To establish a Cd-induced cell transformation model, we treated immortalized human bronchial epithelial cells (BEAS-2B) to Cd at the concentration of 2.5 $\mu$M twice a week. The transformation process was monitored by the soft agar colony formation assay monthly. After 9 months of exposure, the Cd-treated cells displayed more than 50 times of colony formation, compared to the passage-matched control-treated cells (**Figure 2.1A**), suggesting that cell transformation by Cd was achieved. Meanwhile, Cd-induced cell transformation was further analyzed by determining the cancer stem cell (CSC)-like property and tumorigenicity of Cd-exposed cells (Cd-T). The suspension culture sphere formation assay showed that Cd-T cells form significantly more suspension spheres than the passage-matched control cells (**Figure 2.1B**). Furthermore, the first generation sphere cells from Cd-transformed cells formed significantly more secondary spheres (**Figure 2.1B**), demonstrating the self-renewal capacity of this distinct population within the transformed cells. CD133 (Prominin-1), a transmembrane glycoprotein, has been used as a CSC surface marker in many cancer types, including lung adenocarcinoma (Miyata et al., 2017). As shown in **Figure 2.1C**, the number of CD133 positive cells in Cd-transformed cells is 5 times more than that in control cells, providing another evidence that chronic Cd exposure induces CSC-like property. Moreover, Cd transformed cells were further sorted into CD133 positive and negative populations and applied to suspension

sphere formation. It was found that CD133$^+$ cells displayed a much stronger sphere-forming capacity than the CD133$^-$ cells (**Figure 2.1D**), suggesting that CD133 could serve as one of the cell surface markers of the CSC-like population induced by chronic Cd exposure. Moreover, we further examined several stemness-related markers at their protein levels. Elevated expressions of KLF4, KLF5, and Nanog were observed in Cd-transformed cells (**Figure 2.1E**). Since CSC or CSC-like cells are considered as tumor initiating cells, we also determined the tumor forming capability of Cd-transformed cells. To study tumorigenic capacity of Cd-transformed cells, we injected Cd-T cells, as well as the passage-matched control group cells, into the right flank of nude mice. Comparing to the control group which had no tumor formed, 60% of tumor incidence in the Cd-T group was observed (**Figure 2.1F**). Together, these results demonstrated that long-term exposure to a low dose of Cd causes cell malignant transformation, along with the induction of CSC-like property and tumorigenesis.

2.4.2 Chronic exposure to a low dose of Cd does not induce significant DNA damage, but causes long non-coding RNA dysregulations

Next, we set to determine the mechanism by which chronic low dose of Cd exposure induces CSC-like property. We first determined whether chronic low dose of Cd exposure causes genetic toxicity in BEAS-2B cells. We performed immunofluorescence staining to examine the presence of DNA damage marker phospho-histone H2A.X ($\gamma$H2AX) in passage-matched control BEAS-2B cells and Cd-T cells. **Figure 2.2A** shows that no significant amount of $\gamma$H2AX is present in

the control cells and Cd-transformed cells. We next determined the genotoxic effect of acute low dose and high doses of Cd exposure on control BEAS-2B cells. While treating control BEAS-2B cells with Cd 2.5 μM, no significant γH2AX formation was detected, treating control BEAS-2B cells with 10 μM of Cd significantly induced γH2AX formation (**Figure 2.2B**), indicating large amount of DNA damage. These results suggested that the Cd exposure concentration of 2.5 μM is not genotoxic and that the cell malignant transformation could be the result of other non-genotoxic effects such as epigenetic modifications. To further determine the mechanism of Cd inducing CSC-like property, we performed lncRNA microarray analysis and the results were deposited to the NCBI data repository (Access ID: GSE175472). The lncRNA microarray results revealed that 225 lncRNAs were up-regulated in Cd-T cells, while 75 were down-regulated (with cut-off 2-fold change) (**Figure 2.2C**). Among the up-regulated lncRNAs, there were four lncRNAs identified as oncogenic by other studies (**Table 2.1**) and the expression levels were 2.5 times or higher in Cd-transformed cells than the control cells: LUCAT1; LINC00473; HOTAIRM1; and *DUXAP10* (**Figure 2.2D**). Further qPCR analysis confirmed the up-regulation of the 4 oncogenic lncRNAs: *DUXAP10* was up-regulated around 5.6-fold, while HOTAIRM1 and LINC00473 were up-regulated around 3-fold, and LUCAT1 was up-regulated less than 2-fold. As *DUXAP10* was confirmed the highest expression level in Cd-transformed cells (**Figure 2.2E**), we decided to focus on *DUXAP10*.

### 2.4.3 Knockdown of *DUXAP10* in Cd-T cells significantly reduces their CSC-like property

The lncRNA *DUXAP10* has been shown oncogenic in various cancer models, including non-small cell lung cancer (Wei et al., 2017). Our bioinformatics analysis shown in **Figure 2.3A** demonstrated that its overexpression is associated with significantly worse overall survival (OS) for lung cancer patients, further confirming its oncogenic role in lung cancer. To perform functional studies, we knocked down *DUXAP10* by small interfering RNA which's efficiency was around 50% (**Figure 2.3B**). After the knockdown, the stemness markers which were shown upregulated in Cd-T cells decreased at the protein levels, including KLF4 and Nanog (**Figure 2.3C**). Furthermore, sphere formation with *DUXAP10* knockdown dropped by 50%, compared to the Cd-T – control siRNA cells (**Figure 2.3D**). In addition, we examined the stem cell surface marker CD133 by flow cytometry. In Cd-T cells with *DUXAP10* knockdown, CD133 positive population decreased 60% (**Figure 2.3E**). These results demonstrate the importance of *DUXAP10* in maintaining CSC-like property of Cd-transformed cells.

### 2.4.4 The Hedgehog pathway is highly activated in Cd-T cells promoting their CSC-like property

As the previous results revealed the induced CSC-like property in Cd-T cells, we next set to explore the pathways associated with this property. Downstream targets of three stemness-related pathways were screened first, including the

Hedgehog pathway, Notch pathway, and Wnt/β-catenin pathway. Glioma-associated oncogene homolog 1 (GLI1) acts as the effector of the Hedgehog signaling, and is also one of the downstream targets of this pathway. Transcription factor HES1 plays an important role during embryogenesis and is the downstream target of the Notch signaling pathway. The transcription factor 12 (TCF12) is one of important target genes of the Wnt/β-catenin pathway. The qPCR results showed 2.3-fold increase in GLI1 expression, while the levels of HES1 and TCF12 show no change between the control cells and Cd-T cells (**Figure 2.4A**). Important proteins involved in the Hedgehog pathway were then checked by Western blot. We found upregulated levels of GLI1, Protein patched homolog 2 (PTCH), and Sonic hedgehog protein (SHH) in Cd-T cells, while the levels of Smoothened (SMO) and Suppressor of fused homolog (SUFU) remained unchanged between control and Cd-T cells (**Figure 2.4B**). Translocation of GLI1 from cytoplasm to nucleus is essential to activate the transcription of Hedgehog downstream target genes. Here, we checked the cellular localization of GLI1 in the control BEAS-2B and Cd-T cells by immunofluorescence staining. In Cd-T cells, GLI1 is mostly localized in the nucleus as indicated by the pink color resulting from the overlapping of nuclear DAPI staining in blue and GLI1 staining in red (**Figure 2.4C**). On the contrary, in the BEAS-2B control cells, the nucleus color remained blue, which demonstrates no significant amount of GLI1 nuclear translocation (**Figure 2.4C**). Cyclopamine, an inhibitor of the Hedgehog pathway (Incardona et al., 1998), was then utilized to confirm that Hedgehog pathway plays a critical role in the CSC-like property of Cd-T cells. Immunofluorescence staining showed no significant GLI1 nucleus

translocation under the treatment of cyclopamine at 10 μM. (**Figure 2.4D**). At the same time, treatment of 10 μM of cyclopamine abolished the sphere forming capability of Cd-T cells (**Figure 2.4E**). Furthermore, protein levels of stemness markers KLF4, KLF5, Nanog, as well as GLI1 in Cd-T cells, were down-regulated by the cyclopamine treatment (**Figure 2.4F**). Together, these results indicated that the Hedgehog pathway activity is essential to maintain the CSC-like properties in Cd-T cells.

2.4.5 Knockdown of *DUXAP10* inactivates the Hedgehog pathway in Cd-T cells

We next determined whether *DUXAP10* regulates the Hedgehog pathway activity in Cd-transformed cells. **Figure 2.5A** shows that knockdown of *DUXAP10* leads to decreased levels of GLI1, SHH, and PTCH in the Cd-T cells. Immunofluorescence staining revealed no significant presence of GLI1 in the nucleus while *DUXAP10* was knocked down (**Figure 2.5B**). These results suggest that *DUXAP10* plays an important role in activating the Hedgehog signaling pathway. We then further determined how *DUXAP10* activates the Hedgehog pathway. Modes of lncRNA actions in tumor cells could be: (1) mediating transcription by binding with proteins such as transcription factors; (2) acting as scaffold molecule to assemble protein complex; (3) acting as decoy or guide molecule to regulate functions of DNA, mRNA and miRNA (Gao et al., 2020). Though with little evidence presented regarding the regulatory role of *DUXAP10*, the previous studies hinted a higher chance of *DUXAP10* interacting with proteins

(Wei et al., 2017; Xu et al., 2018). We next proceeded to predict the interaction between *DUXAP10* and the proteins in the Hedgehog pathway by RPIseq (RNA-Protein Interaction Prediction, powered by Iowa State University). The outcome indicated that the interaction probability between *DUXAP10* and GLI1 is 0.9, while it is 0.7 between *DUXAP10* and SHH (**Table 2.2**). RNA pulldown assay was then performed to confirm the interaction between the lncRNA *DUXAP10* and the proteins. The results showed that *DUXAP10* sense strain binds to GLI1, with its antisense as the negative control (**Figure 2.5C**). However, the RNA pulldown assay revealed no interaction between *DUXAP10* and SHH. As the interaction of *DUXAP10* and GLI1 was confirmed, we next study the impact of this interaction on GLI1 level. Previously, a study suggested that destruction of GLI1 is regulated by proteosome degradation (Huntzicker et., 2005). Here, we treated the cells with proteosome inhibitor MG132, and observed increased level of GLI1 in Cd-T cells, which confirmed that GLI1 stability could be regulated by the proteosome mechanism. MG132 treatment also increased the level of GLI1 in the Cd-T with *DUXAP10* knockdown (**Figure 2.5D**). This demonstrates that *DUXAP10* contributes to the stability of GLI1 to promote the downstream signaling.

2.4.6 Chronic Cd exposure increases the expression of Pax6 to up-regulate *DUXAP10* level

We further determined how chronic low dose Cd exposure up-regulates *DUXAP10* level. Pax6 has been inferred as a putative transcription factor for *DUXAP10*. The predicting binding site of Pax6 locates at the end of *DUXAP10*

promoter region (**Figure 2.6A**). In Cd-T cells, we observed significantly elevated expression level of Pax6 (**Figure 2.6B**). This is the first study to show that Cd exposure induces the expression of Pax6. Further bioinformatics analysis shows that the expression level of this transcription factor is negatively corelated to the overall survival rate of lung cancer patients (**Figure 2.6C**). ChIP-qPCR analysis revealed that Pax6 binds to *DUXAP10* promoter region (**Figure 2.6D**). Furthermore, knockdown of Pax6 decreased the expression of *DUXAP10* by 50% (**Figure 2.6E**), as well as down-regulating GLI1 level (**Figure 2.6F**). Immunofluorescence staining also shows decreased nuclear localization of GLI1 in the Cd-T with knockdown of Pax6 (**Figure 2.6G**). Finally, the knockdown of Pax6 also led to reduced sphere formation by 50% (**Figure 2.6H**) in Cd-T cells.

## 2.5 DISCUSSION

Cd is a known carcinogen to lung cancer. However, as the most of those studies utilized cancer cell models, the exact mechanism of Cd carcinogenesis remains to define. CSCs or CSC-like cells play important roles in cancer initiation and progression. Moreover, ours and other recent studies showed that CSC-like cells may be also play critical roles in metal carcinogenesis (Dai et al., 2017; Wang et al., 2018, Wang and Yang, 2019). However, whether and how Cd induces CSC-like population remains unknown. In the present study, immortalized human bronchial epithelial cells were exposed to Cd at a low dose for 9 months and utilized for studying the underlying mechanisms. Our results demonstrated that Cd

exposure led to cell malignant transformation and induced CSC-like property through dysregulation of oncogenic lncRNA *DUXAP10* (**Figure 2.7**).

It is generally accepted that Cd is relatively low genotoxic. Most studies thus focused more on the non-genotoxic effects caused by Cd exposure, especially DNA methylation. Venza et al. and Yuan et al. found that Cd contributes to silencing of tumor suppressor p16 through DNA hypermethylation in melanoma and lymphoma cells (Venza et al., 2015; Yuan et al., 2013). Aberrant DNA methylation profiles have also been shown in breast cancer cells exposed to Cd (Liang et al., 2020; Liang et al., 2021). On the other hand, little is known about the role of non-coding RNA(s) in Cd oncogenic effect. Huang et al. and Zhou et al. reported overexpression of lncRNA MALAT1 and lncRNA-ENST00000446135 in the Cd-transformed16HBE cells and the lungs of Cd-exposed rats, as well as in the blood of the workers exposed to Cd (Huang et al., 2017; Zhou et al., 2020). However, no study has reported the role of lncRNAs in cancer stem cell-like populations induced by this heavy metal.

The findings from this study suggested a potential role of the oncogenic lncRNA *DUXAP10* in the induced stemness of Cd-T cell. *DUXAP10* was first identified oncogenic in the study of Wei et al. in 2017, in which the results demonstrated *DUXAP10* inhibited the expression of tumor suppressors Large tumor suppressor 2 (LATS2) and Ras-related associated with diabetes (RRAS) (Wei et al., 2017). In addition, it has been shown that *DUXAP10* enhances cell proliferation and metastasis through activating the PI3K/AKT pathway in hepatocellular carcinoma (Sun et al., 2019; Han et al., 2019; Yue et al., 2019) and

40

AKT/mTOR pathway in papillary thyroid carcinoma (Li et al., 2020). Our study provides the first evidence to show that *DUXAP10* contributes to CSC-like property. Furthermore, our mechanistic studies delineated that *DUXAP10* contributes to Cd-induced CSC-like property likely by regulating the sonic hedgehog pathway.

It has been shown that lncRNAs could interact with various macro molecules, including DNA, RNA, and protein, to exert biological functions (Xu et al., 2021; Ming et al., 2021; Jiang et al., 2021). *DUXAP10* has been shown to interacts with histone demethylase lysine specific demethylase 1 (LSD1) in non-small cell lung cancer (Wei et al., 2017). The interaction between *DUXAP10* and LSD1 was also reported by Lian et al. later, which suppressed the expression of p21 and phosphatase and tensin homolog (PTEN) in colorectal cancer cells (Lian et al., 2017). Our study showed that *DUXAP10* interacts with GLI1 protein and stabilizes GLI1 to activate the Hedgehog pathway. We identified a new protein binding partner for *DUXAP10*, offering a new mechanism for understanding the oncogenic role of *DUXAP10*.

In addition to stabilizing GLI1, *DUXAP10* also elevated the levels of SHH and PTCH2 in Cd-T cells. As the driving force of the Hedgehog pathway, upregulated SHH and its receptor PTCH would further enforce the downstream signaling. The facts that *DUXAP10* stabilizes GLI1 and that *DUXAP10* enhances the level of SHH and PTCH altogether presented a novel oncogenic function of *DUXAP10* contributing not only to the initiation of the Hedgehog pathway but also augmenting the positive feedback loop within the pathway. Our RNA pull-down studies did not detect the interaction between *DUXAP10* and SHH, further studies

are needed to determine the mechanism by which *DUXAP10* up-regulates the protein levels of SHH and PTCH.

CD133 has been regarded as one of the stemness markers for various cancers, including lung cancer (Alama et al., 2015; Bertolini et al., 2009; Wu et al., 2014), and is one of the downstream targets of the Hedgehog pathway. Cd is a known carcinogen for lung cancer, yet there is no study discussing the relationship of Cd carcinogenesis and CD133 in lung cancer. In the present study, we first demonstrated that Cd promotes CD133 level through *DUXAP10* dysregulation in Cd-transformed cells. Moreover, CD133 positive cells among Cd-T cells could form significantly more spheres in the suspension culture than CD 133 negative cells, suggesting that CD133 is potentially a cell surface marker of the Cd-induced CSC-like population. This representative role of CD133 for the Cd carcinogenesis may serve as a predictive biomarker and potentially benefit prognostics and diagnostics for the lung cancer patients exposed to Cd.

While the studies of *DUXAP10* all focused on its oncogenic regulations, little is known about how *DUXAP10* expression level is upregulated. Pax6 is predicted as one of the putative transcription factors for *DUXAP10*. Here we provided the first evidence showing that Pax6 serves as a transcription factor for *DUXAP10*. Pax6 has been shown indispensable for neurodevelopmental processes, particularly for neuroectodermal epithelial tissues. Aberrant expression of Pax6 has been reported in various cancer types, including colon cancer, colorectal cancer, breast cancer, and lung cancer. However, Pax6's oncogenic role is debatable. Down regulation of Pax6 due to its promoter hypermethylation was

found significantly correlated to poorer prognosis and lower overall survival rate of NSCLC patients (Zhang et al., 2015). Kiselev et al. have elucidated that Pax6 acts as a tumor suppressor, given the significant correlation between high Pax6 level and longer disease-specific survival in NSCLC patients (Kiselev et al., 2018). On the contrary, several studies provided an opposite view toward the role of Pax6 in cancer. There were studies revealing that the level of Pax6 is positively correlated to tumor cell proliferation, migration, and invasion (Liu et al., 2020; Jiang et al., 2020; Qian et al., 2018). In addition, Ooki et al. reported that Pax6 is responsible for the cancer stem cell characteristics (Ooki et al., 2018). With these studies discussing the role of Pax6 in cancer cells, its role in heavy metal carcinogenesis has not been reported yet. The present study is the first one to show that the expression of Pax6 is elevated in the Cd transformed cells and that Pax6 acts as a transcription factor of *DUXAP10*. As we described the oncogenic role of Pax6 here, the mechanism underlying its overexpression would need to be further examined. However, Pax6 has been described to be upregulated due to Cd-induced oxidative stress in rat cerebellum model (P M et al., 2018). This could provide a direction for further study.

In summary, long term exposure to a low dose of Cd induces cell malignant transformation and CSC-like property. The evoked stemness is regulated by Pax6-up-regulated oncogenic lncRNA *DUXAP10*, which in turn activates the sonic hedgehog signaling pathway. This study shows an important role of *DUXAP10* for Cd-induced CSC-like property and tumorigenesis.

Table 2.1 Up-regulated oncogenic lncRNAs in Cd-transformed cells.

| LncRNA | Chromosomal location | Cancer type | binding partner(s)/associated signaling pathway | Regulation target (s) | Function(s) | References |
|---|---|---|---|---|---|---|
| LUCAT1 | 5q14.3 | papillary thyroid cancer | | CDK1, EZH2, p57, HDAC1, DNMT1, NRF2 | proliferation, invasion, cell cycle, oxidative stress, apoptosis | Luzon-Toro et al., 2019 |
| | | colorectal cancer | UBA52 | RPL40, p53 | cell cycle progression, apoptosis | Zhou et al., 2019 |
| | | glioma | miR-375 | | cell viability, invasion | Gao et al., 2018 |
| LINC00473 | 6q27 | head & neck squamous cell carcinoma | Wnt/β-catenin pathway | | proliferation, cell survival, radioresistance | Han P-B et al., 2018 |
| | | gastric cancer | | MMP2, MMP9 | migration, invasion | Zhang W, et al., 2018 |
| | | glioma | miR-195-5p; Hippo pathway | YAP/TEAD1 | proliferation, migration, invasion, cell survival | Wang et al., 2019 |
| | | breast cancer | p-CREB | CCND1 | proliferation | Shi et al., 2019 |
| | | glioma | miR-637 | CDK6 | proliferation, invasion,EMT | Zhang et al., 2019 |
| HOTAIRM1 | 7q15.2 | glioblastoma multiforme | G9a, EZH2, DNMTs | HOXA1 | proliferation, migration, invasion, cell survival | Li et al., 2018 |
| | | hepatocellular carcinoma | Wnt/β-catenin pathway | | proliferation, cell survival | Zhang et al., 2018 |
| | | thyroid cancer | | miR-148a, Wnt10 | proliferation, invasion | Li et al., 2021 |
| | | leukemia | | miR-148a, miR-152, miR0148b | proliferation, cell survival | Hu et al., 2019 |
| DUXAP10 | 14q11.2 | hepatocellular carcinoma | Wnt/β-catenin pathway, PI3K/Akt pathway | | proliferation, metastasis | Han et al., 2019 |
| | | chronic myeloid leukemia | | PTEN | proliferation, cell survival | Yao et al., 2018 |
| | | esophageal squamous carcinoma | EZH2 | p21 | cell cycle | Wang et al., 2018 |
| | | renal cell carcinoma | | cyclin D./E, CDK4, N-cadherin, vimentin | proliferation, migration, invasion | Chen et al., 2020 |

Table 2.2 Interaction probability between *DUXAP10* and GLI1, SHH, respectively.

| Interaction probabilities | DUXAP10-GLI1 | DUXAP10-SHH |
|---|---|---|
| Prediction-RF classifier | 0.8 | 0.65 |
| Prediction-SVM classifier | 0.99 | 0.97 |

*The predictions were performed on RPISeq powered by Iowa State University and based on Random Forest (RF) or Support Vector Machine (SVM) classifiers.
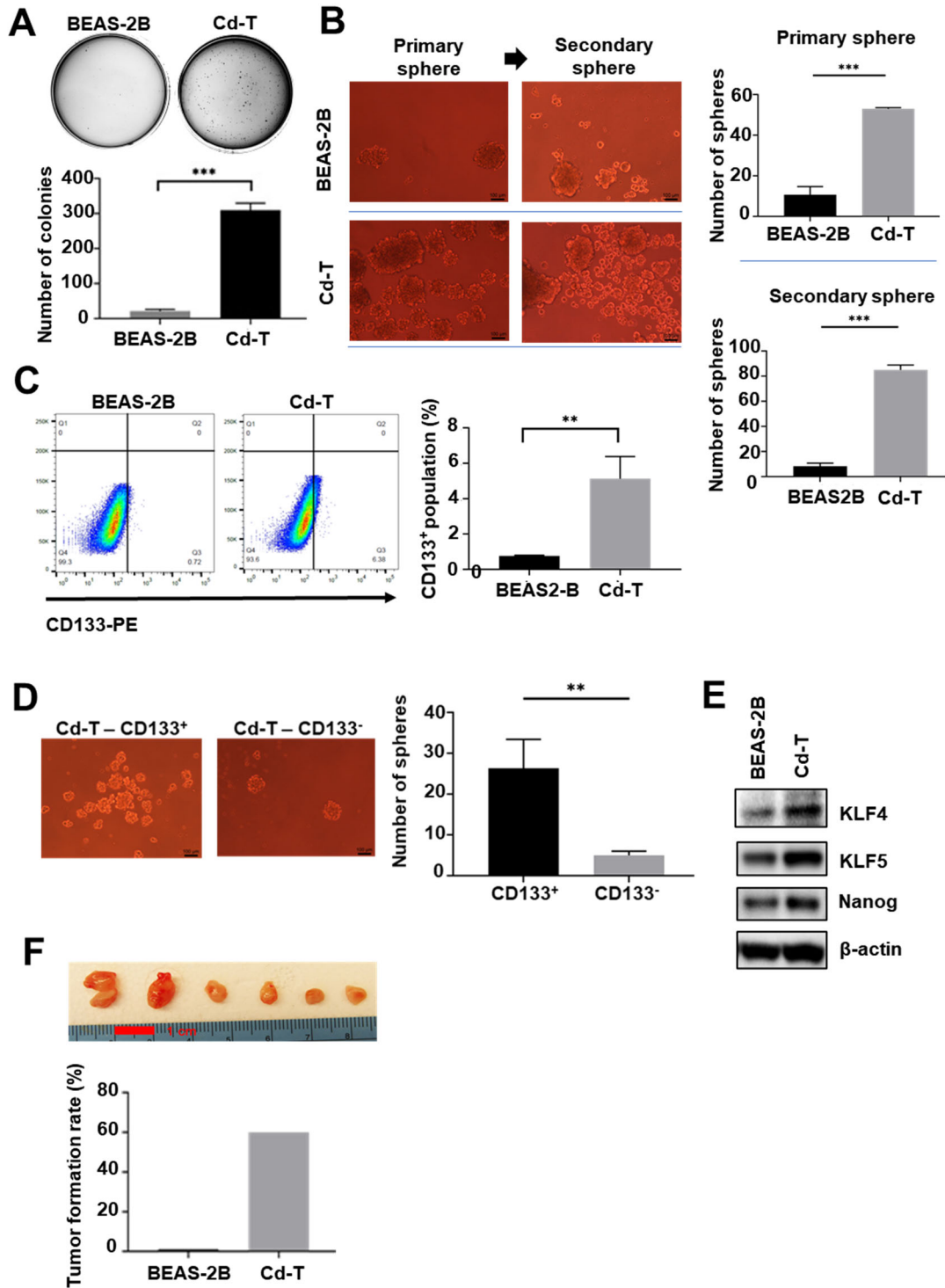
**Figure 2.1** Chronic exposure to a low dose of Cd induces CSC-like property and

tumorigenesis. (A) Representative images of soft agar colonies formed from the

passage-paired BEAS-2B cells and the Cd transformed BEAS-2B cells (Cd-T) (means ± SD, n=3), ***$p<$ 0.001. (B) Representative images of the first and the second generation of suspension spheres formed from the passage-paired BEAS-2B cells and Cd-T cells. Scale bar: 100 $\mu$m. The bar graph represents the average numbers of the spheres formed in the repeated assays (means ± SD, n=3), ***$p<$ 0.001. (C) Representative images of flow cytometry analysis of CD133 positive cells in the control BEAS-2B cells and Cd-T cells. The Bar graph shows the average percentage of CD133$^+$ population in each group (means ± SD, n=3), **$p<$ 0.01. (D) Representative images of suspension spheres formed from the FACS-sorted CD133$^+$ and CD133$^-$ Cd-T cells. Scale bar: 100 mm. The bar graph represents the average numbers of the spheres formed in the repeated assays (means ± SD), **$p<$ 0.01. (E) Representative Western blot analysis images of stemness marker levels in the control BEAS-2B and Cd-T cells. The assay was repeated, and similar results were obtained. (F) Nude mouse xenograft tumorigenesis study as described in Materials and Method (n=10).
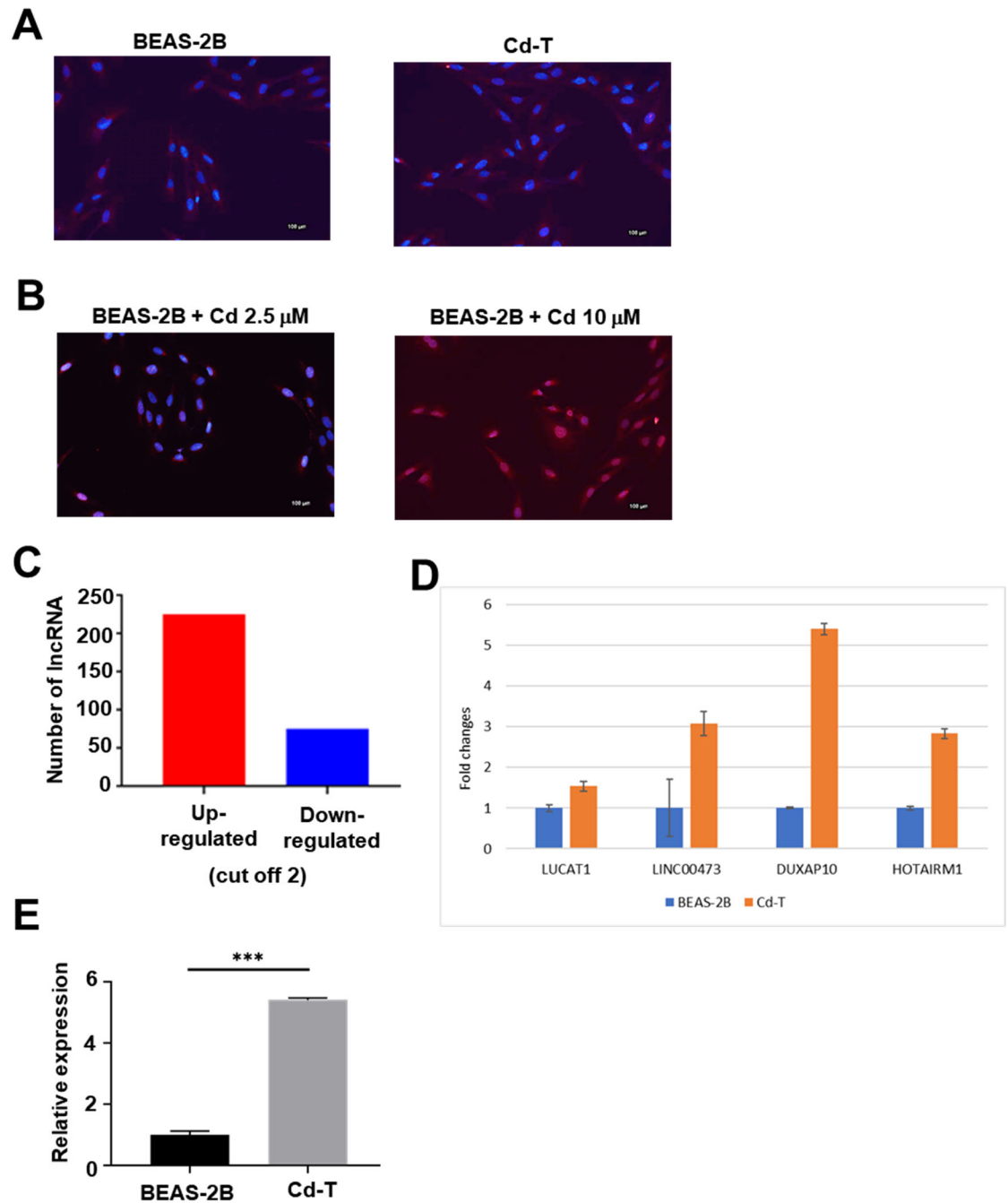
**Figure 2.2** Chronic exposure to Cd does not induce significant DNA damage but cause long non-coding RNA dysregulations. (A) Representative IF staining overlaid images of $\gamma$H2A.X in red fluorescence and DAPI in blue fluorescence from control BEAS-2B and Cd-T cells. Scale bar: 100 $\mu$m. (B) Representative IF staining

overlaid images of γH2A.X in red fluorescence and DAPI in blue fluorescence from

the BEAS-2B treated with Cd 2.5 μM or 10 μM, respectively. Scale bar: 100 μm.

(C) Microarray result shows 225 lncRNA upregulated and 75 lncRNA

downregulated (cut off 2). (D) Quantitative PCR analysis of the relative lncRNA

levels in control BEAS-2B and Cd-T cells. The RNA level in the Cd-T is expressed

relative to control BEAS-2B cells. (E) Quantitative PCR analysis of the relative

*DUXAP10* level in control BEAS-2B and Cd-T cells. The RNA level in the Cd-T is

expressed relative to control BEAS-2B cells (means ± SD, n=3), ***p< 0.001.
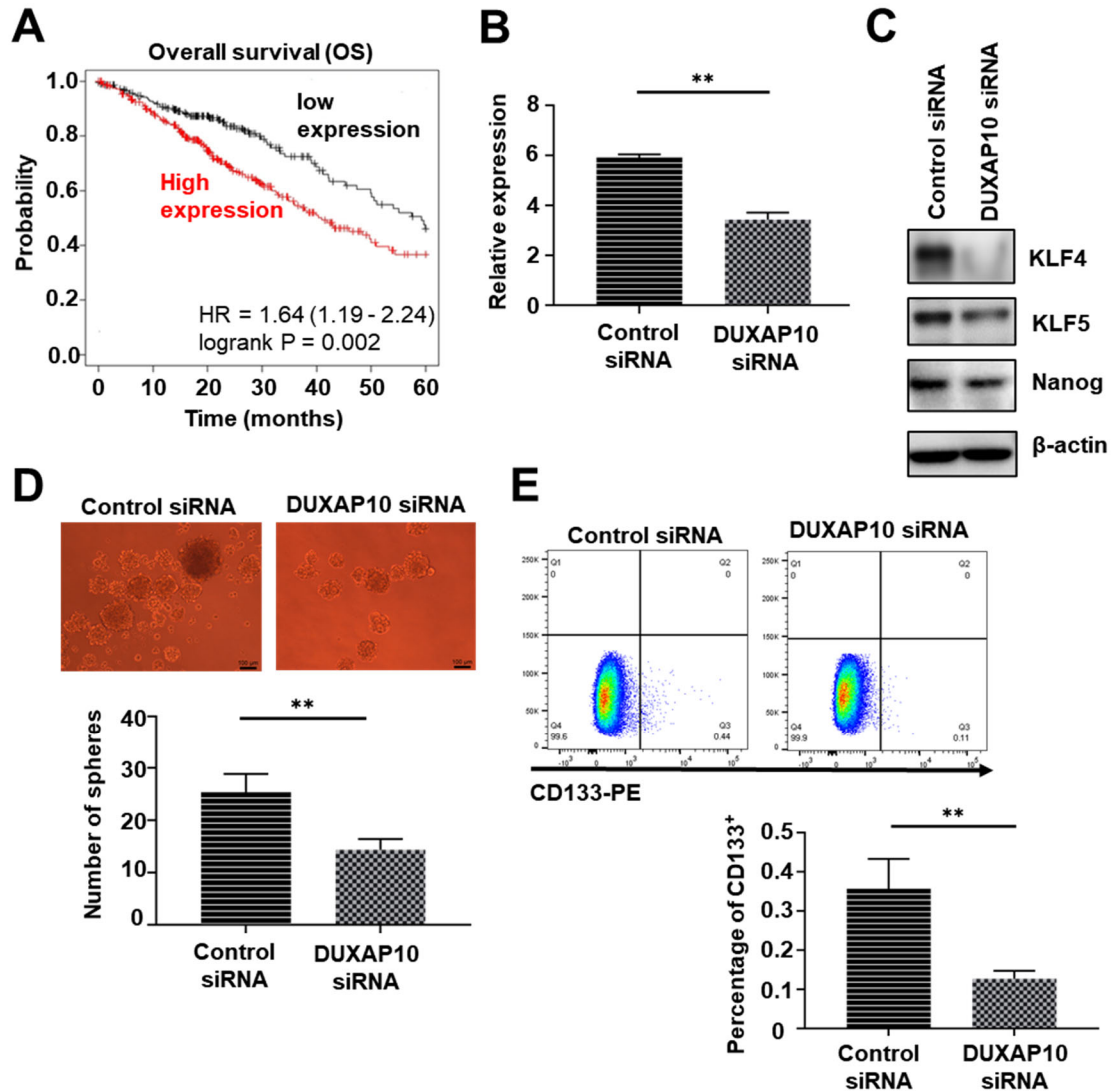
**Figure 2.3** Knockdown of *DUXAP10* in Cd-T cells significantly reduces their CSC-like property. (A) Kaplan-Meier plotter survival analysis revealed negative correlation between *DUXAP10* level and the overall survival rate, relapse-free survival rate in lung cancer patients. (B) Quantitative PCR analysis of the relative *DUXAP10* level in Cd-T cells transfected with control siRNA and the siRNA targeting *DUXAP10*. The RNA level in the Cd-T with *DUXAP10* knockdown is expressed relative to the control group (means ± SD, n=3), **p< 0.01. (C) Representative Western blot images of stemness marker levels in Cd-T cells

transfected with control siRNA or the siRNA targeting *DUXAP10*. The assay was repeated, and similar results were obtained. (D) Representative images of suspension spheres formed from Cd-T cells transfected with control siRNA or *DUXAP10* siRNA. Scale bar: 100 μm. The bar graph represents the average numbers of the spheres formed in the repeated assays (means ± SD, n=3), **$p<$ 0.01. (E) Representative images of flow cytometry analysis of CD133 levels in the Cd-T cells transfected with control siRNA or *DUXAP10* siRNA. The Bar graph shows the average percentage of CD133$^+$ population in each group (means ± SD, n=3), **$p<$ 0.01.
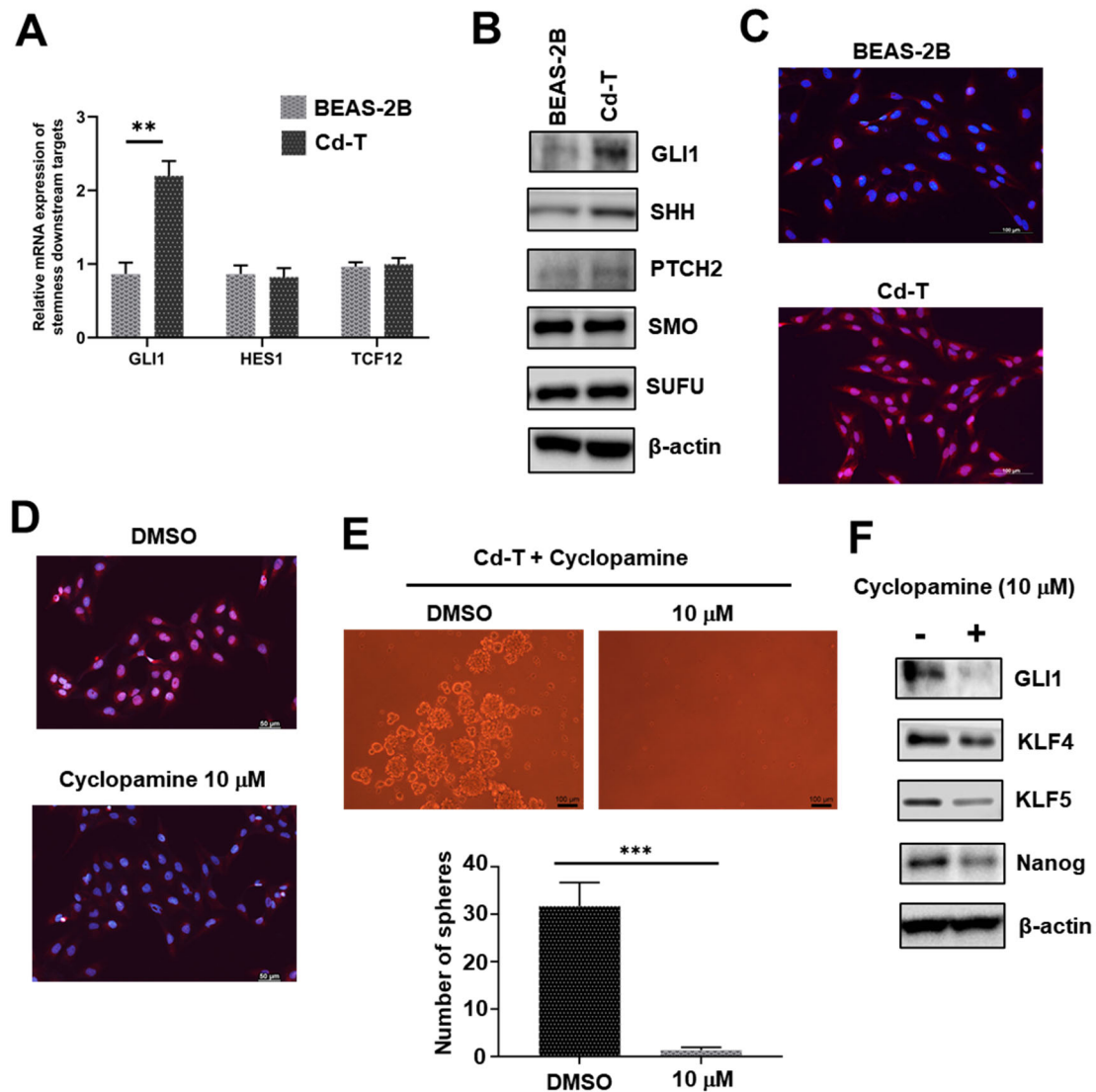
**Figure 2.4** The Hedgehog pathway is highly activated in Cd-T cells promoting their CSC-like property. (A) Quantitative PCR analysis of the relative levels of GLI1, HES1, TCF12 mRNA in control BEAS-2B and Cd-T cells. The mRNA levels in the Cd-T are expressed relative to the control group (means ± SD, n=3), **$p < 0.01$. (B) Representative Western blot images of the levels of GLI1, SHH, PTCH2, SMO, SUFU in control BEAS-2B and Cd-T cells. The assay was repeated, and similar results were obtained. (C) Representative IF staining overlaid images of GLI1 in

red fluorescence and DAPI in blue fluorescence from control BEAS-2B and Cd-T cells. Scale bar: 100 μm. (D) Representative IF staining overlaid images of GLI1 in red fluorescence and DAPI in blue fluorescence from Cd-T cells treated with DMSO (vehicle control) and cyclopamine (10 μM), respectively. Scale bar: 100 μm. (E) Representative images of suspension spheres formed from Cd-T cells treated with DMSO (vehicle control) or cyclopamine (10 μM), respectively. Scale bar: 100 μm. The bar graph represents the average numbers of the spheres formed in the repeated assays (means ± SD, n=3), ****$p$< 0.0001. (F) Representative Western blot images of the levels of GLI1, KLF4, KLF5, Nanog in Cd-T cells treated with DMSO (vehicle control) or cyclopamine (10 μM). The assay was repeated, and similar results were obtained.
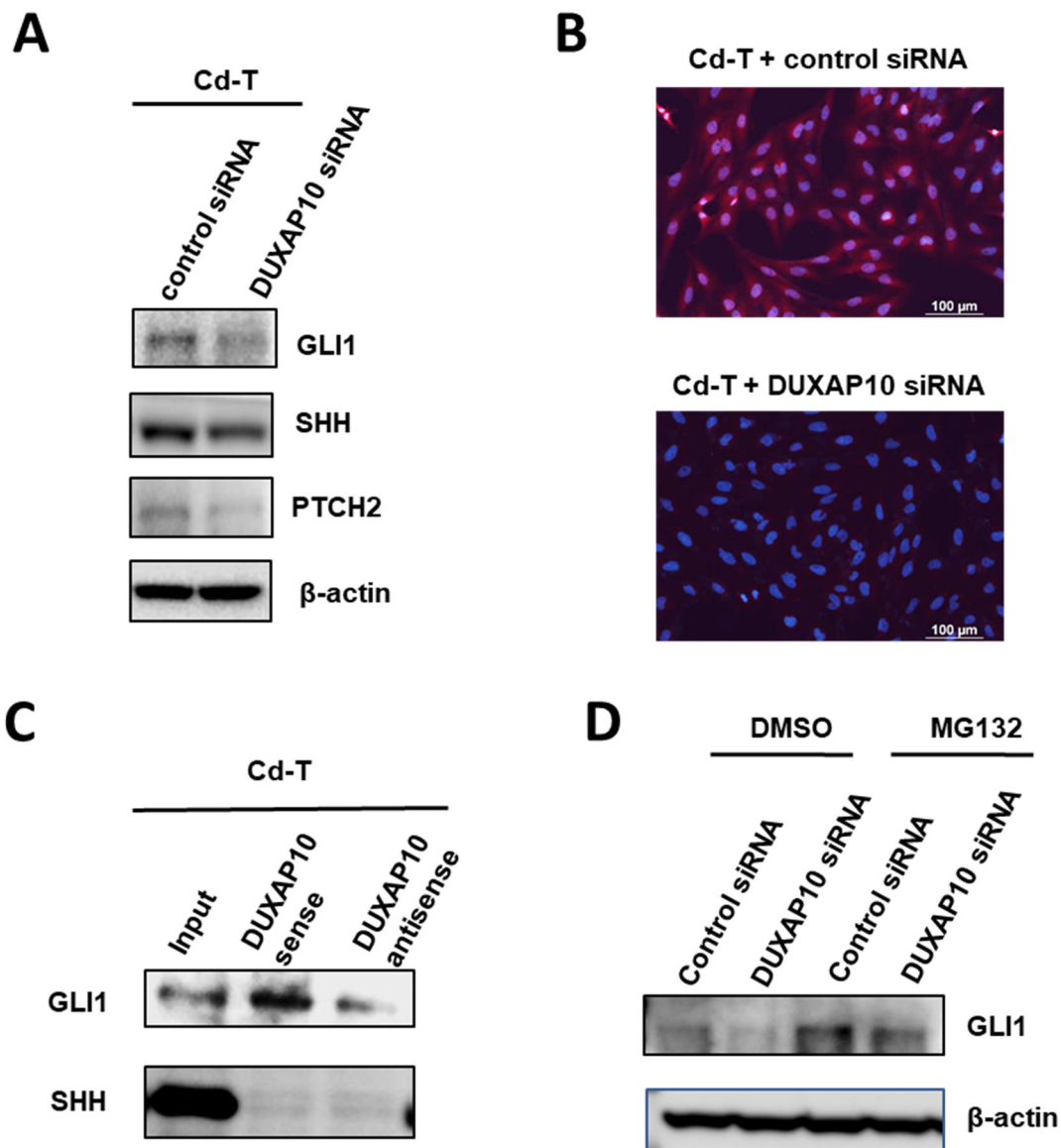
**Figure 2.5** Knockdown of *DUXAP10* inactivated the hedgehog pathway in Cd-T cells. (A) Representative Western blot images of the levels of GLI1, SHH, PTCH2 in Cd-T cells transfected with control siRNA or *DUXAP10* siRNA. The assay was repeated, and similar results were obtained. (B) Representative IF staining overlaid images of GLI1 in red fluorescence and DAPI in blue fluorescence from the Cd-T cells transfected with control siRNA or *DUXAP10* siRNA. Scale bar: 100 μm. (C)

Representative Western blot images of the levels of GLI1 and SHH in the Cd-T protein lysates applied to *DUXAP10*-sense and *DUXAP10*-antisense biotinylated RNA pull down, respectively. The assay was repeated, and similar results were obtained. (D) Representative Western blot images of the level of GLI1 in Cd-T cells transfected with control siRNA or *DUXAP10* siRNA and treated with 10 $\mu$M MG132 or a vehicle control DMSO, respectively. The assay was repeated, and similar results were obtained.
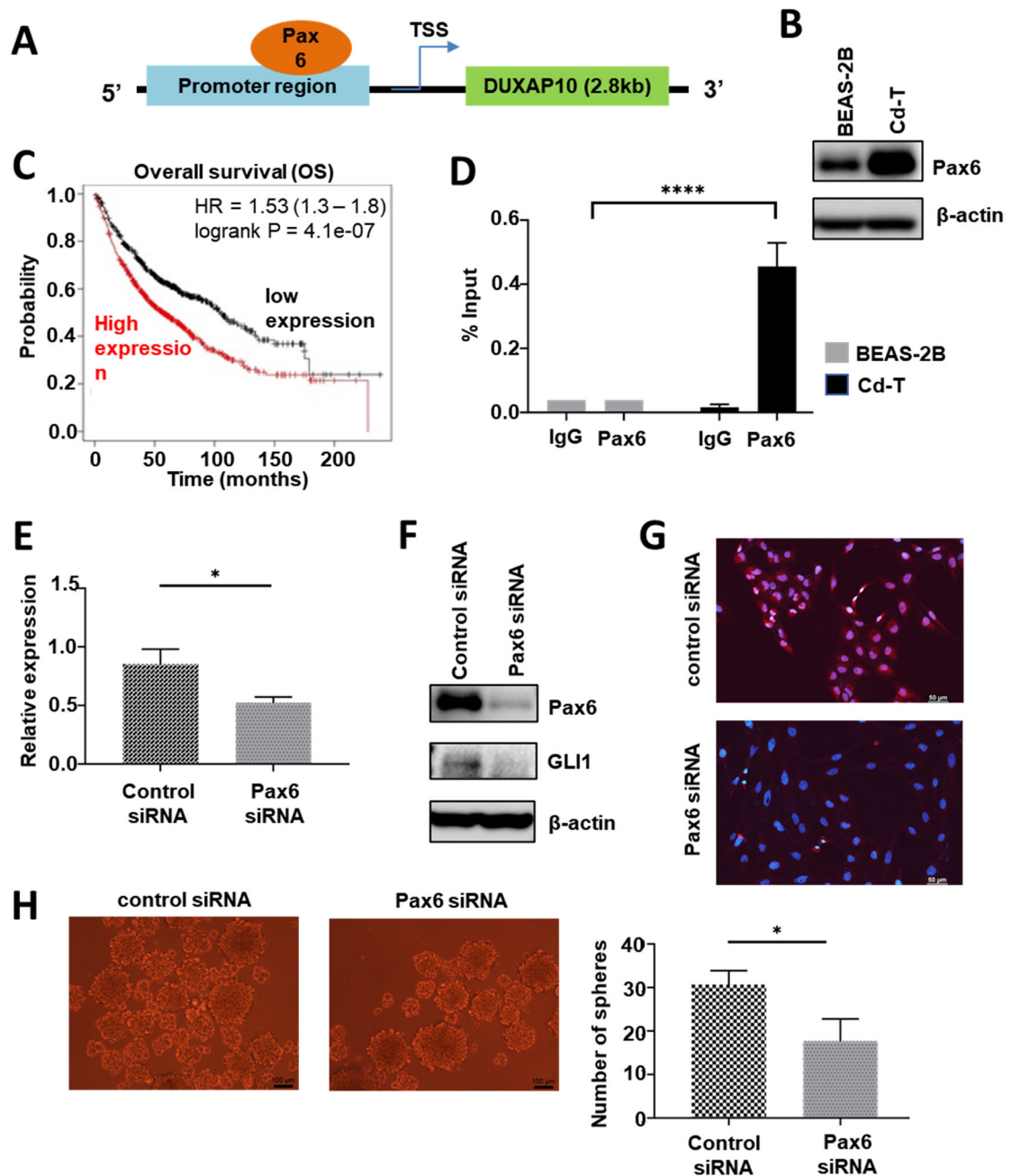
**Figure 2.6** Chronic Cd exposure increases the expression of Pax6 to upregulate *DUXAP10* level. (A) Schematic map shows that the putative binding site of Pax6 locates 3 kb upstream of the *DUXAP10* transcription start site, close to the 3' end of the promoter region. (B) Representative Western blot images of Pax6 level in control BEAS-2B and Cd-T cells. The assay was repeated, and similar results were

obtained. (C) Kaplan-Meier plotter survival analysis revealed negative correlation between the expression level of Pax6 and the overall survival rate in lung cancer patients. (D) ChIP qPCR analysis of relative level of *DUXAP10* promoter bound by Pax6 in control BEAS-2B and Cd-T cells. Rabit IgG was used as negative control. Percentage of input method was adopted to analyze the raw data. The repeated results are presented as means ± SD (n=3), ****$p$< 0.0001. (E) Quantitative PCR analysis of the relative level of *DUXAP10* in Cd-T cells transfected with control siRNA or siRNA targeting Pax6, respectively. The RNA level in the Cd-T with Pax6 knockdown is expressed relative to the control group (means ± SD, n=3), *$p$< 0.05. (F) Representative Western blot images of levels of Pax6 and GLI1 in Cd-T cells transfected with control siRNA or Pax6 siRNA, respectively. The assay was repeated, and similar results were obtained. (G) Representative IF staining overlaid images of GLI1 in red fluorescence and DAPI in blue fluorescence from the Cd-T cells transfected with control siRNA or Pax6 siRNA. Scale bar: 100 μm. (H) Representative images of suspension spheres formed from the Cd-T cells transfected with control siRNA or Pax6 siRNA. Scale bar: 100 μm. The bar graph represents the average numbers of the spheres formed in the repeated assays (means ± SD, n=3), *$p$< 0.05.
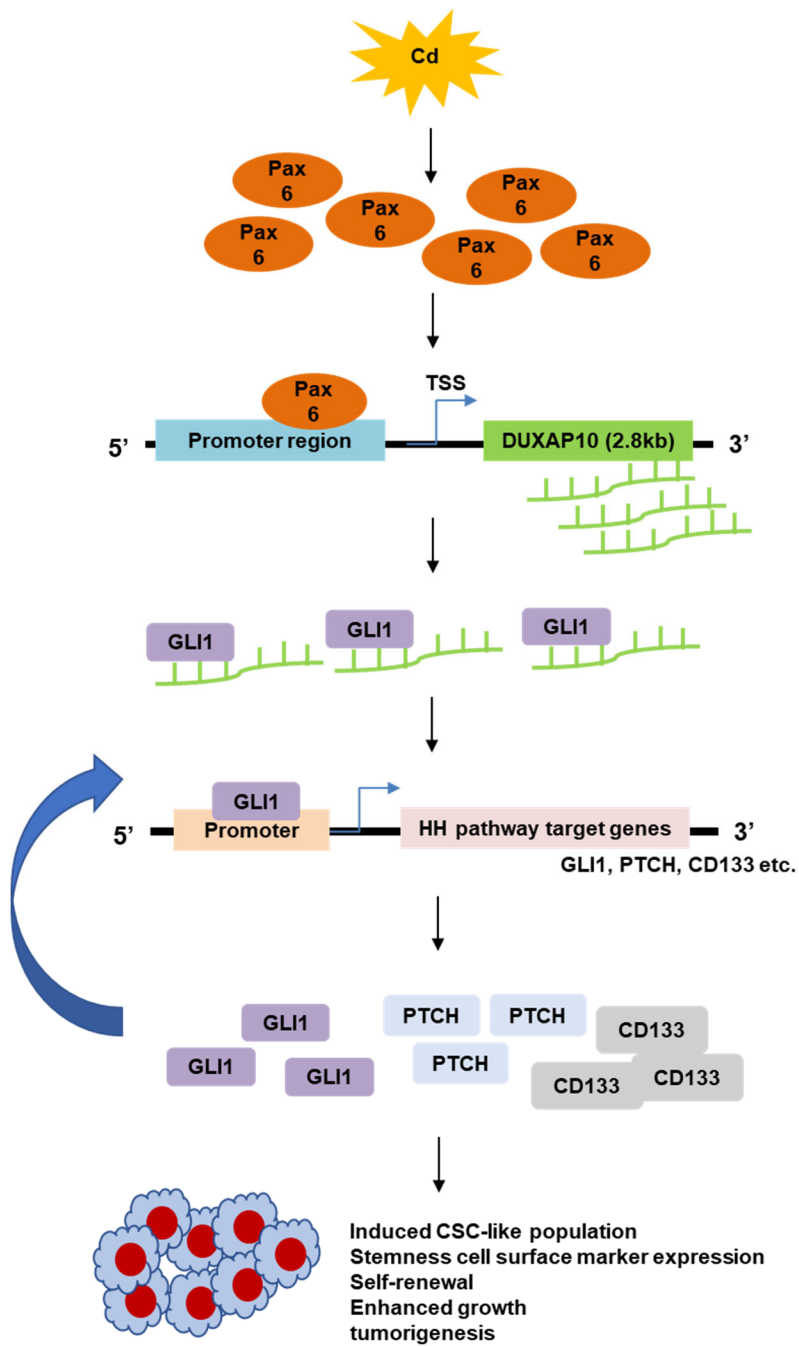
**Figure 2.7** A schematic summary of the mechanism of Cd-induced CSC-like property and tumorigenesis through *DUXAP10* dysregulation.

# CHAPTER 3. DOWN-REGULATION OF LONG NON-CODING RNA *MEG3* PROMOTES CHRONIC LOW DOSE CADMIUM EXPOSURE-INDUCED CELL TRANSFORMATION

## 3.1 ABSTRACT

Cadmium (Cd) is a toxic heavy metal and one of carcinogens that cause lung cancer. However, the exact mechanism of Cd carcinogenesis remains unclear. To investigate the mechanism of Cd carcinogenesis, we exposed human bronchial epithelial cells (BEAS-2B) to a low dose of Cd (2.5 $\mu$M, CdCl$_2$) for 9 months, which caused cell malignant transformation and generated cancer stem cell (CSC)-like cells. The goal of this study is to investigate the underlying mechanism. The long non-coding RNA (lncRNA) microarray analysis showed that the expression level of a tumor suppressive lncRNA maternally expressed 3 (*MEG3*) is significantly down-regulated in Cd-transformed cells, which is confirmed by further q-PCR analysis. Mechanistically, it was found that chronic Cd exposure up-regulates the levels of DNA methyltransferases (DNMTs), which increases the methylation of the differentially methylated region (DMR) 1.5 kb upstream of *MEG3* transcription start site to reduce *MEG3* expression. Functional studies showed that stably overexpressing *MEG3* in Cd-transformed cells significantly reduces their transformed phenotypes. Moreover, stably overexpressing *MEG3* in parental non-transformed human bronchial epithelial cells significantly impaired the capability of chronic Cd exposure to induce cell transformation and CSC-like property. Further mechanistic studies revealed that the cell cycle inhibitor p21 level is reduced and

retinoblastoma protein (Rb) phosphorylation is increased in Cd-transformed cells to promote cell cycle progression. In addition, Cd-transformed cells also expressed higher levels of Bcl-xL and displayed apoptosis resistance. In contrast, stably overexpressing *MEG3* increased p21 levels and reduced Rb phosphorylation and Bcl-xL levels in Cd-exposed cells and reduced their cell cycle progression and apoptosis resistance. Together, these findings suggest that *MEG3* down-regulation may play important roles in Cd-induced cell transformation and CSC-like property by promoting cell cycle progression and apoptosis resistance.

Key words: cadmium; carcinogenesis; epigenetics; long non-coding RNA; *MEG3*

## 3.2 INTRODUCTION

Lung cancer is the leading cause of cancer mortality around the world. The risk factors contributing to lung cancer could be gene mutations (Kosaka et al., 2004; Román et al., 2018; Gadepalli et al., 2014) or exposure to environmental carcinogens including toxicants in tobacco smoke (Kleinjans et al., 1993; Luo et al., 2011). Cadmium (Cd) is a toxic heavy metal and has been widely used in the production of paint and batteries. Other than industrial usage, cigarette smoke also contains a high level of Cd. Its prevalence in contaminated water, soil, and air represents a critical environment health concern. Cd has been listed as one of the carcinogens for lung cancer by International Agency for Research on Cancer (IARC). However, the exact mechanism of Cd carcinogenesis remains to be clearly defined.

Cd has been seen as a week mutagen, especially at low doses it is barely genotoxic (Misra et al., 1998; Waalkes, 2000). Hence, studies of its oncolytic effects have mostly focused on non-genotoxic modifications, such as epigenetic alterations. Aberrant DNA methylation caused by DNA methyltransferases (DNMTs) is a type of epigenetic dysregulations commonly found in carcinogenesis. In lung cancer, elevated DNMT activity has been shown associated with silence of tumor suppressors such as p16 and IRX1 (Küster et al., 2020; Liu et al., 2019). However, the role of dysregulated DNA methyltransferases (DNMTs) activity involved in Cd malignant effects remain ambiguous. Studies have shown that Cd exposure leads to an increase of DNMTs expression which results in silencing of tumor suppressor genes such as p16 and RASSF1A (Yuan et al., 2013; Benbrahim-Tallaa et al., 2007). On the other hand, it has also been shown that Cd exposure leads to a decrease of DNMTs expression which resulted in regional or global genomic hypomethylation in cancer cells (Ghosh et al., 2020; Iftode et al., 2021; Doi et al., 2011). Further studies on the role of dysregulated DNA methylation in Cd carcinogenesis is needed.

Long non-coding RNAs (lncRNAs) are a group of non-protein coding transcripts exceeding 200 base pairs. Often referred as pseudogenes, this type of transcripts are found to have various biological functions, including regulations of DNA replication, gene transcription, and post-transcriptional modifications. In cancers, lncRNAs could function as either oncogenic or tumor suppressive. Abnormal lncRNA expressions and activities have been reported associated with cancer development and progression. LncRNA *MEG3* (Maternally expressed 3) is

an imprinted pseudogene expressed by the maternal allele on human chromosome 14q32 (Han et al., 2015; Budkova et al., 2020). In various cancer types, *MEG3* has been shown to be downregulated, which favors proliferation and survival of cancer cells (Zhang et al., 2019; Wu et al., 2019; Dan et al., 2018). In metal carcinogenesis, so far nickel is the only one that has been shown to decrease the expression of *MEG3*, in turn leading to cell malignant transformation (Zhou et al., 2017). However, it is unknown whether Cd and other metal carcinogen exposures downregulate *MEG3* expression and whether *MEG3* downregulation plays an important role in other metal carcinogenesis.

To investigate the mechanism of Cd carcinogenesis, we continuously exposed human bronchial epithelial cells (BEAS-2B) to a low dose of Cd (2.5 $\mu$M, CdCl$_2$) for 9 months, which caused cell malignant transformation and generated cancer stem cell (CSC)-like cells. The goal of this study is to investigate the underlying mechanism focusing on the role of Cd exposure caused *MEG3* dysregulation.

## 3.3 MATERIALS AND METHODS

### 3.3.1 Cell culture and generation of MEG3 stably expressing cells

Immortalized human bronchial epithelial BEAS-2B cell line was purchased from America Type Culture Collection (ATCC, Manassas, VA). BEAS-2B cells were exposed to 2.5 $\mu$M of CdCl$_2$ (Sigma-Aldrich) or a vehicle control (H$_2$O) for 9 month to generate Cd-transformed BEAS-2B cells (Cd-T) and the passage-paired BEAS-

2B control cells (BEAS-2B). All cells were cultured in Dulbecco's Modified Eagle Medium (DMEM) (Thermo Fisher, MA) supplemented with 5% fetal bovine serum (FBS) and 1% Penicillin-Streptomycin (P/S). To generate *MEG3* stable expressing cells, the lentiviral particles purchased from Transomic Technologies (Huntsville, AL) for the vector control and *MEG3* overexpression were transduced into the parental BEAS-2B cells at early passage or Cd-transformed BEAS-2B cells (Cd-T cells). After 48 h of puromycin (1 $\mu$g/mL) selection following the procedure described in our previous study (Humphries et al., 2017), the cells were harvested and *MEG3* overexpression was confirmed by quantitative PCR (q-PCR).

### 3.3.2 Cell transformation by chronic exposure of MEG3 stably expressing parental BEAS-2B cells to cadmium (CdCl$_2$)

The chronic cell transformation was performed following our published procedure (Wang et al., 2011). Briefly, the generated *MEG3* stably overexpressing parental BEAS-2B cells (BEAS-2B-*MEG3*) and the parental BEAS-2B cells with control vector (BEAS-2B-vector) were continuously exposed to a vehicle control (H$_2$O) or 2.5 $\mu$M of CdCl$_2$ (Sigma-Aldrich). When reaching about 80-90% confluence after exposure, cells were sub-cultured. Cd was freshly added to cells each time after overnight cell attachment. Soft agar colony formation assay was performed after every 4-week Cd exposure to assess cell transformation. This process was repeated for 9 months (38 weeks).

### 3.3.3 Anchorage-independent soft agar colony formation

The soft agar colony formation assay was carried out in 60 mm cell culture dishes for each group as previously described (Yang et al., 2005). Briefly, cultured cells were collected by trypsinization and suspended in DMEM containing 10% FBS at density of $0.25 \times 10^4$ cells/mL. Normal melting point agarose (4 mL of 0.6% agarose in DMEM containing 10% FBS) was placed into each 60 mm cell culture dish as the bottom layer. After solidification, 4 mL of cell mixture consisting of 2 mL of cell suspension and 2 mL of 0.8% low melting point agarose in DMEM containing 10% FBS were poured over the bottom layer agarose. After solidification of the upper layer, 3 mL of DMEM containing 10% FBS was added, and dishes were incubated at 37℃ in cell incubator with 5% $CO_2$. After 4-week incubation, colonies formed in the agarose dishes were stained with 0.003% crystal violet, photographed and counted.

### 3.3.4 Serum-free suspension culture for sphere formation

The spheroid formation assay was performed following the published protocol (Dontu et al., 2003) with minor modifications. Briefly, single cells were plated in ultra-low attachment 24-well culture plates (Corning, NY) at a density of $2 \times 10^3$ cells per well suspended in serum-free DMEM containing human recombinant basic fibroblast growth factor (bFGF, 20 ng/mL) (R&D, Minneapolis, MN), human recombinant epidermal growth factor (EGF, 20 ng/mL) (R&D, Minneapolis, MN), B27 (Invitrogen, Carlsbad, CA) and heparin (4 $\mu$g/mL, Sigma-Aldrich). Plates were

incubated at 37℃ in cell incubator with 5% $CO_2$. Spheres > 50 μm were viewed, photographed and counted under a phase-contrast microscope after 10-day culture.

### 3.3.5 Western blot

Cells were lysed using lysis buffer following our published protocol (Yang et al., 2006; Wang et al., 2014). The cell lysates were then applied to the bicinchoninic acid assay (Bio-rad) to determine protein concentration, followed by SDS-polyacrylamide gel electrophoresis (PAGE) (20-30 μg of protein/lane). The separated proteins were then transferred to polyvinylidene fluoride membrane (PVDF, Millipore, MA). Five percent milk in PBS was applied for the blocking step before primary antibody incubation. The following primary antibodies were used: anti-DNMT1, anti-DNMT3A, anti-DNMT3B, anti-phospho-Rb (S780), anti-phospho-Rb (S807/811), anti-Rb, anti-E2F1, anti-p21, anti-Mcl-1, anti-Bcl-xL, anti-Puma, anti-Bim, anti-Bik, anti-Bid, anti-Bax, anti-Bad, anti-cleaved caspase 3, anti-caspase 3, anti-cleaved PARP, anti-PARP (Cell Signaling Technology, Beverly, MA) (dilution 1:1000); and anti-β-actin (Millipore Sigma, St. Louis, MO) (dilution 1:8000). After overnight primary antibody incubation at 4 °C, the membranes were washed and then incubated with HRP-conjugated antibodies for 1 h at room temperature. Images were developed by Amersham Imager 680 (GE Healthcare Life Sciences, MA).

*3.3.6 The lncRNA microarray analysis*

The passage-paired BEAS-2B control and Cd-transformed cells were used for total RNA extraction using the TRIzol reagent following the manufacturer's protocol (Invitrogen, CA). The resulted total RNA samples were provided to Arraystar Inc. (Rockville, MD) for the lncRNA microarray analysis. The array results were deposited to the National Center for Biotechnology Information (NCBI)'s data repository (Access ID: GSE175472).

*3.3.7 Bisulfite conversion and pyrosequencing for DNA methylation analysis*

Genomic DNA was extracted from cultured cells following the manufacturer's procedure (DNeasy® Blood & Tissue Kit, Qiagen) and digested by HindIII (NEB). Bisulfite conversion was then carried out using 1 $\mu$g of digested DNA according to the manufacturer's instructions (EZ DNA Methylation-Lightning kit, Zymo Research). Converted DNA was applied to the following PCR with the primer designed on Bisulfite Primer Seeker (http://bpsbackup.zymoresearch.com) powered by Zymo Research. PCR was performed using ZymoTaq PreMix with the following program: (1) 95°C 10 min; (2) 95°C 30 sec; (3) annealing temperature (depending on the primer pair) 40 sec; (4) 72°C 45 sec; (5) repeat steps 2-4 for 40 cycles; (6) 72°C 7 min. Gel-purified PCR products were applied to blunt-end modification using Ent-It-DNA End-Repair kit (Epicentre, Charlote, NC), followed by subcloning into pUC19 vector. Primers set 1: (Forward) ATGTTTTTGTGGGGTTGTAG; (Reverse)

TAACCACAATATTAATAACTAAAAAACA. Primer set 2: (Forward) GAATGYGAGTTTTTTGTTAATG; (Reverse) CTTACACAACAAAAACRCCC. Ten to fifteen clones from each PCR product were sequenced (University of Chicago Comprehensive Cancer Center DNA Sequencing and Genotyping Facility). Raw data analysis was performed using BiQ Analyzer to determine the percentage of converted cytosine residues at specific CpG sites in the sequence.

### 3.3.8. MTT assay

Thiazolyl Blue Tetrazolium Bromide (MTT) was purchased from Sigma-Aldrich (St Louis, MO). The assay was performed as described previously (Wang et al., 2014). Briefly, cells were seeded into 96-well plates ($10^3$ cells/well in 100 $\mu$L of culture medium) for 4 time points: 0, 24, 48, and 72 h. At the end of incubation, 50 $\mu$L of the MTT reagent (5 mg/mL) was added to each well and incubated for 4 h, followed by another 1 h incubation with 200 $\mu$L of dimethyl sulfoxide (DMSO). The plate was read using a microplate reader (SpectraMaxi3x, Molecular Devices, Sunnyvale, CA) at the wavelength of 570 nm. The inhibition on relative cell growth was determined by the following formula: Cell Viability (%) = (Absorbance at 570 nm of SOCS3 overexpressing cells)/ (Absorbance at 570 nm of control cells) ×100.

### 3.3.9 Cell cycle analysis

Cell cycle synchronization was first carried out by maintaining the cells in serum-free medium for 24 h. In 24 h, the cells re-enter the cell cycle by resuming normal

culture condition with serum. After 24 h of incubation, the cells were harvested and suspended in 70% ethanol and placed at 4 °C for 2 h. Then cells were proceeded to Propidium iodide (PI) staining (20 $\mu$g/mL of PI, 200 $\mu$g/mL of RNase A, 0.1% Triton X-100), followed by flow cytometry analysis performed by cytometer BD LSRII (Becton Dickinson). The acquired data were further analyzed by ModFit LT software.

### 3.3.10 Quantitative PCR

Total RNA extraction was performed by TRIzol reagent following the manufacturer's instruction (Invitrogen, CA). Quality and Quantity of extracted RNA was determined by NanoDrop$^{TM}$ spectrophotometer (Thermo Fisher, MA) before applying to TaqMan gene expression assays. Quantitative PCR was performed by ABI QuantStudio 3 qPCR System (Applied Biosystems). The $2^{-\Delta\Delta}$ ct analysis method was utilized to quantify relative RNA expression levels of each gene, with human 18S RNA as the internal control.

### 3.3.11 RNA interference

Cells were seeded into 6-well plates or 60 mm dishes (Corning) 24 h before transfection in DMEM supplemented with 5% FBS and 1% P/S. Before transfection, the culture medium was refreshed with serum-free DMEM. siRNA was then transfected using Lipofectamine 3000 (Invitrogen) according to the manufacturer's protocol. Four hours after, equal volume of DMEM with 10% FBS

and 1% P/S was added to the plates/dishes. The cells would be ready for further analysis in 48 h.

### 3.3.12 Statistical analysis

The statistical analyses for the significance of differences in presented numerical data (mean ± SD) were carried out by testing different treatment effects using two-tailed t-tests for comparison of two data sets. A *p*-value of < 0.05 was considered statistically significant.

## 3.4 RESULTS

### 3.4.1 *MEG3* is down-regulated and DNMTs are up-regulated in cadmium-transformed cells and inhibition of DNMTs increases *MEG3* expression levels and reduces their transformed phenotypes

To study the mechanism of Cd carcinogenesis, we performed the lncRNA microarray analysis in Cd-transformed cells and the passage-matched control cells. It was found that the most significantly down-regulated (almost undetectable) tumor suppressive lncRNA in Cd-transformed cells is *MEG3* which was confirmed by further q-PCR analysis (**Figure 3.1A**). MTT analysis revealed that Cd-transformed cells (Cd-T cells) grow significantly faster than the passage-pair BEAS-2B control cells (**Figure 3.1B**). Western blot analysis showed that Cd-T cells have higher expression levels of DNA methyltransferases (DNMTs), including

DNMT1, DNMT3A, and DNMT3B (**Figure 3.1C**). As shown in others' studies, *MEG3* downregulation in cancer cells was often due to hypermethylation of its promoter region (Dong et al., 2017; Guo et al., 2017; Ding et al., 2019). Here, as we observed elevated levels of the DNMTs, we next treated the Cd-T cells with a DNMT inhibitor 5-Aza-2-deoxycytidine (5-Aza). Q-PCR analysis revealed that 5-Aza treatment significantly increases the expression levels of *MEG3* in Cd-transformed cells (**Figure 3.1D**). Moreover, MTT analysis showed that inhibition of DNMTs by 5-Aza treatment dose-dependently reduces the proliferation of Cd-T cells (**Figure 3.1E**). Treating the cells with 5-Aza also effectively reduced colony formation in the anchorage-independent soft agar assay, as the colony number in the group dropped almost 90 percent, compared to the vehicle control (DMSO)-treated group (**Figure 3.1F**). Furthermore, serum-free suspension culture sphere formation assay showed that inhibition of DNMTs also significantly decreases sphere formation by Cd-T cells (**Figure 3.1G**).

3.4.2 The differentially methylated region upstream of *MEG3* transcription start site is highly methylated in Cd-transformed cells

To further determine the mechanism that contributes to chronic Cd exposure-caused downregulation of *MEG3*, we next examined methylation status of the CpG island containing 30 CpGs about 1.5 kb upstream of *MEG3* by performing bisulfite-conversion and sequencing (**Figure 3.2A**). *MEG3* is an imprinted pseudogene which under normal conditions, the paternal allele is methylated to remain off, while the maternal allele is much lower in methylation to

70

allow for the expression of the lncRNA. However, in cancers *MEG3* has been found to be downregulated from hypermethylation in the promoter. Here We found that in the Cd-T cells there is an hypermethylation across the CGI – 98% Cd-T to 65% passage-matched BEAS-2B control cells (**Figure 3.2B**, right). We also highlight 15 CpG sites that had a significant increase in methylation of at least 18% (p<0.05) (**Figure 3.2B**, left). These sites that are hypermethylated, in combination with the DNMT expression, could lead to the downregulation of *MEG3* in the Cd-T cells.

3.4.3 Stably overexpressing *MEG3* in Cd-transformed cells significantly reduces their transformed phenotypes

While 5-Aza treatment significantly increased *MEG3* expression levels in Cd-transformed cells and reduced their proliferation, soft agar colony and suspension culture sphere numbers, these results only suggest a negative co-relationship between *MEG3* expression levels and the extent of malignant behaviors of Cd-transformed cells. To further determine the contribution of *MEG3* down-regulation to the malignant behaviors of Cd-transformed cells, we next used a genetic approach to stably overexpress *MEG3* in Cd-transformed cells. Successful generation of *MEG3* overexpression and vector control cells were confirmed by q-PCR analysis. **Figure 3.3A** shows that the lentiviral infection increased the *MEG3* expression level by 2 folds in Cd-transformed cells. The MTT assay showed that enforced expression of *MEG3* reduces Cd-T cell proliferation, compared to the vector-control cells (**Figure 3.3B**). Anchorage-independent soft agar assay results demonstrated significantly reduced colony formation in Cd-T

with *MEG3* expression (**Figure 3.3C**). Moreover, stable expression of *MEG3* also significantly decreased suspension culture sphere formation in Cd-T cells, compared to the Cd-T vector control cells (**Figure 3.3D**).

### 3.4.4 Stably overexpressing *MEG3* in parental non-transformed BEAS-2B cells significantly reduces the capability of chronical low dose of Cd exposure to induce cell transformation and CSC-like property

Next, we would like to further examine whether overexpression of *MEG3* in parental non-transformed cells could reduce cell transformation induced by chronic low dose exposure of Cd. We first stably overexpressed *MEG3* in parental BEAS-2B cells (BEAS-2B-*MEG3*) and generated vector control BEAS-2B cells (BEAS-2B-vector) as well. Before initiating chronic exposure of Cd at low dose (2.5 $\mu$M, CdCl$_2$), *MEG3* overexpression was confirmed by the q-PCR analysis (**Figure 3.4A**). MTT assay showed that *MEG3* overexpression does not significantly affect cell proliferation before Cd exposure (**Figure 3.4B**). After 9 months of Cd exposure, the expression level of *MEG3* was examined again. The q-PCR result showed that after the long term Cd exposure process, the level of *MEG3* in *MEG3* overexpression cells was decreased, but still maintained at 2.5 fold higher than the vector control cell group (**Figure 3.4C**). In the MTT assay BEAS-2B *MEG3* overexpression cells with Cd exposure (BEAS-2B *MEG3*-Cd) displayed significantly slower cell proliferation, compared to BEAS-2B vector control cells with Cd exposure (BEAS-2B vector-Cd cells) (**Figure 3.4D**). In addition, BEAS-2B vector-Cd cells displayed enhanced colony formation capacity like Cd-T cells in

soft agar assay, while BEAS-2B *MEG3*-Cd cells showed only limited colony formation (**Figure 3.4E**). Moreover, we examined the CSC-like property in the Cd-exposed cells by serum-free suspension culture. BEAS-2B vector-Cd cells were found to form around 2 times more spheres than the BEAS-2B *MEG3*-Cd cells (**Figure 3.4F**). These results suggested the importance of *MEG3* to inhibit cell transformation and CSC-like property induced by chronic Cd exposure.

3.4.5 LncRNA *MEG3* reduces cell cycle progression by regulating the levels of cell cycle proteins

Next, we determined the mechanism of how Cd exposure affect cell proliferation. We first analyzed cell cycle progression in control, Cd-transformed cells, BEAS-2B vector-Cd and BEAS-2B *MEG3*-Cd cells by flow cytometry. **Figure 3.5A** shows that more Cd-transformed cells stayed in the S phase but less in the G1 phase, and vice versa in the passage-matched control BEAS-2B cells, indicating that Cd-T cells were actively undergoing cell proliferation. However, this trend was reversed by the overexpression of *MEG3*. After 9 months of Cd exposure, while the vector control cells (BEAS-2B vector-Cd) demonstrated active cell cycle progression, the *MEG3* overexpression cells (BEAS-2B *MEG3*-Cd) displayed halted cell cycle, given that more of its subpopulation stayed in the G1 phase but less in the S phase (**Figure 3.5B**). The levels of some cell cycle related proteins were further examined. By comparing BEAS-2B control cells and Cd-T cells, it was found that phospho-Rb proteins (S780, S807/S811), total Rb protein, and E2F1 were upregulated in Cd-T cells, but p21 in Cd-T cells was downregulated

73

(**Figure 3.5C**). Such trend of regulations was also found in BEAS-2B vector-Cd cells, while in BEAS-2B *MEG3*-Cd cells, phospho-Rb proteins, total Rb protein, and E2F1 were decreased and p21 was elevated (**Figure 3.5D**). These results demonstrated that *MEG3* inhibited cell proliferation by regulating the levels of important cell cycle-related proteins.

3.4.6 LncRNA *MEG3* reverses Cd exposure-induced apoptosis resistance by reducing the level of Bcl-xL

Apoptosis resistance has also been shown to be associated with cancer stemness (Kruyt et al., 2010; Safa, 2016). Next, we examined whether Cd-transformed cells display apoptosis resistance. We first screened the levels of proteins related to apoptosis in passage-paired BEAS-2B control cells and Cd-transformed cells, including anti-apoptotic proteins Mcl-1 and Bcl-xL, and pro-apoptotic proteins Puma, Bim, Bik, Bid, Bax, and Bad. Among these proteins, the anti-apoptotic protein Mcl-1 and Bcl-xL were found upregulated in Cd-transformed cells (**Figure 3.6A**). With *MEG3* overexpression, Bcl-xL level was found largely suppressed after 9 month of Cd exposure to the cells (**Figure 3.6B**). Interestingly, *MEG3* expression had no effect on the level of Mcl-1, given that the protein levels in BEAS-2B vector-Cd and BEAS-2B *MEG3*-Cd remained almost the same (**Figure 3.6B**).

To determine whether Cd-transformed cells developed apoptosis resistance, we treated the passage-paired BEAS-2B control cells and Cd-T cells

with a higher concentration of Cd (5 $\mu$M, $CdCl_2$). Previously, several studies have reported that Cd-induced apoptosis could be evidenced by increased levels of cleaved caspase 3 and cleaved PARP (Zhao et al., 2015; Liu et al., 2016; Ou et al., 2021). While the treatment of this high concentration of Cd increased the levels of cleaved caspase 3 and cleaved PARP in the passage-paired BEAS-2B control cells, no significant cleavage of these apoptotic proteins was observed in Cd-T cells (**Figure 3.6C**), suggesting that Cd-transformed cells display apoptosis resistance. Next, we treated BEAS-2B vector-Cd and BEAS-2B *MEG3*-Cd cells with Cd at 5 $\mu$M or a pan-Bcl-2 family inhibitor ABT 737 at 1.25 $\mu$M. For both treatments, elevated levels of cleaved caspase 3 and accordingly decreased total caspase 3 were observed in BEAS-2B *MEG3*-Cd cells, while in BEAS-2B vector-Cd cells only minor cleavage of caspase 3 was shown and accompanied by higher levels of total caspase 3 (**Figure 3.6D**). These results suggest that stably overexpressing *MEG3* reverses chronic Cd exposure-induced apoptosis resistance. Finally, we further determined the role of the anti-apoptotic protein Bcl-xL in Cd-induced apoptosis resistance. Cd-T cells were first transfected with a control siRNA (control si) or the siRNA targeting Bcl-xL (Bcl-xL si), then treated with 5$\mu$M of Cd or 1.25 $\mu$M of ABT 737. For both treatments, we observed increased levels of cleaved caspase 3 in Cd-T cells with Bcl-xL knockdown (**Figure 3.6E**). Together, these results suggested that *MEG3* overexpression suppresses Cd-induced cell transformation and CSC-like property is likely through reducing Cd-induced Bcl-xL expression.

## 3.5 DISCUSSION

Cd has been listed as one of the carcinogens for lung cancer. However, the mechanism of Cd carcinogenesis has not been clearly defined. As Cd has been shown a weak mutagen, it has been speculated that its oncolytic effect is non-genotoxic, and studies of Cd carcinogenesis have focused on its non-genotoxic effects such as epigenetic modifications. Cd has been shown to induce oxidative stress (Kiran Kumar et al., 2016; Al Olayan et al., 2020). It has also been shown that Cd-induced oxidative stress leads to aberrant DNA methylation (Wu and Ni, 2015). Aberrant DNMT activity has been revealed to be associated with Cd toxicity, in which DNMT downstream targets include glucose transporter 3 (GLUT3), tumor suppressors RASSF1A and p16 (Benbrahim-Tallaa et al., 2007; Yuan et al., 2013; Xu et al., 2016). In addition, it has been shown that the elevated DNMT led to silencing of several DNA repair genes, such as hOGG1, hMSH2, ERCC1, and XRCC1 (Zhou et al., 2012). In the present study, we first determined that elevated DNMT activity induced by Cd exposure led to downregulation of tumor suppressive lncRNA *MEG3*, as well as abnormal cell proliferation and the induced CSC-like property. Further assays by restoring *MEG3* expression demonstrated reversed malignant effects, such as reduced cellular anchorage-independent growth and the CSC-like property. Further investigations show that *MEG3* regulates the levels of key cell cycle proteins and apoptotic proteins. Our study presents the first evidence demonstrating that DNMT-mediated *MEG3* down-regulation plays an important role in Cd-induced cell transformation and CSC-like property (Fig. 7A).

Previous studies have shown different mechanisms of *MEG3* silencing in cancers. Han et al. and Qin et al. have reported histone methyltransferase EZH2-mediated H3K27 enrichment at the *MEG3* promoter region, resulting in silencing of this lncRNA (Han et al., 2020; Qin et al., 2020). On the other hand, DNA hypermethylation of the *MEG3* promoter has also been discovered in retinoblastoma and myeloma (Benetatos et al., 2008; Gao et al., 2017). In the present study, the bisulfite sequencing results revealed that the differentially methylated region (DMR) upstream of *MEG3* transcription start site was highly methylated in Cd-transformed cells, which prevents the transcription of the area downstream of the DMR. This finding indicates that the elevated DNMTs in Cd-transformed cells facilitates the silencing of *MEG3* expression.

Mounting evidence has suggested that *MEG3* exerts diverse functions in a wide spectrum and regulating stemness is one of those. *MEG3* has been reported to regulate differentiation of various stem cells/progenitors, including human bone marrow stem cells, human adipose derived stem cells, and dental pulp stem cells, by interacting with various proteins or miRNAs. In cancer, though with relatively less reports, *MEG3* has been found downregulated in liver and lung cancer stem cells, in which its function is to impede the action of miRNA 650 or to assist the action of another tumor suppressor p53 (Hsieh et al., 2021). Interestingly, a study with a contrast point of view demonstrated that *MEG3* is inessential in hematopoietic stem cells (Sommerkamp et al., 2019). Here, we observed that restoring *MEG3* expression in Cd-transformed cells inhibited the Cd-induced CSC property. Moreover, in the study of Yew et al., they provided evidence showing that

p21 level is associated with the expression of stemness markers in human mesenchymal stem cells (Yew et al., 2011). In our study, we observed increased p21 level along with decreased stemness in the cells with *MEG3* overexpression. Though the underlying mechanism of how *MEG3* down-regulation contributes to Cd-induced CSC-like property needs to be further investigated, its effect on p21 expression level might be a critical point.

While most studies on *MEG3* have been performed in cancer cell models, or in the cells which have already turned malignant such as our Cd model to determine the function(s) of *MEG3*, it has not been shown that whether overexpressing *MEG3* could inhibit cell transformation. To assess the effect of *MEG3* on chronic Cd exposure-induced cell transformation, we overexpressed *MEG3* in parental non-transformed cells and initiated the chronic exposure of Cd. We found that *MEG3* could suppress Cd-induced cell transformation by inhibiting cell cycle progression and reversing apoptosis resistance. Evidence has shown that *MEG3* halts cell cycle by regulating cell cycle inhibitor p16 or p21 in various cancer cells (Tao et al., 2021; Chak et al., 2017). As an important cyclin dependent kinase inhibitor regulating cell cycle phase transition through G1 to S phase, p21 has been shown to mediate Rb protein dephosphorylation and degradation (Deng et al., 1995; Gartel et al., 2005; Broude et al., 2007). Such regulatory axis might explain what we found in this study. In the cells with *MEG3* expression, the levels of p21 was increased, whereas phospho-Rb proteins were shown decreased at different serine sites.  Meanwhile, our study presents the first evidence showing that *MEG3* leads a determinant role for E2F1 level. E2F1, which poses dual

characteristics in terms of the role for tumorigenesis, is subjected to various post translational modifications for its activity and stability (Johnson, 2000; Shats et al., 2017; Costa et al., 2013; Wu and Yu, 2009). Binding to Rb protein is one of the mechanisms for E2F1 stabilization (Campanero and Flemington, 1997). We thus speculate that the reduced level of E2F1 is attributed by *MEG3* through downregulation of phosphor-Rb proteins. Further studies would need to examine this hypothesis. In addition, while the mechanism of Rb phosphorylation has been well perceived, another mechanism for Rb protein inactivation is degradation in a caspase-dependent manner (Chial, 2008). In our Cd-transformed cells that are apoptosis-resistant, this might explain why we observed accumulated total Rb protein, even with the increased phospho-Rb.

At last, accumulated level of Bcl-xL was observed in Cd-transformed cells, which was largely decreased in Cd-exposed cells with *MEG3* overexpression. It is unclear how *MEG3* regulate the level of Bcl-xL. However, it has been documented that E2F1 contributes to stabilization of Bcl-xL (Vuillier et al., 2018). Given the consistent pattern of altered levels of E2F1 and Bcl-xL in our results, it suggests that Cd-induced E2F1 leads to accumulation of Bcl-xL, resulting in apoptosis resistance of Cd-transformed cells. Moreover, several studies have revealed that targeting Bcl-2 family proteins benefits eradicating cancer stem cells and cancer therapy. The studies of Lagadinou et al. and Qiu et al. demonstrated that inhibition of Bcl-2 resulted in elimination of leukemia and glioblastoma stem cells (Lagadinou et al., 2013; Qiu et al., 2012). Zeuner et al. reported that targeting Bcl-xL elicited cytotoxicity towards NSCLC stem cells (Zeuner et al., 2014). The study of Yang et

al. also presented the critical role of another Bcl-2 family member Mcl-1 for the induced CSC-like property of the cells transformed by arsenic and benzo[a]pyrene co-exposure (Yang et al., 2020). These results suggest that apoptosis resistance-mediated by Bcl-2 protein family contributes to cancer stemness. In the present study, *MEG3* overexpression reduced the level of Bcl-xL, apoptosis resistance and inhibited Cd-induced CSC-like property, suggesting an important role of apoptosis resistance in Cd-induced CSC-like property.

In conclusion, chronic exposure to a low dose of Cd up-regulates the expressions of DNMTs, which increases the methylation of differentially methylated region upstream of the lncRNA *MEG3* transcription start site reducing *MEG3* expression. Cd exposure-caused *MEG3* down-regulation leads to enhanced cell cycle progression and apoptosis resistance promoting Cd-induced cell transformation and CSC-like property.
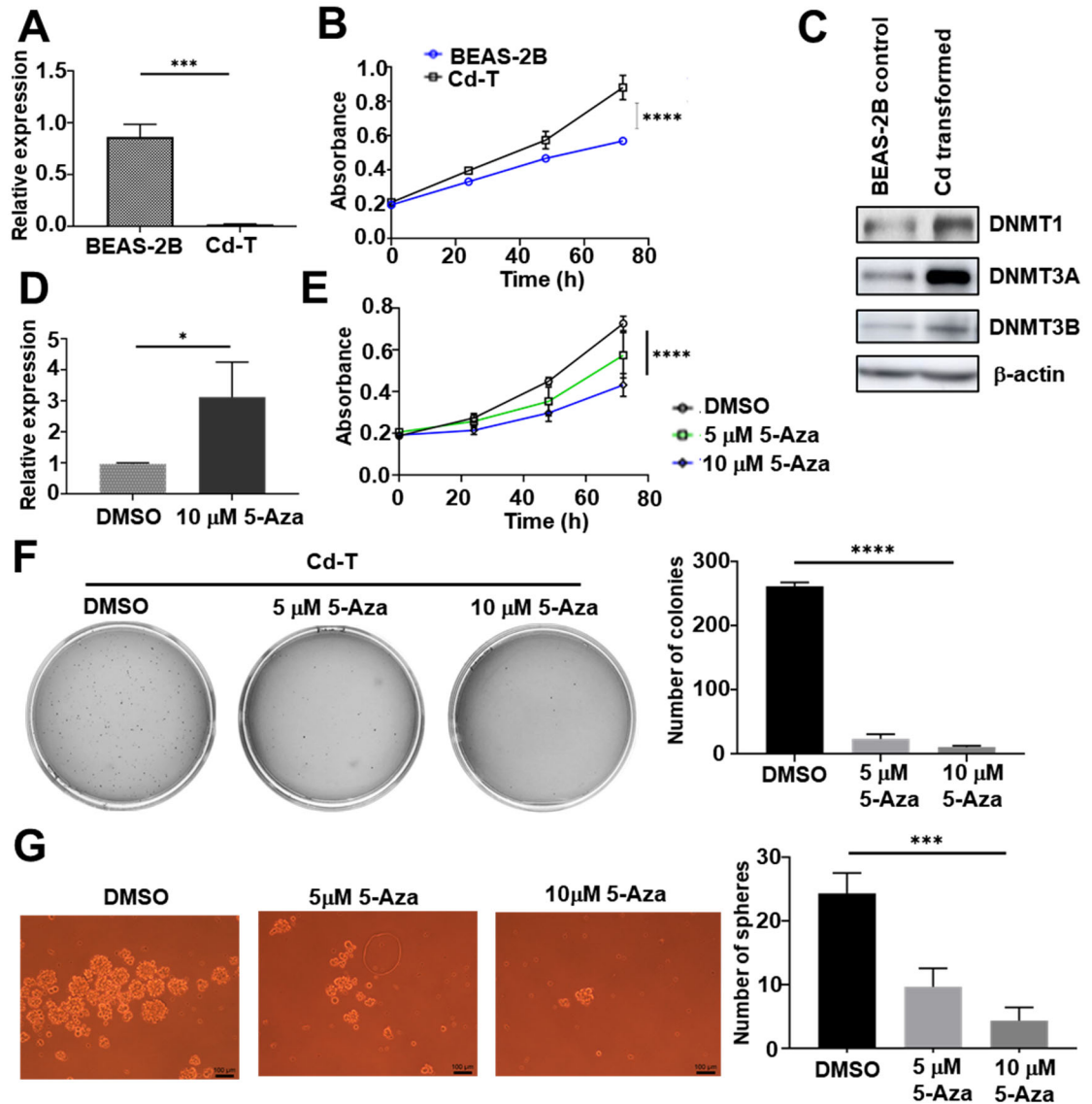
**Figure 3.1** *MEG3* is down-regulated and DNMTs are up-regulated in Cd-transformed cells and inhibition of DNMTs increases *MEG3* expression levels and reduces their transformed phenotypes. (A) Q-PCR analysis of the relative *MEG3* levels in passage-paired control BEAS-2B and Cd-T cells. The *MEG3* level in the Cd-T is expressed relative to control BEAS-2B cells (means ± SD, n=3), ***$p< 0.001$. (B) MTT analysis of passage-paired BEAS-2B control and Cd-T cells. The results are presented as means ± SD (n=5), ****$p<0.0001$. (C) Representative

Western blot analysis images of DNMTs levels in passage-paired control BEAS-2B and Cd-T cells. The assay was repeated, and similar results were obtained. (D) Q-PCR analysis of the relative *MEG3* levels in Cd-T cells treated with 5-Aza (10 $\mu$M). DMSO was used as a vehicle control. The *MEG3* level in the Cd-T with 5-Aza treatment is expressed relative to the control group (means ± SD, n=3), *$p$< 0.05. (E) MTT analysis of Cd-T cells treated with 5-Aza of 5 and 10 $\mu$M. DMSO was used as a vehicle control. The results are presented as means ± SD (n=5), ****$p$<0.0001. (F) Representative images of soft agar colonies formed from Cd-T treated with different concentration of 5-Aza (5 and 10 $\mu$M) (means ± SD, n=3), ****$p$<0.0001. (G) Representative images of suspension spheres formed from Cd-T cells treated with DMSO (vehicle control) or 5-Aza (5 and 10 $\mu$M), respectively. Scale bar: 100 $\mu$m. The bar graph represents the average numbers of the spheres formed in the repeated assays (means ± SD, n=3), ***$p$<0.001.
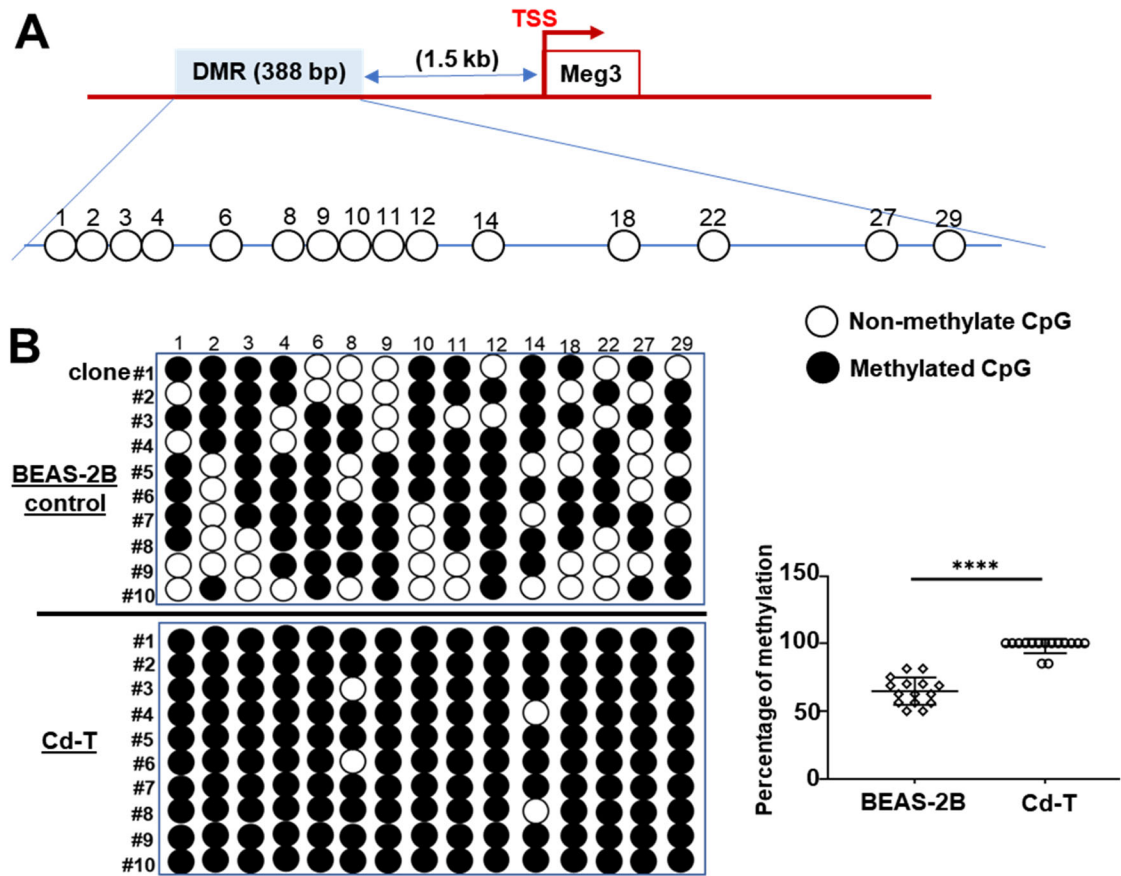
**Figure 3.2** Differentially methylated region upstream of *MEG3* transcription start site is highly methylated in Cd-transformed cells. (A) The CpG island examined at the differentially methylated region upstream of *MEG3* transcription start site. (B) Lollipop presentation of methylation status at the examined differentially methylated region upstream of *MEG3* transcription start site in passage-paired BEAS-2B control and Cd-T cells (open circle: nonmethylated; filled circle: methylated). The bar graph represents the percentage of methylation at each CpG site (n=16), ****$p< 0.0001$.
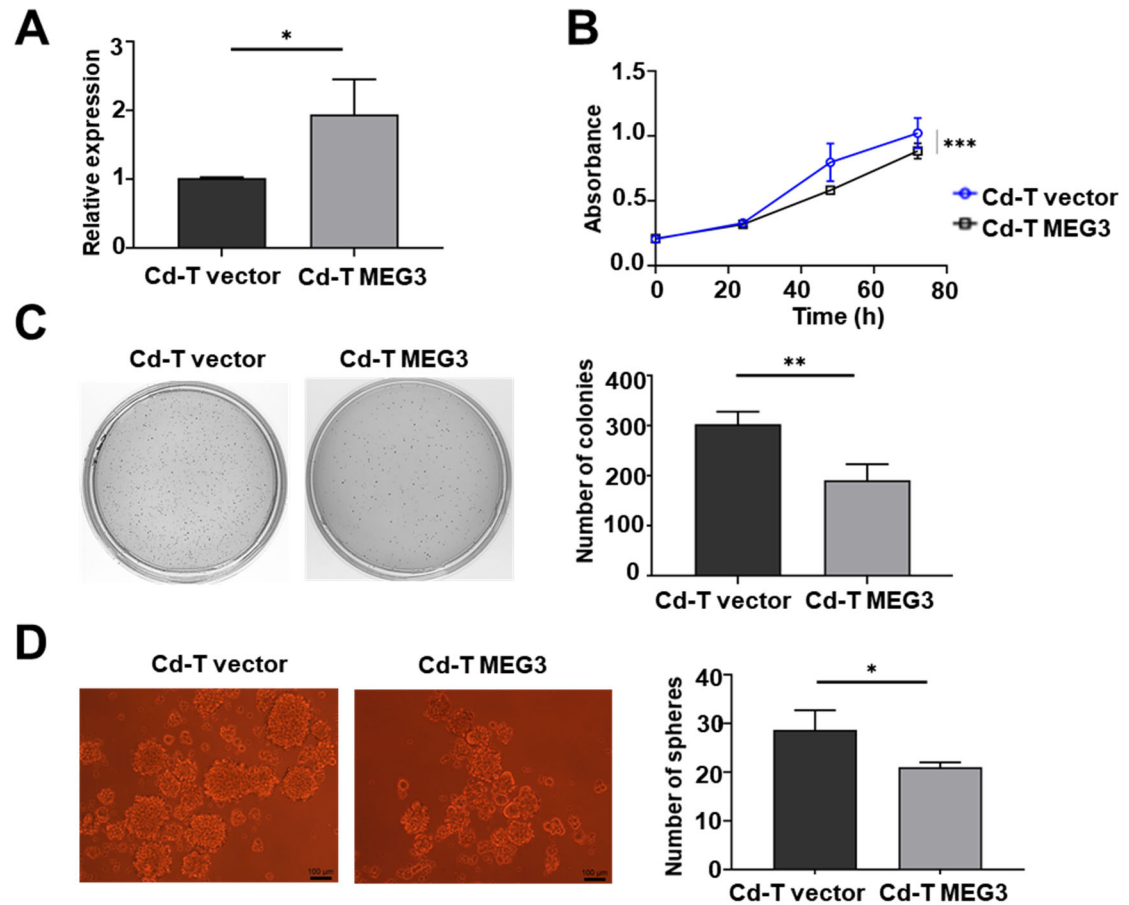
**Figure 3.3** Stably overexpressing *MEG3* in Cd-transformed cells significantly reduces their transformed phenotypes. (A) Q-PCR analysis of the relative *MEG3* levels in Cd-T vector control and Cd-T *MEG3* overexpressing cells. The *MEG3* level in the Cd-T *MEG3* overexpressing cells is expressed relative to the vector control cells (means ± SD, n=3), *$p < 0.05$. (B) MTT analysis of Cd-T vector control and Cd-T *MEG3* overexpressing cells. The results are presented as means ± SD (n=5), ***$p < 0.001$. (C) Representative images of soft agar colonies formed from Cd-T vector control and Cd-T *MEG3* overexpressing cells. The bar graph represents the average numbers of the soft agar colonies formed in the repeated assays (means ± SD, n=3), *$p < 0.05$. (D) Representative images of suspension

spheres formed from Cd-T vector control and Cd-T *MEG3* overexpressing cells.

Scale bar: 100 $\mu$m. The bar graph represents the average numbers of the spheres

formed in the repeated assays (means ± SD, n=3), *p<0.05.
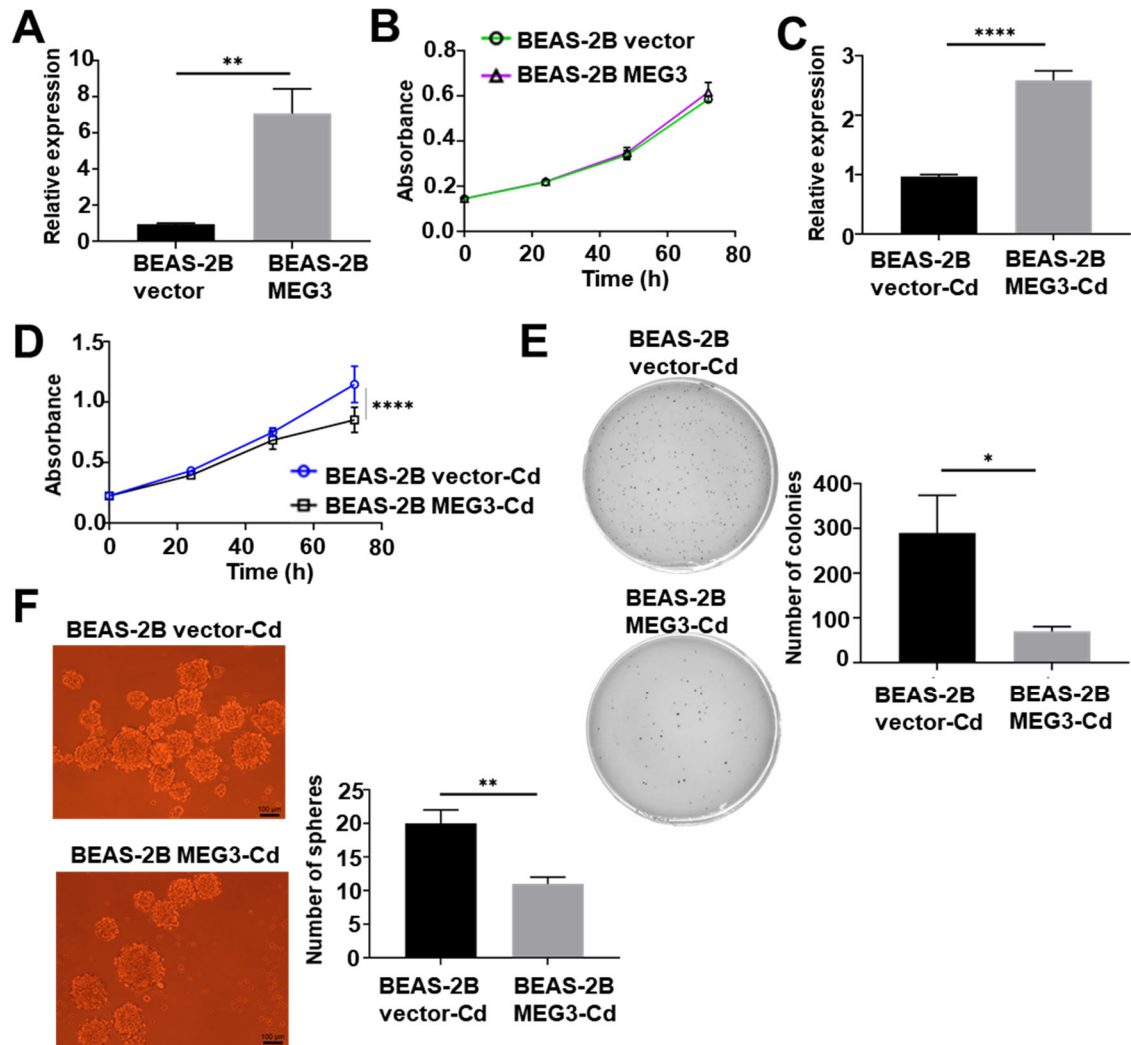
**Figure 3.4** Stably overexpressing *MEG3* in parental BEAS-2B cells reduces the capability of chronic low dose Cd exposure to induce cell transformation and CSC-like property. (A) Q-PCR analysis of the relative *MEG3* levels in BEAS-2B vector control and BEAS-2B *MEG3* overexpressing cells. The *MEG3* level in the *MEG3* overexpressing cells is expressed relative to the vector control cells (means ± SD, n=3), **$p< 0.01$. (B) MTT analysis of BEAS-2B vector control and BEAS-2B *MEG3* overexpressing cells. The results are presented as means ± SD (n=5). (C) Q-PCR analysis of the relative *MEG3* levels in BEAS-2B vector-Cd and BEAS-2B *MEG3*-

Cd cells. The *MEG3* level in the BEAS-2B *MEG3*-Cd cells is expressed relative to BEAS-2B vector-Cd cells (means ± SD, n=3), ****$p$< 0.0001. (D) MTT analysis of BEAS-2B vector-Cd and BEAS-2B *MEG3*-Cd cells. The results are presented as means ± SD (n=5), ****$p$< 0.0001. (E) Representative images of soft agar colonies formed from BEAS-2B vector-Cd and BEAS-2B *MEG3*-Cd cells. The bar graph represents the average numbers of the soft agar colonies formed in the repeated assays (means ± SD, n=3), *$p$< 0.05. (F) Representative images of suspension spheres formed from BEAS-2B vector-Cd and BEAS-2B *MEG3*-Cd cells. Scale bar: 100 μm. The bar graph represents the average numbers of the spheres formed in the repeated assays (means ± SD, n=3), **$p$<0.01.
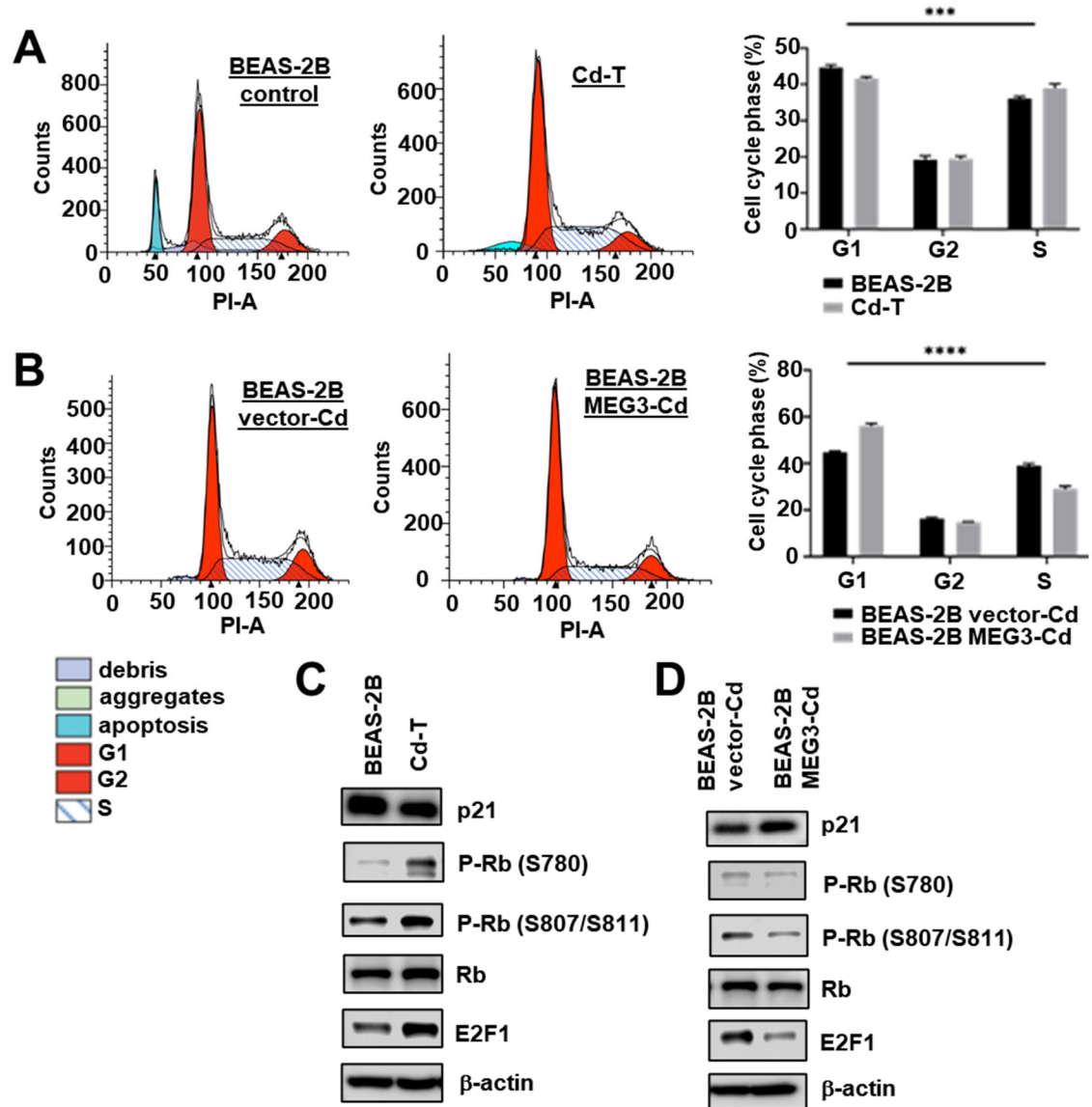
**Figure 3.5** *MEG3* overexpression reduces cell cycle progression by regulating the levels of cell cycle proteins. (A) Representative image of flow cytometry analysis of cell cycles in passage-paired BEAS-2B control cells and Cd-T cells. The bar graph shows the average percentage of each population at distinct cell cycle phase (means ± SD, n=3), ***$p < 0.001$. (B) Representative image of flow cytometry analysis of cell cycles in BEAS-2B vector-Cd and BEAS-2B *MEG3*-Cd cells. The bar graph shows the average percentage of each population at distinct cell cycle

phase (means ± SD, n=3), ****$p$< 0.0001. (C) Representative Western blot analysis images of cell cycle protein levels in passage-paired BEAS-2B control and Cd-T cells. The assay was repeated, and similar results were obtained. (D) Representative Western blot analysis images of cell cycle protein levels in BEAS-2B vector-Cd and BEAS-2B *MEG3*-Cd cells. The assay was repeated, and similar results were obtained.
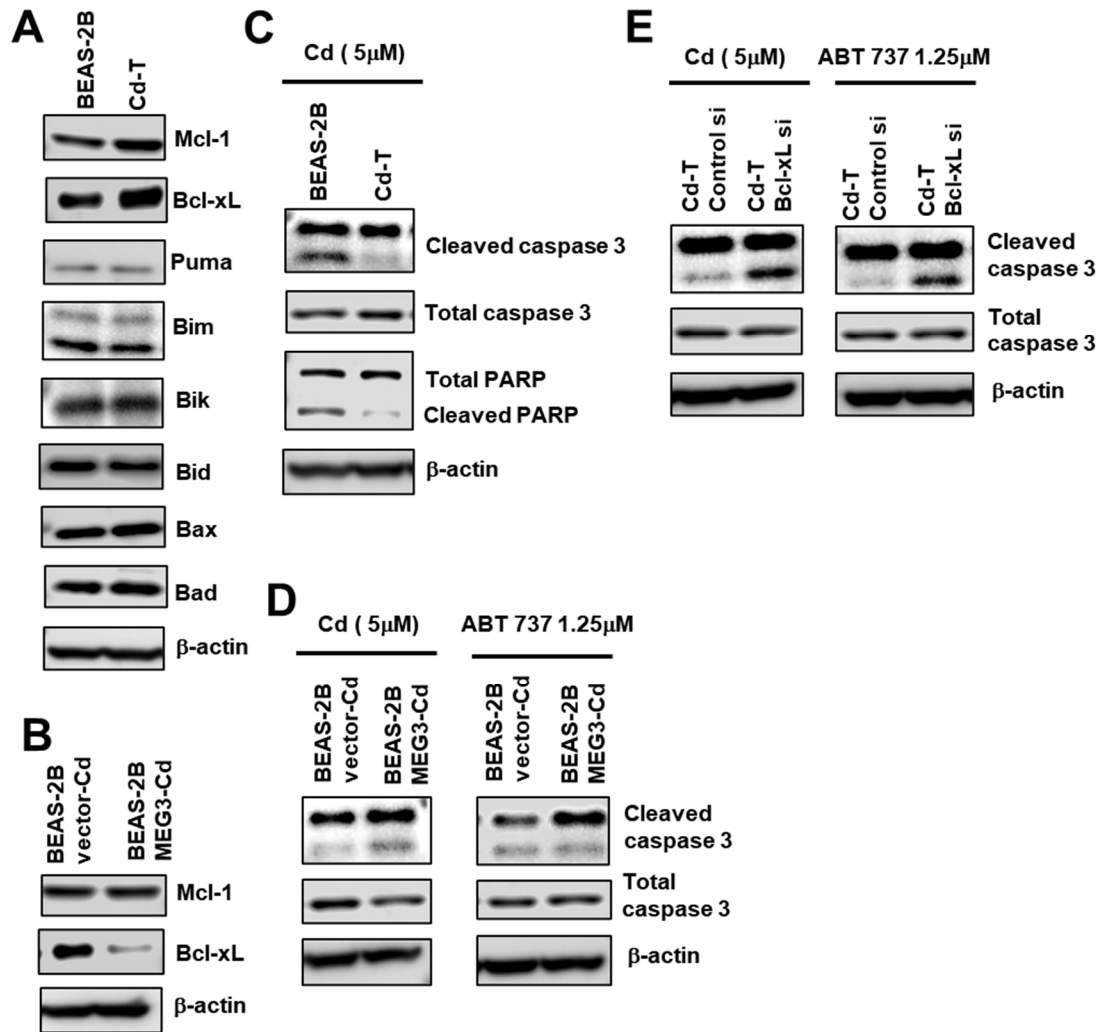
**Figure 3.6** *MEG3* overexpression reverses chronic Cd exposure-induced apoptosis resistance by reducing the level of the anti-apoptotic protein Bcl-xL. (A) Representative Western blot analysis images of apoptotic protein levels in passage-paired BEAS-2B control and Cd-T cells. The assay was repeated, and similar results were obtained. (B) Representative Western blot analysis images of apoptotic protein levels in BEAS-2B vector-Cd and BEAS-2B *MEG3*-Cd cells. The assay was repeated, and similar results were obtained. (C) Representative Western blot analysis images of apoptotic protein levels in passage-paired BEAS-

2B control and Cd-T cells treated with Cd (5 $\mu$M). The assay was repeated, and similar results were obtained. (D) Representative Western blot analysis images of apoptotic protein levels in BEAS-2B vector-Cd and BEAS-2B *MEG3*-Cd cells treated with Cd (5 $\mu$M) or ABT 737 (1.25 $\mu$M). The assay was repeated, and similar results were obtained. (E) Representative Western blot analysis images of apoptotic protein levels in Cd-T cells transfected with control siRNA or Bcl-xL siRNA and treated with Cd (5 $\mu$M) or ABT 737 (1.25 $\mu$M). The assay was repeated, and similar results were obtained.
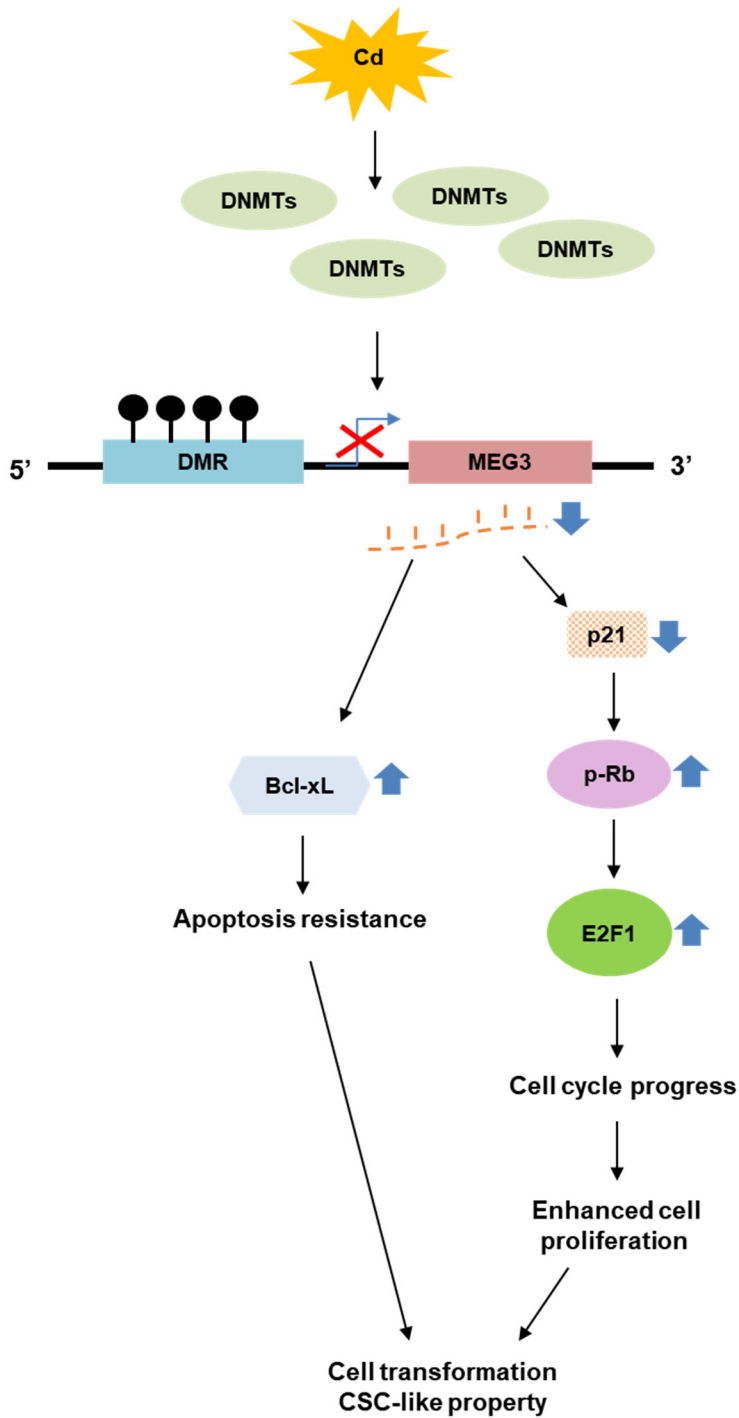
**Figure 3.7** A schematic summary of the mechanism of chronic Cd exposure-caused *MEG3* down-regulation and its role in Cd-induced cell transformation and CSC-like property.

# CHAPTER 4. SOCS3 ACTS AS A TUMOR SUPPRESSOR BY DOWNREGULATING YAP AND REVERSING TUMOR IMMUNOSUPPRESSIVE MICROENVIRONMENT IN LUNG CANCER WITH EGFR MUTATION

## 4.1 ABSTRATCT

Enhanced EGFR signaling contributes to 60% of NSCLC cases. However, there is an unmet need to solve acquired resistance to tyrosine kinase inhibitors for the lung cancer patients. In recent year, development of immunotherapy has been under extensive investigation. However, low objective response rate has been observed in the patients with mutant EGFR lung cancer. Uninflamed tumor microenvironment has been found a major feature in the lung cancer with mutant EGFR. This study was performed to investigate the role of suppressor of cytokine signaling 3 (SOCS3) as tumor suppressor and to explore the potential of its regulatory axis as therapeutic target for the development of novel approach to lung cancer with EGFR mutations. First, in our transgenic mouse model, overexpression of SOCS3 significantly inhibited tumor formation with mutant EGFR. Further investigation for the underlying mechanism revealed that SOCS3 downregulates the yes-associated protein (YAP) through increasing the level of the large tumor suppressor kinase 1/2 (LATS1/2). Decrease of YAP contributes to suppression of Bcl-2 family proteins, which sensitizes the tumor cells to conventional chemotherapy reagent. Consistent with the in vitro result, external YAP inhibitor was also shown to efficiently inhibit the growth of tumor organoids. Furthermore, it was found that SOCS3 downregulating YAP leads to modified

tumor immune microenvironment, evidenced by the decreased levels of the immunosuppressive cytokines, including colony stimulatory factor 1 (CSF-1), the C-X-C motif chemokine 5 (CXCL5), and the C-C motif chemokine ligand 2 (CCL2). In vivo studies further demonstrated the reversed ratio of type I and type II macrophages, as well as decreased populations of exhausted T cells and regulatory T cells in the mice with SOCS3 overexpression. Lastly, SOCS3 was often found to be silenced in various cancer types, including lung cancer. To mimic this circumstance, the therapeutic efficacy of utilizing external YAP inhibitor combined with anti-PD-L1 showed promising outcomes. These results suggest the critical role of SOCS3 as a biomarker for the oncolytic immune environment and provide a novel insight for improving lung cancer immunotherapy.

Key words: immunotherapy; SOCS3; YAP; PD-L1; CSF-1; CXCL5; CCL2

## 4.2 INTRODUCTION

Lung cancer is the leading cause of tumor death for both males and females in the US. Clinically, lung cancer has two major subtypes: non-small cell lung cancer (NSCLC) which accounts for 85% of lung cancer cases, and small cell lung cancer (SCLC) which includes 10-15% of the total. Lung cancer has no symptoms at the early stages, and it usually already spreads by the time of diagnostics in around 70% of the patients, which make it challenging for the treatment and with low 5-year survival rate for both SCLC and NSCLC (Blandin Knight et al., 2017; Schabath et al., 2019). As lung cancer has been often described as a highly

heterogenous disease, common features have been extensively studied for identifying therapeutic targets, such as epidermal growth factor receptor (EGFR).

EGFR is a transmembrane protein and a member of ErbB family proteins. Upon binding of its ligands, dimerization of EGFR with its homodimer or other ErbB family members activates the downstream signaling cascades, including MAPK/ERK pathway and PI3K/AKT pathway, to modulate cell activities such as migration, proliferation and adhesion (Li et al., 2015; Freudlsperger et al., 2011; Hynes et al., 2009). Aberrant EGFR signaling has been proof oncogenic in many cancers and correlated to poor outcomes, including lung cancer (Kanematsu et al., 2003; Lee et al., 2015; Huang et al., 2019; Liu et al., 2020). Conventional chemotherapy and radiation therapy were the two standard methods for the treatment. With the discovery of the oncogenic role of EGFR, targeted therapy, including tyrosine kinase receptor inhibitors (TKIs) and monoclonal antibody (e.g., Cetuximab) have been introduced for improving therapeutic efficacy (Mazzarella et al., 2018; Tan et al., 2018). While inhibiting EGFR by targeted therapy displayed promising outcomes in patients, however, the built-up resistance and relapse tumor progression after a period of treatment have become the major obstacles and challenges for the anti-cancer therapy (Ruppert et al., 2009; Nagano et al., 2018; Kauffmann-Guerrero et al., 2019). Among the mechanisms of the acquired resistance, 60% were resulted from the mutation T790M at exon 20 of EGFR (Huang et al., 2018). This point mutation appears at the tyrosine kinase activity site where ATP binds, which has been seen as the "gate keeper" of the domain and prevents the binding of the first and the second generation of TKIs (Yun et al.,

2008). Though the third generation TKI Osimertinib and other targeted therapy have demonstrated improvement in clinical endpoints, patients' response rate still varies depending on heterogeneity of tumor cells and the various EGFR subtypes (Kobayashi et al., 2018; Cheng et al., 2014; Passaro et al., 2020; Lim et al., 2019; O'Kane et al., 2017).

In recent years, much effort has been made to establish novel therapeutic approach and to investigate the efficacy of combining different types of therapy including TKIs, tradition chemotherapy, and immunotherapy. With the discovery of immune checkpoint proteins, such as programmed cell death protein-1 (PD-1) and its ligand (PD-L1), utilizing immune checkpoint inhibitors have led into a new era of cancer therapy (Hamanishi et al., 2016; Gong et al., 2018; Jiang et al., 2019; [3]Wang et al., 2020). So far, four immune checkpoint inhibitors against PD-1/PD-L1, Durvalumab, Atezolizumab, Nivolumab, and Pembrolizumab, have been approved by the US Food and Drug Administration (FDA) for advanced NSCLC. However, the data of the clinical trials revealed only 14-19% response rate of NSCLC patients with multiple EGFR mutations. On the other hand, higher response rate (44.8%) to the immune checkpoint inhibitor was observed in NSCLC patients with wild-type EGFR (Hsu et al., 2019). This outcome implied that immunotherapy might favor the patients with wild-type EGFR and further pointed out the difficulties of NSCLC immunotherapy with EGFR mutation and the unmet need for solving immunotherapy resistance.

Suppressor of cytokine signaling 3 (SOCS3) is a member of the cytokine-induced negative regulator family which in turn modulates cytokine signaling. It is

often found silenced in various diseases, mostly through hypermethylation of its promoter (Tao et al., 2021; Dhar et al., Dees et al., 2020). In cancers, silence of SOCS3 has been shown to corelate to enhanced proliferation and invasion (Chu et al., 2017; Weber et al., 2005). However, studies regarding its tumor suppressing function have been rarely linked to its conventional role – overseeing various immune response. SOCS3 is critical to fine tune the cytokine signaling to maintain immune homeostasis in local tissues. In a disease state, the presence of SOCS3 tends to create a pro-inflammatory environment which facilitates immune response against the micro-invaders. It has been shown that SOCS3 promotes the expression of interleukin 17 in human T cells in response to the mycobacteria infection (Kleinsteuber et al., 2012). In addition, the presence of SOCS3 promotes macrophage polarization towards inflammatory in the local environment of pneumonia (Chi et al., 2019). Luckey at al. have also reported that enhanced expression of SOCS3 suppressed the generation of regulatory T cells (Luckey et al., 2020). In contrast, aberrant expression of SOCS3 is usually associated with more immune-tolerant microenvironment. It has been shown that suppression of SOCS3 led to macrophage type II polarization after intracerebral hemorrhage (Ji et al., 2020). In breast cancer, deficient SOCS3 resulted in IL-6-induced proliferation of early stage myeloid-derived suppressor cells (MDSCs) and thus create an immunosuppressive tumor microenvironment ([1]Zhang et al., 2018). With the extensive studies in these diseases, however, the functions of SOCS3 in modulating the tumor immune microenvironment in lung cancers remains to be explored.

Uninflamed tumor microenvironment often found to be an important characteristic and responsible for the resistance to immunotherapy (Yu et al., 2018; Soo et al., 2018). The goal of this study was set to revisit the role of SOCS3 as a tumor suppressor in the tumor microenvironment and to further investigate the potential of its regulatory axis against immunotherapy resistance for lung cancer with mutant EGFR. The present study is first to report that SOCS3 inhibited tumor progression through downregulating oncogenic protein YAP and modulating oncolytic immunosuppressive microenvironment. Furthermore, the results provide a new insight of SOCS3, not only as a tumor suppressor, but also as a biomarker for lung cancer diagnosis and prognosis.

## 4.3 MATERIALS AND METHODS

### 4.3.1 Cell culture and generation of SOCS3 stably overexpressing cells

Human lung cancer cell lines H1975, PC9GR4, and PC9 were gifts kindly provided by Dr. Christine F. Brainson at the University of Kentucky. The cells were cultured in Roswell Park Memorial Institute 1640 medium (RPMI 1640, Gibco) supplemented with 10% fetal bovine serum (FBS, Sigma) and 1% Penicillin-Streptomycin (Pen Strep, 10000 U/mL, Gibco). To generate SOCS3 stably overexpressing cells, the lentiviral particles (Invitrogen) for the vector control and SOCS3 overexpressing were transduced into the parental cell lines H1975, PC9GR4, and PC9. After the blasticidin (10 mg/mL) selection based on the

procedures described in our published study (Wang et al., 2019), the cells were harvested and SOCS3 overexpression was confirmed by Western blot analysis.

### 4.3.2 Establishment of 3D tumor organoid cultures for drug treatment

The lungs with tumor burden were collected from the EGFR$^{mut}$ mice. The minced lung tissues were then mixed with tumor organoid culture medium [DMEM-Ham's 12 (Gibco) supplemented with 4 mM L-glutamine, 1 % Pen Strep, 10 % FBS, 10 mg/mL insulin (Sigma-Aldrich), 5 mg/mL ITS (Sigma-Aldrich), 0.1 mg/mL cholera toxin (Sigma-Aldrich), 25 ng/mL EGF, 25 ng/mL bFGF, and 30 mg/mL bovine pituitary extract (Invitrogen)], and growth factor reduced Matrigel (Corning), followed by seeding into transwell insert (0.4 mm). After the primary tumor organoid was observed, 100 mL of dispase was added to each insert liquify the Matrigel. After centrifugation, the retrieved organoids were disassociated by trypsinization. The disassociated organoids were proceeded to cell counting and 5000 cells were seeded back to the transwell inserts. After two passages, drug treatment was started by adding Verteporfin to the medium at the lower chamber. The media were changed every other day. After a week of incubation, the grown tumor organoids were counted and photographed.

### 4.3.3 MTT assay

Thiazolyl Blue Tetrazolium Bromide (MTT) was purchased from Sigma-Aldrich (St Louis, MO). The assay was performed as described previously ([1]Wang et al.,

2014). Briefly, cells were seeded in 96-well plates ($10^3$ cells/well in 100 μL of culture medium) for 4 time points: 0, 24, 48, and 72 hr. At the end of incubation, 50 μL of the MTT reagent (5 mg/mL) was added to each well and incubated for 4 hr, followed by another 1 hr incubation with 200 μL of dimethyl sulfoxide (DMSO). The plate was read using a microplate reader (SpectraMaxi3x, Molecular Devices, Sunnyvale, CA) at the wavelength of 570 nm. The inhibition on relative cell growth was determined by the following formula: Cell Viability (%) = (Absorbance at 570 nm of SOCS3 overexpressing cells)/ (Absorbance at 570 nm of control cells) ×100.

### 4.3.4 Serum free suspension culture for sphere formation

The spheroid formation was performed following the published protocol with minor modifications (Dontu et al., 2003). Briefly, single cells were plated in ultra-low attachment 24-well culture plates (Corning, NY) at a density of 2 x $10^3$ cells per well suspended in serum-free DMEM containing human recombinant basic fibroblast growth factor (bFGF, 20 ng/mL) (R&D, Minneapolis, MN), human recombinant epidermal growth factor (EGF, 20 ng/mL) (R&D, Minneapolis, MN), B27 (Invitrogen, Carlsbad, CA) and heparin (4 mg/mL, Sigma-Aldrich). Plates were incubated at 37℃ in cell incubator with 5% $CO_2$. Spheres > 50 mM were viewed, photographed and counted under a phase-contrast microscope after 10-day culture.

### 4.3.5 Western blot analysis

Cells were lysed using lysis buffer following our published protocol ([1]Wang et al., 2014). The cell lysates were then applied to the bicinchoninic acid assay (Bio-rad) to determine protein concentration, followed by SDS-polyacrylamide gel electrophoresis (PAGE) (20-30 mg of protein/lane). The separated proteins were then transferred to polyvinylidene fluoride membrane (PVDF, Millipore, MA). 5% milk in PBS was applied for the blocking step before primary antibody incubation. The following primary antibodies were used: anti-SOCS3, anti-KLF4, anti-KLF5, anti-Phospho-p44/42 MAPK (p-ERK), anti-Phospho-Akt (Ser473), anti-LATS1, anti-LATS2, anti-Phospho-YAP (Ser127), anti-YAP, anti-Cleaved Caspase-9, anti-Cleaved Caspase 3, anti-Cleaved PARP, anti-Bcl-xL, anti-Mcl-1, anti-Bcl-2, anti-PD-L1 (Cell Signaling Technology, Beverly, MA) (dilution 1:1000); and anti-b-actin (Millipore Sigma, St. Louis, MO) (dilution 1:8000). After overnight primary antibody incubation at 4 °C, the membranes were washed and then incubated with HRP-conjugated antibodies for 1 hr at room temperature. Images were developed by Amersham Imager 680 (GE Healthcare Life Sciences, MA).

### 4.3.6 Immunofluorescence (IF) staining, H&E

For immunofluorescence staining, the cells were seeded on cover-glass placed in 6-well plate and cultured for 48 hr (including the inhibitor treatment or RNA interference) before the antibody staining. For the treatment groups, 24 hr after seeding, Rapamycin and Wortmannin (Cayman Chemical, MI) were added to the

cells and continued for another 24 hr. For the staining process, the cells were first washed first and fixed with 4% paraformaldehyde for 20 min at room temperature. Permeabilization was performed using 1% Triton X-100 in PBS and incubated for 1.5 min at room temperature, followed by blocking with 3% bovine serum albumin (BSA) for 30 min. The primary antibody YAP (Cell Signaling Technology) was diluted in PBS with 1% BSA at ratio of 1:200. Following the primary antibody incubation for overnight at 4°C, the cells were washed before the secondary antibody incubation (Alexa 546 goat anti-mouse/rabbit IgG, 1:300, Invitrogen). After 1 hr of incubation at room temperature, the cells were washed again and stained with nuclear 4'6-diamidino-2-phenylinodole (DAPI) for 10 min before mounting. The IF staining pictures taken under a Nikon fluorescent microscope are the overlaid images of YAP staining in red fluorescence with nuclear 4'6-diamidino-2-phenylinodole (DAPI) staining in blue fluorescence. The images were overlaid using Nikon NIS-Elements software. The H&E staining of the mouse lung tissue sections was carried out following our previous procedures (Zhao et al., 2010).

## 4.3.7 RAN extraction and quantitative PCR

Total RNA extraction from cultured cells and the mouse lung tissue were performed using the TRIzol reagent (Invitrogen) following the manufacturer's protocol. Quality and Quantity of extracted RNA was determined by NanoDrop$^{TM}$ spectrophotometer (Thermo Fisher, MA) before applying to TaqMan gene expression assays. Quantitative PCR was performed by ABI QuantStudio 3 qPCR System (Applied Biosystems). The $2^{-DD}$ CT analysis method was utilized to quantify

relative mRNA expression levels of each gene, with human 18S RNA as internal control.

### 4.3.8 Flow cytometry analysis

The collected mouse lung tissues were cut into small pieces followed by disassociation with collagenase IV (Gibco) and Dispase II (Sigma-Aldrich) at 37°C. After 1 hr of incubation, the isolated lung tissue cells were stained washed with PBS, followed by the antibody staining. The fluorescence-conjugated antibodies used in this study: anti-CD45, anti-CD3, anti-CD8, anti-CD279, anti-CD366, anti-CD4, anti-CD25, anti-CD11b, anti-Ly6G, anti-CD11c, anti-F4/80, anti-CD86, and anti-CD206 (Biolegend, CA). Before anti-FOXP3 (Biolegend, CA) staining, cells were fixed and permeabilized with True-Nuclear™ Transcription Factor Buffer kit following the manufacturer's manual. Fluorescence-activated cell sorting was carried out by the flow cytometer BD LSR II (Becton Dickinson). Raw data was analyzed by using Flowjo software (Becton Dickinson).

### 4.3.9 Preparation of Verteporfin- and Cyanine 7.5 (Cy 7.5)-loaded nanoparticles

The compound encapsulated nanoparticles were prepared by nanoprecipitation method following our published study ([1]Li et al., 2019). Briefly, Lecithin (2 mg), $PEG_{2000}$-DSPE (18 mg) and RGD-$PEG_{2000}$-DSPE (2 mg) were dissolved in 4% ethanol and heated to 65°C. Verteporfin (1 mg/mL in acetone) was mixed with PLGA (1.875 mg) in 0.6 mL acetone and incubated at 65°C for 1 min, then added

into the preheated Lecithin/PEG$_{2000}$-DSPE/RGD-PEG$_{2000}$-DSPE mixed solution. The self-assembled nanoparticle mixture was placed at room temperature overnight, followed by centrifugation using Amicon Ultra-4 centrifugal filter (Millipore, MA) to remove acetone, ethanol and DMSO thoroughly. Sterile PBS was then used to dilute the remaining supernatant to a final concentration of 10 mg/mL, which was further sterilized by 0.4 mm syringe-driven filters. The nanoparticles loaded with Cyanine 7.5 (Cy 7.5) dye were prepared with the same method except replacing Verteporfin with Cy 7.5. Lecithin was obtained from Alfa Aesar (Ward Hill, MA). PEG-DSPE [1,2-distearoyl-sn-glycero-3-phosphoethanolamine-N-carboxy (polyethylene glycol) 2000] was purchased from Jenkem Technology (Allen, TX). RGD peptide was obtained from Peptides International (Louisville, KY). PLGA [Poly (d, L-lactide-co-glycolide)] and Verteporfin were purchased from Sigma-Aldrich. The fluorescence dye Cyanine 7.5 (Cy 7.5) was from Lumiprobe Corporation (Hunt Valley, MD).

*4.3.10 Cy 7.5-RGD-nanoparticle in vivo distribution study*

The Cy 7.5-RGD-nanoparticle (Cy 7.5-RGD-NP) in vivo distribution was studied to evaluate the efficiency of RGD peptide targeting lung tumor cells in the EGFR$^{mut}$ mice. This study was performed following the guidelines approved by the Institutional Animal Care and Use Committee of University of Kentucky. Briefly, Cy 7.5-RGD-NP was injected into the mice with or without tumor formation through tail vein (2.5 mg of Cy 7.5 per mouse). Time course at the 48, 72, 96 hr post

injection, fluorescence imaging (Ex 745 nm/ Em 800 nm) was performed using the IVIS live animal imaging system (PerkinElmer, Waltham, MA).

### 4.3.11 Transgenic mouse models for the tumorigenesis study and therapeutic study

By crossing the mice carrying hetero-EGFR$^{mut}$ (T790M/L858R) with upstream floxed STOP structure and the mice carrying hetero-SOCS3 with upstream floxed STOP structure, two types of breeds were generated for this study: the ones with loxp-STOP-loxp-EGFR$^{mut}$ (T790M/L858R) (abbreviated as EGFR$^{mut}$ mice in the following study) and the ones with both loxp-STOP-loxp-EGFR$^{mut}$ and loxp-STOP-loxp-SOCS3 (abbreviated as SOCS3/EGFR$^{mut}$ mice in the following study). Conditional activation of EGFR$^{mut}$ and SOCS3 genes in the transgenic mice was performed by administering recombinant adeno-associated virus expressing Cre (Ad5CMVCre, University of Iowa) at the age of 6 weeks. For the tumorigenesis study, the mice were sacrificed at different time course and the lungs were collected for tissue RNA extraction or stained with Bouin's fixative solution. For the therapeutic groups, the mice were treated with anti-mouse PD-L1 antibody (100 mg per mouse) (Bio X Cell, NH) twice a week, or Verteporfin-RGD-nanoparticles (10 mg/kg) three time a week, or the combination of the above two. At the end point, the mice were euthanized for collecting the lungs for flow cytometry analysis or fixed with Bouin's solution.

*4.3.12 Statistical analysis*

The statistical analyses for the significance of differences in presented numerical data (mean ± SD) were carried out by testing different treatment effects using two-tailed t-tests for comparison of two data sets or one-way analysis of variance (ANOVA) for multiple data sets. A p-value of < 0.05 was considered statistically significant.

## 4.4. RESULTS

### 4.4.1 SOCS3 overexpression suppresses lung cancer cell proliferation, CSC properties, and tumor formation

To study the potential tumor suppressing function of SOCS3, we first generated SOCS3 overexpression cells with three lung cancer cell lines bearing different EGFR mutation points: H1975 (T790M/L858R), PC9GR4 (del E746-A750/T790M), and PC9 (del E746-A750). **Figure 4.1A** shows upregulated SOCS3 in the three cell lines after transfection (H1975-SOCS3, PC9GR4-SOCS3, PC9-SOCS3). MTT assay was first performed to study the impact of SOCS3 overexpression. Decreased cell proliferation was observed in H1975-SOCS3 and PC9GR4-SOCS3 (**Figure 4.1B**) but has no effect on PC9-SOCS3 (data not shown). Similarly, overexpressing SOCS3 in H1975 and PC9GR4 inhibited sphere formation in serum-free suspension culture, but in PC9, only minor inhibition was observed (**Figure 4.1C**). To further understand the impact of SOCS3 on CSC property at the molecular level, expression of pluripotency marker KLF4 and KLF5

106

was evaluated by Western blot. SOCS3 overexpression decreased KLF4 and KLF5 in all three cell lines, though the effect on KLF4 in PC9 was less strong as on the other two (**Figure 4.1D**). In addition to the in vitro study, two mice models were applied to the present study to determine whether SOCS3 could suppress tumorigenesis in the lungs of the mice bearing EGFR mutation (**Figure 4.2A**). The first model is the mice carrying EGFR$^{mut}$ (T790M/L858R) with upstream floxed STOP structure (abbreviated as EGFR$^{mut}$ mice in the following study). Another model is the mice carrying SOCS3 and EGFR$^{mut}$ (T790M/L858R) with upstream floxed STOP structure (abbreviated as SOCS3/EGFR$^{mut}$ mice in the following study). Conditional activation was induced by administering recombinant adeno-associated virus expressing Cre (Ad5CMVCre, University of Iowa). 17 weeks post viral induction, SOCS3 overexpression inhibited tumor formation in the lungs of the SOCS3/EGFR$^{mut}$ mice by at least 50%, compared to the EGFR$^{mut}$ mice (**Figure 4.2B**). Furthermore, time course study revealed that SOCS3 delayed massive tumorigenesis in the SOCS3/EGFR$^{mut}$ mice till the 12$^{th}$ week post viral induction, while the same number of tumors were already forming in the lungs of the EGFR$^{mut}$ mice at the 10$^{th}$ week post viral induction (**Figure 4.2C**). These results demonstrate a critical role of SOCS3 as tumor suppressor for lung cancer, particularly with EGFR mutation.

### 4.4.2 SOCS3 downregulates PI3K/MAPK signaling and leads to decreased level of oncogenic protein YAP

Next, we would like to determine the underlying molecular mechanism of SOCS3 inhibiting tumorigenesis. **Figure 4.3A** shows dramatic decreases of phospho-Akt (p-Akt) in the three cell lines with SOCS3 overexpression, and downregulated phospho-ERK (p-ERK) in H1975-SOCS3 and PC9GR4-SOCS3. Xia et al. reported that PI3K and its downstream signaling regulates the activity of the Hippo pathway effector YAP (Xia et al., 2018). In addition, the study of Mayrhofer et al. demonstrated the association between MAPK signaling and YAP activation in a brain tumor model (Mayrhofer et al., 2016). As both AKT and ERK signaling were inhibited by the presence of SOCS3, Western blot was performed to examine the level of YAP, as well as its phosphorylated form, p-YAP. As a transcription factor, nuclear translocation is critical for YAP to exert its biological function. However, its nuclear localization could be impaired by phosphorylation. While phosphorylation of most proteins represents activation, phosphorylation of YAP demonstrates that it is sequestered in the cytoplasm followed by degradation. Such YAP phosphorylation could be regulated by the protein kinase LATS1/2 which's activity is inhibited by AKT/ERK signaling (Boopathy et al., 2019). It was found that both LATS1 and LATS2 were upregulated in the cell lines with SOCS3 overexpression, although the level of LATS1 in PC9-SOCS3 showed no change. Increase of p-YAP and decrease of total YAP were also observed in H1975-SOCS3, PC9GR4-SOCS3, and PC9-SOCS3, suggesting that SOCS3 overexpression led to downregulation of this oncogenic protein (**Figure 4.3B**).

Immunofluorescence staining was next performed to determine the cellular localization of YAP. In the parental H1975, PC9 cells, YAP accumulated in the nuclei stained with DAPI. On the contrary, in H1975-, PC9-SOCS3 cells, YAP was clearly sequestered in the cytoplasm (**Figure 4.4A**), indicating that SOCS3 prevents YAP from transferring to the nuclei. The treatment of Rapamycin (mTOR inhibitor) and Wortmannin (PI3K inhibitor) to H1975 and PC9 cells also showed inhibited nuclear translocation of YAP, confirming that YAP signaling is upregulated in these lung cancer cells and that such signaling is regulated by PI3K signaling (**Figure 4.4B**). The results mentioned above suggest that SOCS3 inhibiting ERK and AKT signaling, which leads to downregulation of oncogenic YAP through promoted LATS1/2 activity.

4.4.3 Inhibited YAP activity limits the growth of EGFR$^{mut}$ organoids and sensitizes lung cancer cells to chemotherapeutic agent

Next, we set to explore the downstream effect(s) brought by YAP inhibition. Tumors in the lungs of the EGFR$^{mut}$ mice were retrieved for establishing 3D organoid culture which allows us to examine the response of the tumor cells to YAP inhibition in a mimic physiological environment. The derived tumor organoids were treated with YAP inhibitor Verteporfin (Sigma-Aldrich) at the concentration of 2 $\mu$M. It was found that YAP inhibition significantly reduced growth of the organoids by 50% (**Figure 4.5**). To further determine if inhibiting YAP would benefit traditional chemotherapy, H1975 and PC9 were treated with Verteporfin and Cisplatin at gradient concentrations. Levels of cleaved-caspase 3, -PAPR, and –caspase 9

were examined by Western blot. The combination of Verteporfin and Cisplatin displayed synergistic effect on the enhanced apoptosis at dose-dependent manner, though minor difference was observed between the two cell lines. H1975 appeared to be resistant to Cisplatin, evidenced by that single use of Cisplatin barely induced apoptosis, even at the highest concentration 20 $\mu$M. On the contrary, increased levels of cleaved-caspase 9, -caspase 3, and -PARP were shown in PC9 treated with 20 $\mu$M of Cisplatin (**Figure 4.6A**). To delineate the underlying mechanism of the combined therapy promoting apoptosis in the H1975 and PC9, Western blot was performed to screen pro-apoptotic and anti-apoptotic proteins in these two cell lines treated with Verteporfin and Cisplatin. We found that the therapeutic combination significantly reduced the level of Bcl-xL in PC9, and the levels of Mcl-1, Bcl-xL, and Bcl-2 in H1975 (**Figure 4.6B**). These results suggest that inhibited YAP in lung cancer cells leads to downregulation of pro-survival Bcl-2 family proteins and benefits the downstream apoptotic signaling cascade.

4.4.4 SOCS3 downregulating YAP leads to decreased expression of PD-L1 and secretion of immunosuppressive and angiogenic cytokines

Previously, it has been reported that YAP induces the expression of immune checkpoint ligand PD-L1 in lung cancer and melanoma (Miao et al., 2017; Kim et al., 2018). The role of PD-L1 has been regarded as immunosuppressive in the tumor microenvironment (Iwai et al., 2002). For lung cancer with EGFR mutation,

however, the correlation between expression level of PD-L1 and immunotherapy resistance remain inconclusive. In the present study, we proposed to examine the anti-tumor effect of SOCS3 and its downstream regulatory axis applied to immunotherapy. First, PD-L1 level was found significantly decreased in H1975-SOCS3 and PC9R4-SOCS. In PC9, PD-L1 was undetectable in either the parental cells or the ones with SOCS3 overexpression (**Figure 4.7A**). To demonstrate the causal relationship between YAP activity and PD-L1 expression, H1975 and PC9GR4 cells were then treated with Verteporfin at gradient concentration. PD-L1 level was reduced at a dose-dependent manner (**Figure 4.7B**). Furthermore, mRNA levels of cytokines involved in tumor microenvironment were measured in H1975, PC9GR4, PC9 -parental and -SOCS3 overexpression cells by quantitative PCR. Tumor-secreted CSF-1 has been shown to recruit immunosuppressive macrophages in pancreatic cancer (Zhu et al., 2014). In H1975-SOCS3, the level of CSF-1 was down to undetectable; in PC9GR4-SOCS3, CSF-1 was downregulated to 50%. However, in PC9, SOCS3 overexpression has no significant effect on CSF-1 expression (**Figure 4.8A**). Meanwhile, chemoattractant for recruiting pro-angiogenic neutrophils CXCL5 and the cytokine for recruiting anti-inflammatory monocytes CCL2 were also downregulated to undetectable in H1975-SOCS3. Interestingly, both CXCL5 and CCL2 were originally undetectable in PC9GR4 and PC9 parental cells (**Figure 4.8A**). To further demonstrate that SOCS3 downregulates these cytokines through inhibition of YAP, H1975, PC9GR4, and PC9 were treated with Verteporfin at gradient concentrations (**Figure 4.8B**). Consistently, CSF-1 was reduced at a dose-dependent manner in

all three cell lines. Among those, H1975 showed most sensitive to Verteporfin treatment. Downregulation of CXCL5 and CCL2 was also observed in H1975 treated with gradient Verteporfin, though there was no sign of dose-dependent shown. The results stated above described the downstream effects of SOCS3 inhibiting YAP, including decreased PD-L1, CSF-1, CXCL5, and CCL2, and suggested the potential role of SOCS3 for immunotherapy.

4.4.5 SOCS3 overexpression inhibits tumorigenesis by modulating tumor immuno-microenvironment

Consistent with the tumor formation rate shown in Fig. 1, H&E staining results showed significant higher tumor burden in the $EGFR^{mut}$ mice than in $SOCS3/EGFR^{mut}$ mice (**Figure 4.9**). Next, we set to determine if SOCS3 overexpression exerts impact on the cytokine secretion in vivo. Total RNA was extracted from excised mouse lungs bearing tumors and converted to cDNA. Quantitative PCR was then performed to determine relative expression of the cytokines. Consistent with the in vitro results, we observed significantly lower levels of CSF-1 (**Figure 4.10A**) and CXCL5 (**Figure 4.10B**) in the mice with SOCS3 overexpression. In addition, markers of type I and type II macrophages were also examined here. The qPCR results demonstrated that SOCS3 overexpression increases the level of type I macrophage markers Nos2 and TNF, but decreases the levels of markers for type II macrophages, IL-10 and IL-4 (**Figure 4.10C-H**). The live cells isolated from the mice lungs were also stained with antibodies for immune cells analysis by flow cytometry. In the lungs from the

SOCS3/EGFR$^{mut}$ mice, number of type I macrophage (percentage of CD86$^+$ in F4/80$^+$ cells) was found higher than type II (percentage of CD206$^+$ in F4/80$^+$ cells), and vice versa in the EGFR$^{mut}$ mice (**Figure 4.11A**). Regulatory T cells (Treg) have been seen accountable for immunotherapy failure for cancer patients. In out mouse model here, we also found that the number of Treg cells in the SOCS3/EGFR$^{mut}$ mice is only a half of the one in the EGFR$^{mut}$ mice (**Figure 4.11B**). Furthermore, population of exhausted T cells (PD-1$^+$/TIM3$^+$) was found significantly decreased in the SOCS3/EGFR$^{mut}$ mice, compared to the ones in the EGFR$^{mut}$ mice which is around 5 times higher (**Figure 4.11C**). These results suggest that other than an immunosuppressive microenvironment, the presence of SOCS3 turned the pathological microenvironment into more pro-inflammatory, which could further benefit the anti-cancer therapy.

4.4.6 Targeting YAP sensitizes lung cancer with EGFR mutation to immunotherapy

The results in the previous figures indicated that SOCS3 suppresses tumorigenesis by remodeling tumor microenvironment through YAP inhibition, which points out the critical role of YAP for cancer therapy, especially for immunotherapy. As mentioned above, hypermethylation at the promoter region and thus SOCS3 downregulation was often found in lung cancer patients. Under this premise, we would like to examine if inhibiting YAP by external administration would produce similar effects as with the presence of SOCS3 and benefit the immunotherapy. Verteporfin is an extremely hydrophobic compound. In the present study, we package this compound into nanoparticles with specific

targeting. Integrin $\alpha$V has been reported highly expressed in the lung cancer cells. We detected the expression level of this protein in the three cell lines used in this study. Interestingly, only H1975 showed high level of integrin $\alpha$V (**Figure 4.12A**). As the mutation points of EGFR in H1975 are the same as the EGFR$^{mut}$ construct of the mouse model here, this result encouraged us to apply this targeting to the nanoparticle. Next, luminescent dye cyanine 7.5 (Cy 7.5) was packed into the nanoparticle with integrin aV targeting and injected into the control (EGFR$^{mut}$ mice without AdCre viral induction) and the tumor bearing mice (EGFR$^{mut}$ mice with viral induction) through tail vein. 48 hours after the injection, Cy 7.5 signals accumulated at the thoracic area of the tumor bearing mice through 72 hours, and the signal reduced with time through 96 hours (**Figure 4.12B**). This result demonstrated that targeting integrin $\alpha$V could increase the specificity of the therapeutic agent. According to others' studies, Verteporfin encapsulated in the targeted nanoparticles was administered three times a week at the dosage of 10 mg/kg (Fisher et al., 2017). Rat anti-mouse PD-L1 antibody (BE0101, BioXCell) was used as the immunotherapeutic agent and administered 100 mg twice a week (**Figure 4.13A**). Therapeutic groups included Verteporfin alone, anti-PD-L1 alone, anti-PD-L1 plus empty nanoparticles, and anti-PD-L1 plus Verteporfin in the nanoparticles (n=5). And the last group would be no treatment control. After three weeks of therapy, the mice were sacrificed and the lungs were collected for Bouin's staining and FACS analysis, respectively. The combination of Verteporfin and anti-PD-L1 significantly reduced tumor nodules, as compared to other groups (**Figure 4.13B**). The synergistic effect of the combined therapy was further evidenced by the

suppressed level of exhausted T cells (**Figure 4.14A**) and regulatory T cells (**Figure 4.14B**). For the ratio of type I and type II macrophages, we observed no significant difference between the group of Verteporfin alone and Verteporfin combined with anti-PD-L1 (**Figure 4.14C**). To summary, SOCS3 decreases the level of YAP by suppressing PI3K/mTOR signaling and promoting LATS1/2 activity. The reduced YAP signaling results in decreased levels of Bcl-2 family proteins which lead to decreased cell survival. The inhibition of YAP signaling also results in modulated tumor microenvironment for less immunosuppressive. This study describes the critical role of SOCS3 as a tumor suppressor and as a biomarker for immunotherapy and provides a novel insight into combination therapy for lung cancer particularly with EGFR mutations (**Figure 4.15**).

## 4.5 DISCUSSION

Acquired resistance to tyrosine kinase inhibitors has been a major obstacle to effective treatment for lung cancer, particularly with EGFR mutations. Since the discovery of immune checkpoint inhibitors, much effort has been made to the development of immunotherapy. With promising outcomes for various types of cancers, however, objective response is usually low in the patients with mutant EGFR lung cancer (Yu et al., 2016; Soo et al., 2018; Passarelli et al., 2020). Uninflamed tumor microenvironment often found to be an important characteristic and responsible for the resistance to immunotherapy (Dong et al., 2017). Hence, there is an unmet need for novel approaches to solve immunotherapy resistance. SOCS3 has been shown a major regulator of various immune response during

infection and inflammation, such as the signaling induced by IL-6 and IL-17 (Croker et al., 2012; Huang et al., 2016; Kleinsteuber et al., 2012). Furthermore, SOCS3 has been considered a tumor suppressor, given that the presence of this protein was found associated with inhibited tumor cell proliferation and invasion in different cancer types (Barclay et al., 2009; Liu et al., 2018). Nonetheless, the role of SOCS3 in the mutant EGFR lung cancer has not been discussed. In this study, we demonstrated that SOCS3 suppresses the level of oncoprotein YAP via promoting tumor suppressors LATS1/2, which in turn inhibits tumorigenesis of EGFR-mutant lung cancer through inhibition of Bcl-2 family proteins and the immune checkpoint protein PD-L1, as well as modifying uninflamed tumor microenvironment towards more inflammatory (Fig. 7).

To date, more than 40 distinct mutations have been reported within EGFR (Yeh et al., 2013). Among those, primary or secondary T790M at exon 20 has been shown accountable for the resistance to tyrosine kinase inhibitors (Huang et al., 2015). T790M changes the conformation of EGFR, making this gatekeeper more accessible to ATP for constant autophosphorylation and the amplified downstream signaling (Godin-Heymann et al., 2007; Yun et al., 2008). Roughly, EGFR downstream pathways include MAPK pathway, PI3K pathway, and JAK/STAT pathway. As a "master" of various immune activities, the role of SOCS3 in JAK/STAT pathway has been under extensive studied for IL-6 –induced signaling (Babon et al., 2014; Billing et al., 2019). In cancers, it has been shown directly or indirectly that SOCS3 suppresses signaling of PI3K in small cell lung cancer (Wan et al., 2015) or MAPK signaling in prostate cancer (Puhr et al., 2010). In addition,

it has been only reported in gliomas with mutant EGFR, that the absence of SOCS3 leads to activation of STAT3 and FAK (Lindemann et al., 2011). However, the impact of SOCS3 on MAPK and PI3K pathways in EGFR-mutant lung cancer remains unknown. Our study here demonstrates that SOCS3 inhibit signaling of both MAPK and PI3K pathways in the EGFR-mutant lung cancer cells, especially the ones with T790M.

The Hippo signaling pathway is a well-studied and classical signaling pathway for controlling organ sizes during development through regulating cell proliferation and apoptosis. Dysregulation of the Hippo pathway has been shown associated with cancer initiation, metastasis, and cancer stem cells (Zygulska et al., 2017; Gregorieff et al., 2015; Maugeri-Saccà et al., 2015; Chang et al., 2020). LATS1/2 proteins are the core kinases of the Hippo pathway and known for regulating cell cycle (Turenchalk et al., 1999; Xia et al., 2002). As a tumor suppressor, downregulation of LATS has been discussed in various cancers. In an angiogenesis study, it has been shown that both PI3K/MAPK signaling pathways downregulate the level of LATS protein and activate the effector of Hippo pathway YAP/TAZ in response to vascular endothelial growth factor (VEGF) (Azad et al., 2018). In the present study, our results showed that the presence of SOCS3 increased the levels of LATS1/2 with the suppression of PI3K and MAPK signaling, which in turn decreased the level of YAP. This is the first study to demonstrate that SOCS3 regulates the Hippo pathway. In addition, our results revealed reduced stemness proteins and inhibited sphere formations in the cells with SOCS3 overexpression. This is the first study showing that SOCS3 suppresses cancer

117

stem cells which are often found accountable for metastasis at early stage and the hindered therapy for lung cancer. As the altered Hippo signaling shown in the present study, it suggests a potential mechanism contributing to the reduced cancer stemness and would need further investigations to confirm.

The Hippo signaling system has been shown to correlated with the overexpression of PD-L1 in the tumor microenvironment. Hsu et al. reported that the Hippo effector YAP induced the expression of PD-L1 in thoracic cancer (Hsu et al., 2018). In addition, it has been demonstrated that mutated EGFR caused overexpression of PD-L1, which led to impaired immune checkpoint blockade (Dong et al., 2017). Particularly, we observed high level of PD-L1 in the H1975 and PC9GR4 cells, but none in the PC9 cells. In fact, several studies specifically linked T790M mutation with PD-L1 expression, including the study of Inomata et al. which confirmed a positive correlation between T790M and the level of PD-L1 (Inomata et al., 2020). However, if T790M mutation promotes PD-L1 expression, why has low immunotherapy response rate been observed? Interestingly, a contradictory observation has been reported that T790M is associated with low level of PD-L1 (Hata et al., 2017). While the correlation between T790M and PD-L1 level remains debatable, the nature of lung cancer heterogenicity actually suggests that PD-L1 alone might not be enough to predict the oncolytic immune environment, given that the diverse expressions of various immune markers have been observed in NSCLC with T790M mutation which would also need to be taken into account (Suda et al., 2017).

As the major regulator of the immune system, SOCS3 has been shown to oversee the levels of several cytokines and their downstream signaling. It has been reported that tumor derived CXCL5 promotes metastasis of colorectal and pancreatic cancer (Zhao et al., 2017; Ando et al., 2020). CXCL5 was also found to promote lung cancer proliferation and metastasis (Wang et al., 2018). In this study, our results provide the first evidence showing that SOCS3 suppresses the level of CXCL5. In addition, SOCS3 also inhibited the level of CCL2, which was only found in pancreatic model before (Hou et al., 2020). Both cytokines were demonstrated to associate with an immunosuppressive tumor microenvironment in melanoma and glioma (Forsthuber et al., 2019; Chang 2016). Work of Li et al. further showed that the elevated CXCL5 contributes to PD-L1 expression in cancer-associated fibroblasts ([2]Li et al., 2019). Here we have seen that downregulation of YAP led to inhibited CXCL5 and PD-L1, but whether there is a hierarchical regulatory axis between CXCL5 and PD-L1 would need further study to examine. Moreover, SOCS3 has been shown to play an important role of macrophage polarization based on physiological context ([2]Zhang et al., 2018; Chi et al., 2019). Previously, it has been reported that dysregulated Hippo signaling in immunosuppressive glioblastomas was associated with type II macrophage polarization (Kim et al., 2020). The present study provided the first evidence to show that SOCS3 promotes type I macrophage polarization through modulating the Hippo signaling.

As our results revealed the critical role of SOCS3 in the tumor microenvironment, SOCS3, however, has been often found silenced in various cancers by our previous and others' studies (He et al., 2003; Pierconti et al., 2011;

Molavi et at., 2013; [2]Wang et al., 2014; [4]Wang et al., 2020). Hence, we next assessed the therapeutic potential of YAP inhibitor to facilitate immunotherapy in the EGFR[mut] mice. As YAP inhibitor verteporfin is extremely hydrophobic and cannot be directly administered without considering the toxicity of DMSO, we encapsulated the compound into a lipid-polymer hybrid nanoparticle for drug delivery, which's rationale has been described in our previous study ([1]Li et al., 2019). Meanwhile, integrins are the transmembrane proteins responsible for cell-cell and cell-extracellular matrix adhesion, and signal transduction for cell growth and survival. Structurally integrins have a subunits and b subunits with different combination of the isoforms. Overexpression of integrins is usually associated with cancers. It has been revealed that upregulated integrin $\alpha V\beta 3$ promotes cell proliferation in NSCLC (Fu et al., 2020), which indicated that integrin $\alpha V\beta 3$ is a suitable target for increasing therapeutic specificity. Cyclic arginine-glycine-aspartic acid (RGD) peptide is a ligand of $\alpha V\beta 3$ and has been utilized for imaging of this integrin (Chen et al., 2005). Our study is the first one describing the combination of lipid-polymer hybrid nanoparticle and GRD peptide to encapsulate YAP inhibitor for increasing targeting specificity against EFGR-mutant lung cancer.

For lung cancer therapy, particularly the ones with EGFR mutations, improving immunotherapy by tackling the uninflamed tumor microenvironment remains a big yet unsolved issue. Meanwhile, whether the immunosuppressive effects resulted from dysregulated Hippo signaling can be reversed by bringing in a single immune regulator has not been discussed. In the present study, we first demonstrated that SOCS3 inhibits the Hippo effector YAP by inducing the level of

Hippo kinases LATS1/2 which was resulted from the suppressed MAPK/PI3K pathway. The modulated Hippo signaling resulted in the decrease of Bcl-2 family proteins, PD-L1 and immunosuppressive cytokines, leading to pro-inflamed tumor microenvironment which eventually facilitates immunotherapy.
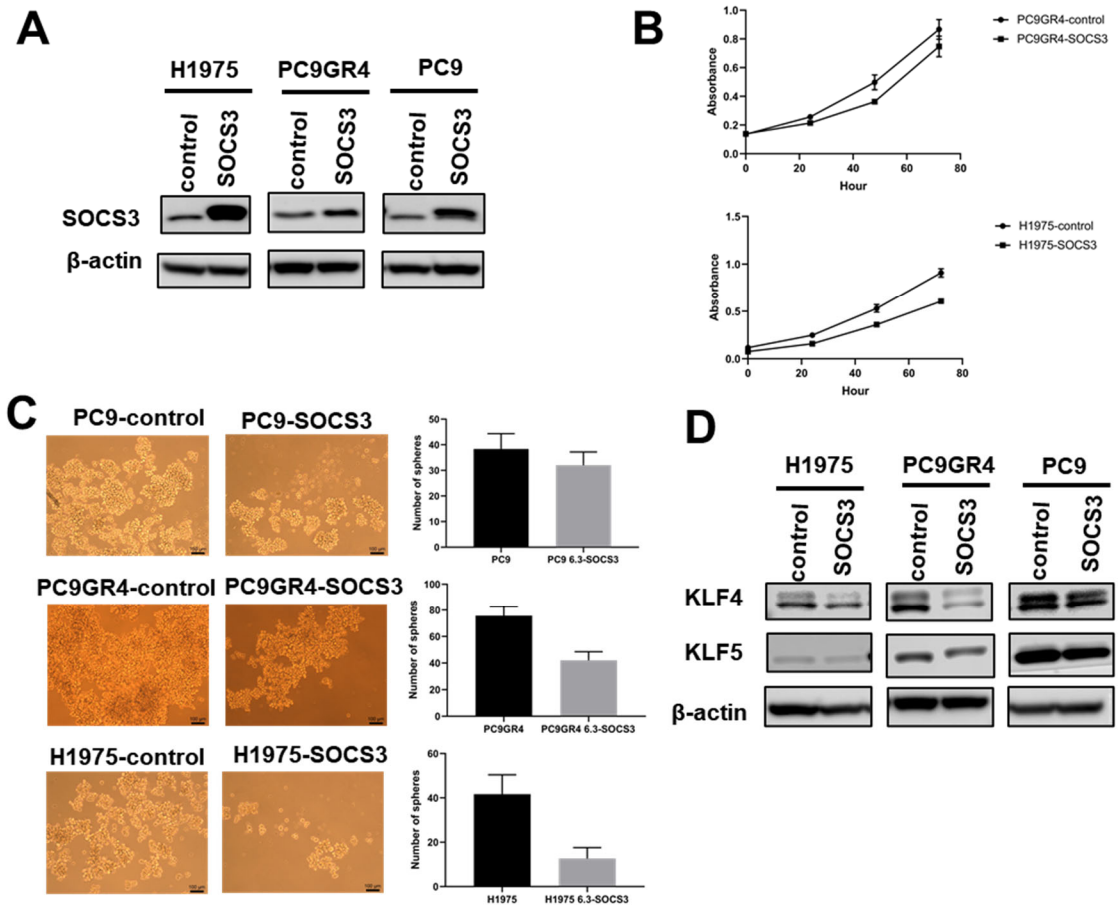
**Figure 4.1** SOCS3 overexpression decreases lung cancer cell proliferation, CSC-like properties. (A) Representative Western blot image of SOCS3 level in parental cells H1975, PC9GR4, PC9, and these three cell lines with stably expressing SOCS3, H1975-SOCS3, PC9GR4-SOCS3, and PC9-SOCS3. The experiment was repeated, and similar results were obtained. (B) MTT analysis of the growth curve of PC9GR4, PC9GR4-SOCS3, H1975, H1975-SOCS3. The results are presented as means ± SD (n=5). (C) Effect of stably expressing SOCS3 in H1975, PC9GR4, and PC9 on sphere formation in suspension culture (means ± SD, n=3), compared to the parental cells. (D) Representative Western blot images of the levels of KLF4 and KLF5 in parental cells H1975, PC9GR4, PC9, and the three

cell lines with stably expressing SOCS3, H1975-SOCS3, PC9GR4-SOCS3, and

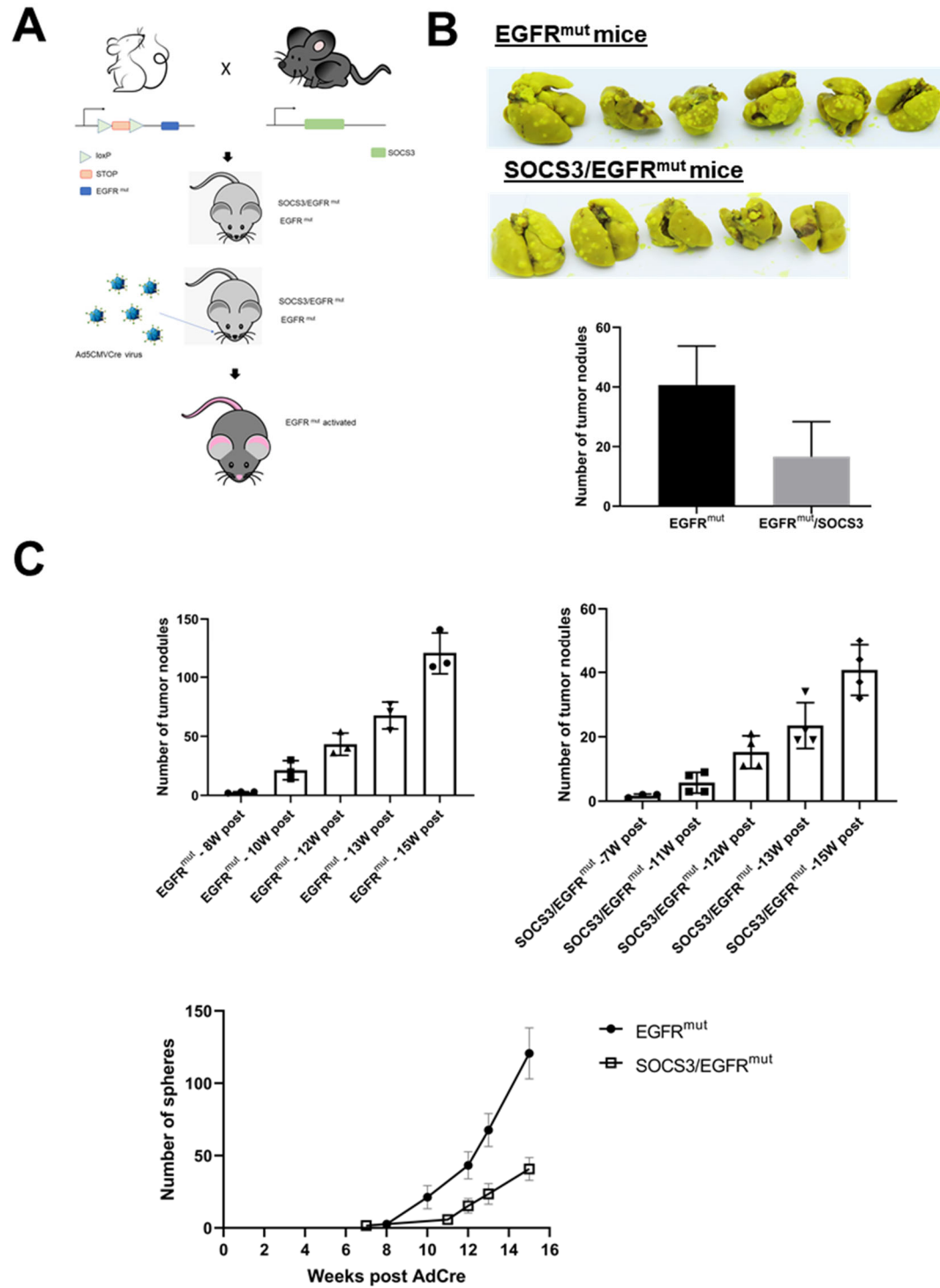PC9-SOCS3.The experiment was repeated, and similar results were obtained.

**Figure 4.2** SOCS3 overexpression decreases tumor formation. (A) The mouse

models used in this study. Cre-lox mice with heterogenous SOCS3 knock-in and

heterogenous EGFR$^{mut}$ (T790M/L858R) knock-in were generated respectively. By crossing the two breeds, the mice with EGFR$^{mut}$ (T790M/L858R) only or SOCS3/ EGFR$^{mut}$ (T790M/L858R) were collected and administered with adenovirus to activate the transgenes at the age of 6 weeks. (B) Images of the lungs of the EGFR$^{mut}$ mice and the SOCS3/ EGFR$^{mut}$ mice 17 weeks post viral activation. The lungs were stained with Bouin solution, and the tumor nodules were counted. The results are presented as means ± SD (n=5). (C) Time course study of tumor formation. The EGFR$^{mut}$ mice and the SOCS3/ EGFR$^{mut}$ mice were euthanized at different time points after viral induction. The lungs were collected and stained with Bouin solution. The tumor nodules were counted and shown as means ± SD (n=5).
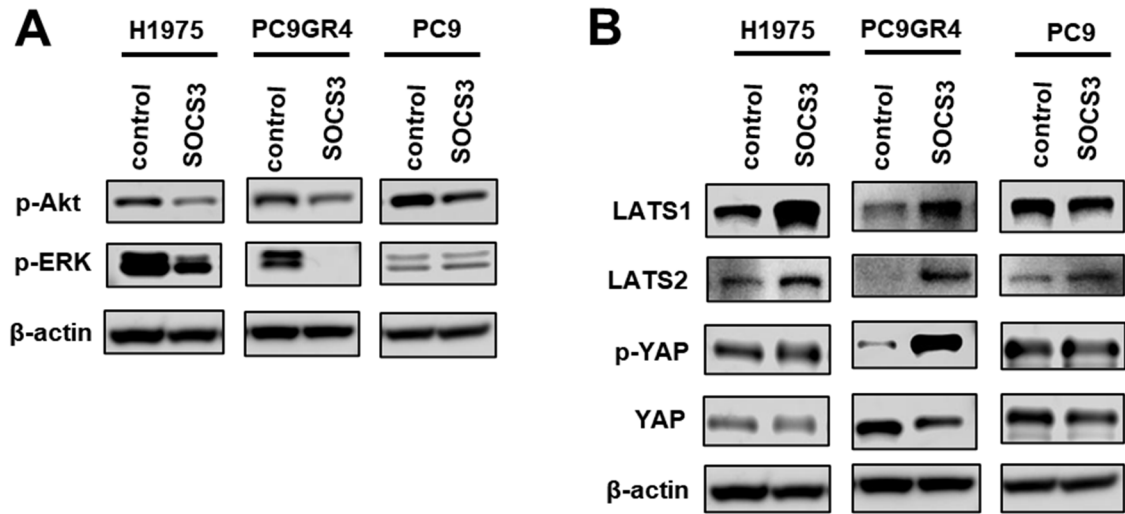
**Figure 4.3** SOCS3 overexpression down-regulates PI3K/MAPK signaling and leads to decreased level of oncogenic protein YAP through enhanced LATS1/2 activity. (A) Representative Western blot image of the levels of phospho-AKT (p-AKT) and phospho-ERK (p-ERK) in parental cells H1975, PC9GR4, PC9, and the three cell lines with stably expressing SOCS3, H1975-SOCS3, PC9GR4-SOCS3, and PC9-SOCS3.The experiment was repeated, and similar results were obtained. (B) Representative Western blot image of the levels of LATS1, LATS2, phospho-YAP (p-YAP), and YAP in in parental cells H1975, PC9GR4, PC9, and the three cell lines with stably expressing SOCS3, H1975-SOCS3, PC9GR4-SOCS3, and PC9-SOCS3. The experiment was repeated, and similar results were obtained.
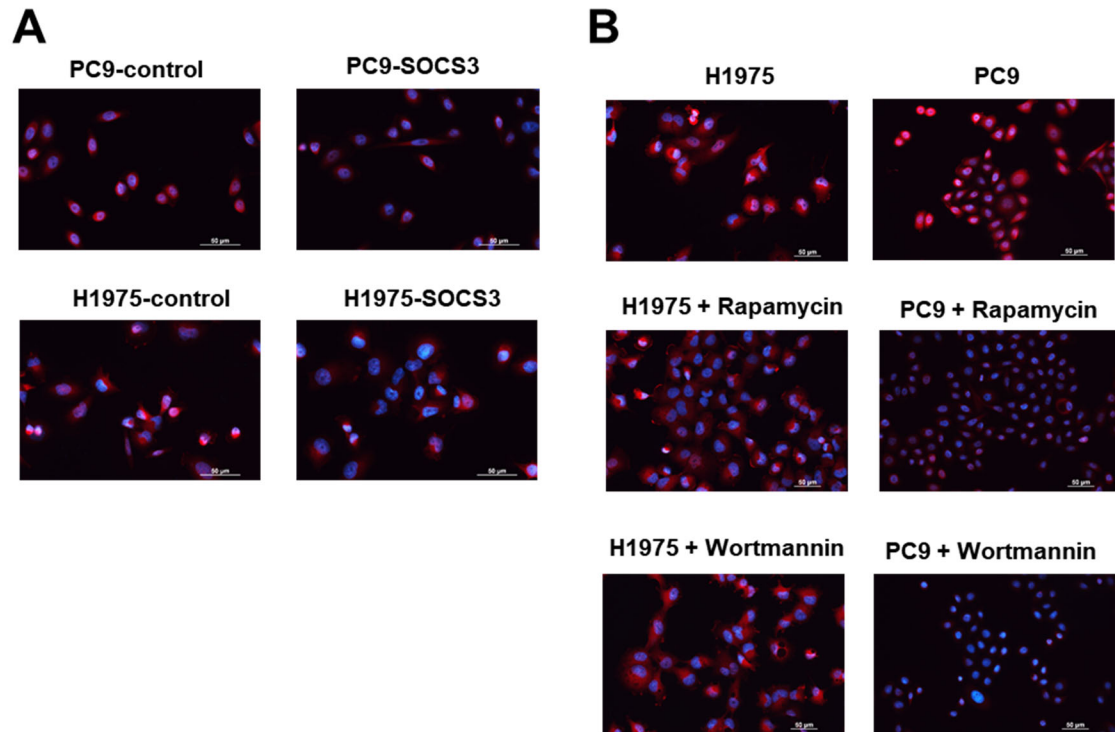
**Figure 4.4** SOCS3 overexpression inhibits YAP nuclear translocation. (A) Representative IF staining overlaid images of YAP in red fluorescence and DAPI in blue fluorescence from the parental cells H1975, PC9, and these two cell lines with stably SOCS3 expressing, H1975-SOCS3 and PC9-SOCS3. Scale bar represents 50 $\mu$m. (B) Representative IF staining overlaid images of YAP in red fluorescence and DAPI in blue fluorescence form H1975 and PC9 cells treated with Rapamycin (1nM) and Wortmannin (2 $\mu$M). Scale bar represents 50 $\mu$m.
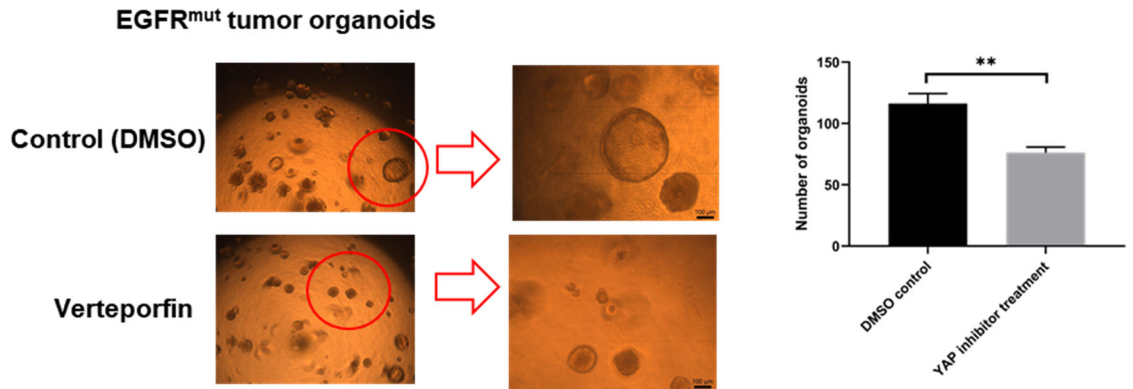
**Figure 4.5** Inhibited YAP activity limits the growth of the EGFR<sup>mut</sup> tumor organoids. Representative images of the tumor organoids treated with DMSO or verteporfin (2 μM). At the end point, the organoids were photographed with different magnifications (the left two images: 4X; the right two images: 10X). The numbers of the organoids were counted and shown as means ± SD (n=3).
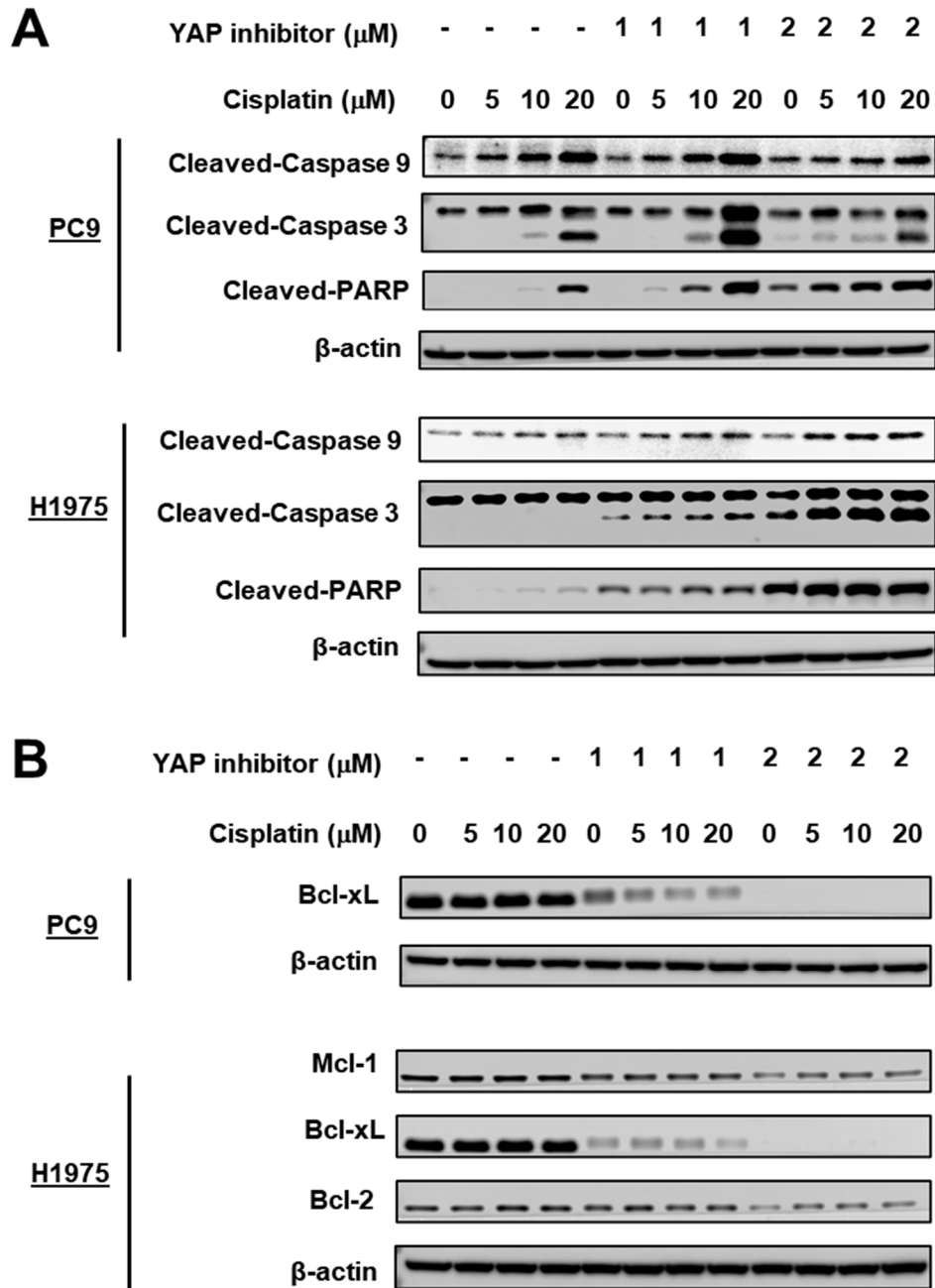
**Figure 4.6** Inhibited YAP activity sensitizes lung cancer cells to chemotherapeutic agent. (A) Representative Western blot image of the levels of cleaved-caspase 9, cleaved-caspase 3, cleaved-PARP in H1975 and PC9 cells treated with verteporfin and cisplatin at different concentrations. The experiment was repeated, and similar results were obtained. (B) Representative Western blot image of the levels of Bcl-

xL, Mcl-1, Bcl-2 in H1975 and PC9 cells treated with verteporfin and cisplatin at different concentrations. The experiment was repeated, and similar results were obtained.
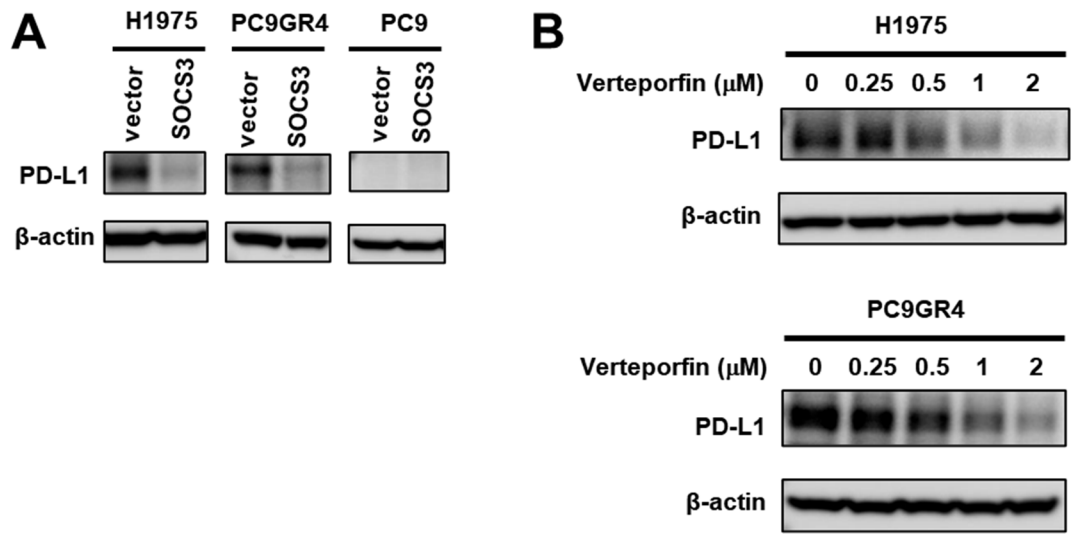
**Figure 4.7** SOCS3 downregulating YAP leads to decreased expression of PD-L1. (A) Representative Western blot image of the level of PD-L1 in parental cells H1975, PC9GR4, PC9, and these three cell lines with stably expressing SOCS3, H1975-SOCS3, PC9GR4-SOCS3, and PC9-SOCS3. The experiment was repeated, and similar results were obtained. (B) Representative Western blot image of the level of PD-L1 in H1975 and PC9GR4 cells treated with verteporfin at gradient concentrations. The experiment was repeated, and similar results were obtained.

**A**

CSF-1 (PC9 / PC9-SOCS3)

CSF-1 (PC9GR4 / PC9GR4-SOCS3)

CSF-1 (H1975 / H1975-SOCS3)

CXCL5 (H1975 / H1975-SOCS3)

CCL2 (H1975 / H1975-SOCS3)

**B**
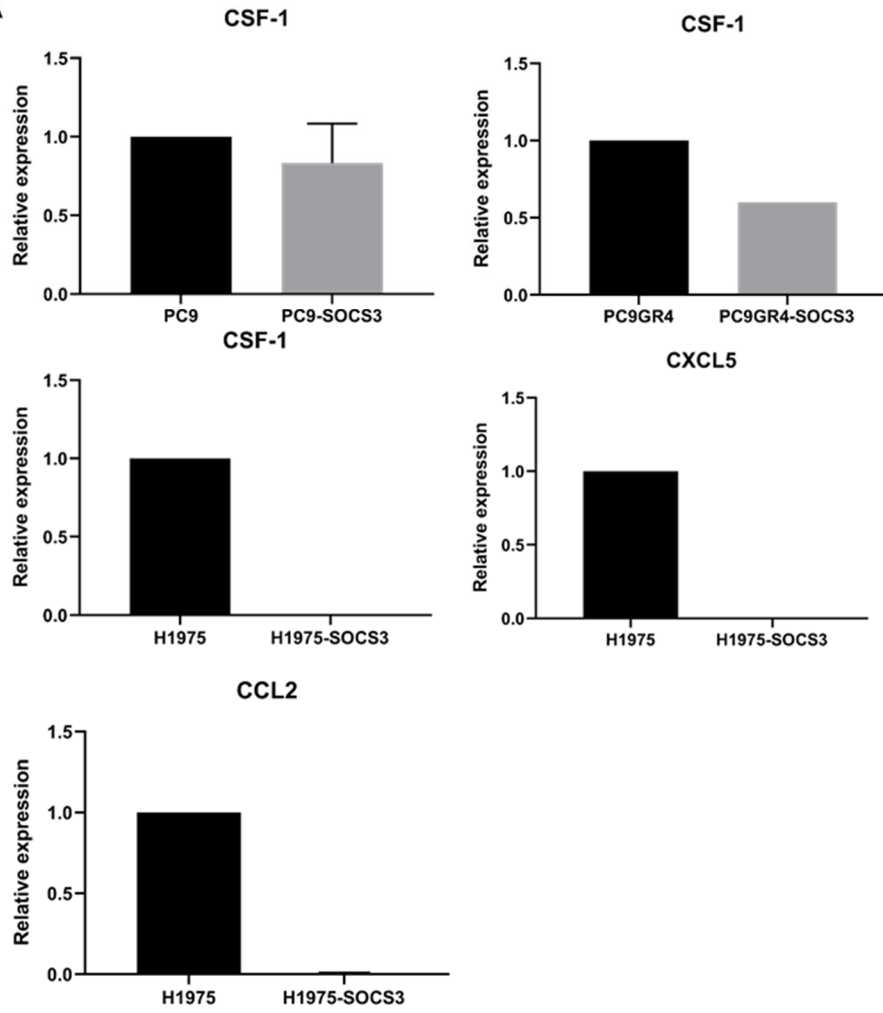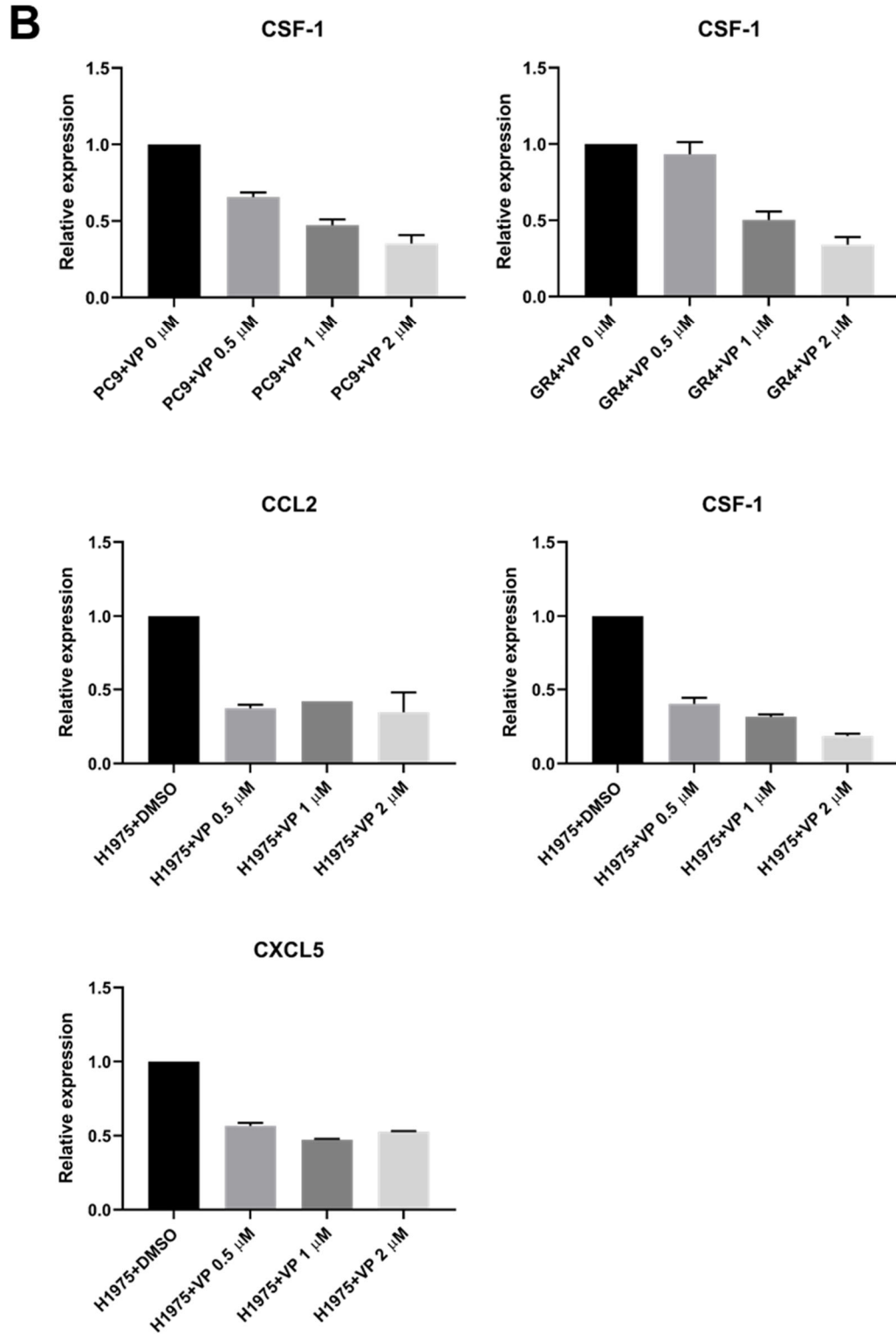


**Figure 4.8** SOCS3 downregulating YAP leads to reduced secretion of immunosuppressive and angiogenic cytokines. (A) Quantitative PCR analysis of

133

the relative mRNA levels of CSF-1, CXCL5, and CCL2 in parental cells H1975, PC9GR4, PC9, and these three cell lines with stably expressing SOCS3, H1975-SOCS3, PC9GR4-SOCS3, and PC9-SOCS3. The mRNA levels are expressed relative to the parental cells (means ± SD, n=3). Human 18S was utilized as internal control. (B) Quantitative PCR analysis of the relative mRNA levels of CSF-1, CXCL5, and CCL2 in H1975, PC9GR4, PC9 cells treated with verteporfin at gradient concentrations. The mRNA levels are expressed relative to the control (non-treated) cells (means ± SD, n=3). Human 18S was utilized as internal control.
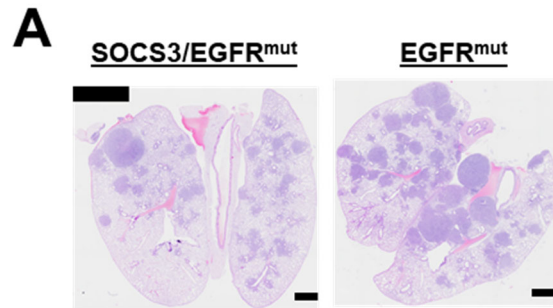
**Figure 4.9** SOCS3 overexpression inhibits tumorigenesis. Representative images of mouse lung section H&E staining from the EGFR$^{mut}$ mice and the SOCS3/EGFR$^{mut}$ mice 17 weeks post viral activation. Scale bar: 1 mm.
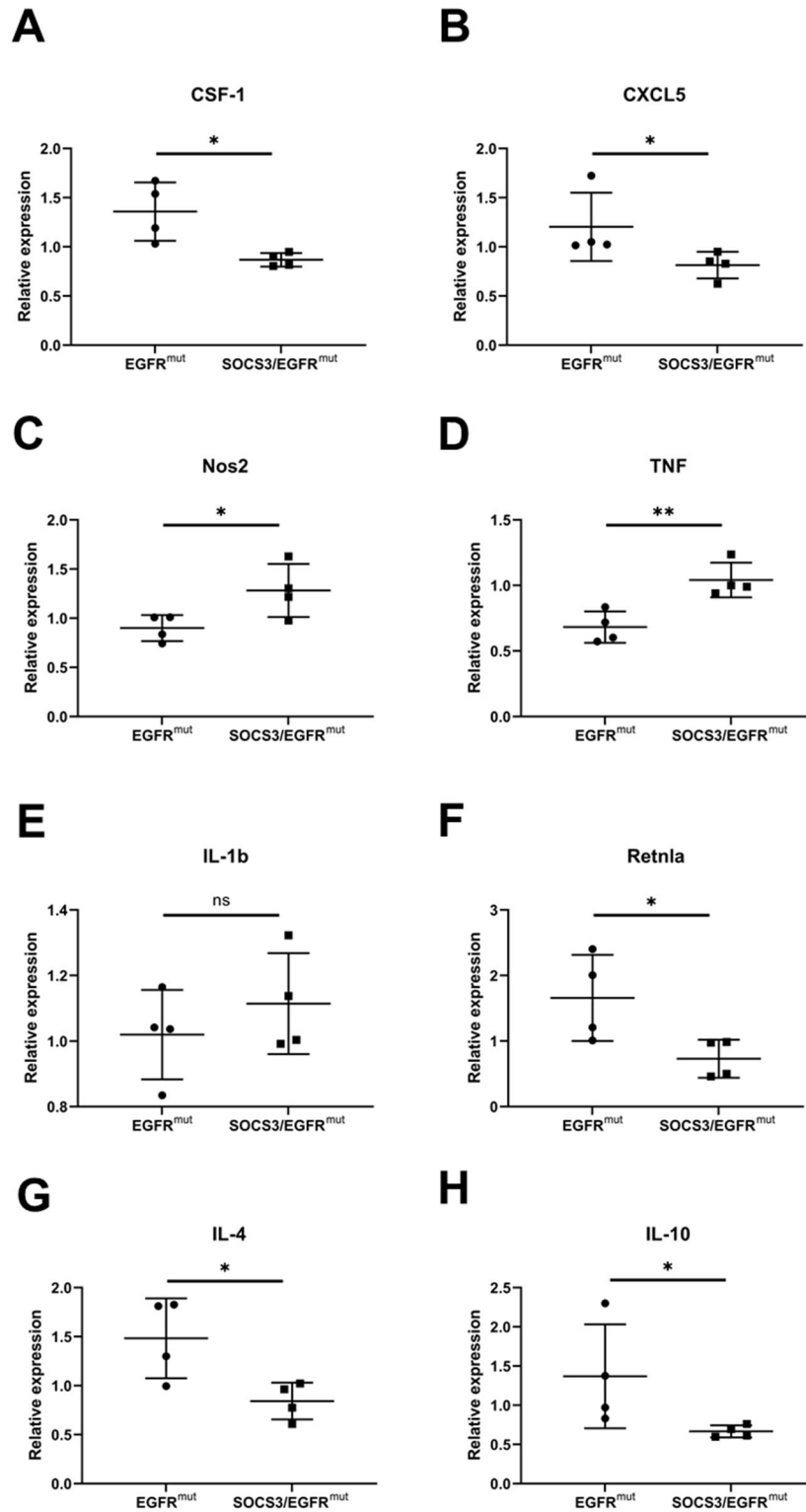
**Figure 4.10** SOCS3 overexpression inhibits tumorigenesis by modulating tumor

microenvironment. (A-H) Quantitative PCR analysis of the relative mRNA levels of

CSF-1, CXCL5, NOS2, TNF, IL-1b, Retnla, IL-4, IL-10 in the lungs of the EGFR$^{mut}$

mice and the SOCS3/ EGFR$^{mut}$ mice. The samples of the SOCS3/ EGFR$^{mut}$ mice

were used as the control groups. The mRNA levels of the samples are expressed

relative to the control (means ± SD, n=4), * $p < 0.05$, ** $p < 0.01$. Murine β-actin

was utilized as internal control.
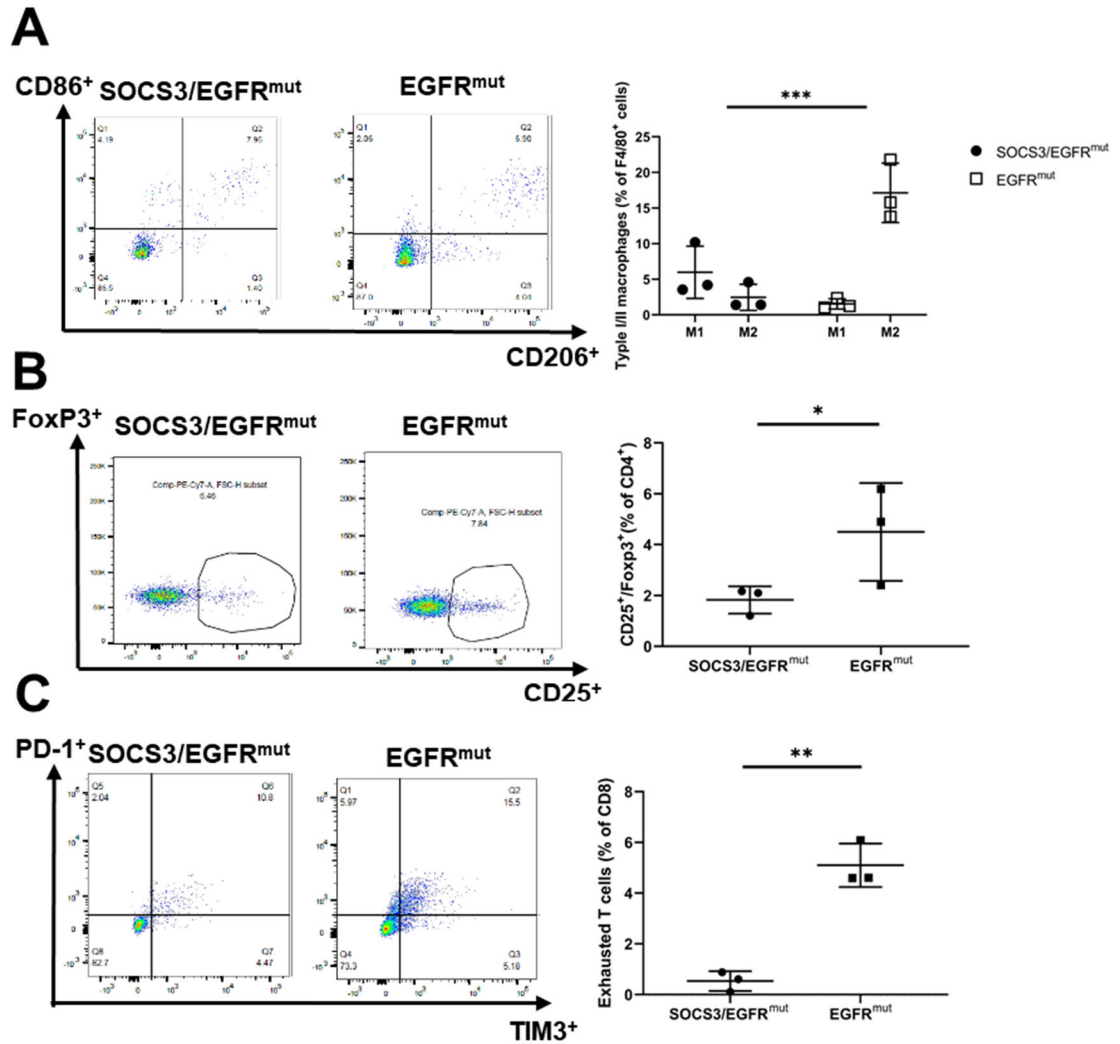
**Figure 4.11** SOCS3 overexpression inhibits tumorigenesis by modulating tumor microenvironment. Representative images of flow cytometry analysis for the cell populations within the lungs of the EGFR^mut mice and the SOCS3/ EGFR^mut mice. The cell populations of the interests are expressed as the percentage of F4/80+ cells (A), CD4+ (B), and CD8+ (C) cells (means ± SD, n=4), * $p < 0.05$, ** $p < 0.01$, *** $p < 0.001$.
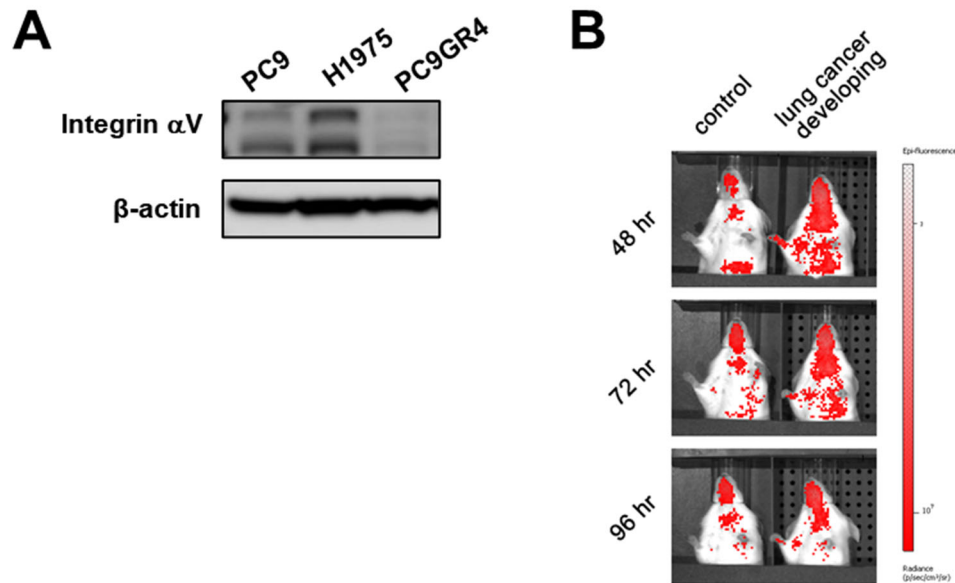
**Figure 4.12** Targeting integrin $\alpha$V increases specificity of the nanoparticles. (A) Representative Western blot image of the level of integrin $\alpha$V in H1975, PC9GR4, and PC9 cells. The experiment was repeated, and similar results were obtained. (B) Representative images showing the accumulation of Cy7.5-labeled GRD-nanoparticles in the lungs of the EGFR$^{mut}$ mice without viral induction (control) and with viral induction (lung cancer developing). The Cy7.5-labeld RGD-nanoparticles were injected into the mice through tail veins. Live animal fluorescence imaging was carried out at 48, 72, and 96 hr post injection, respectively. The mouse abdominal part was covered with a black plastic board for better fluorescence imaging. The experiment was repeated, and similar results were obtained.
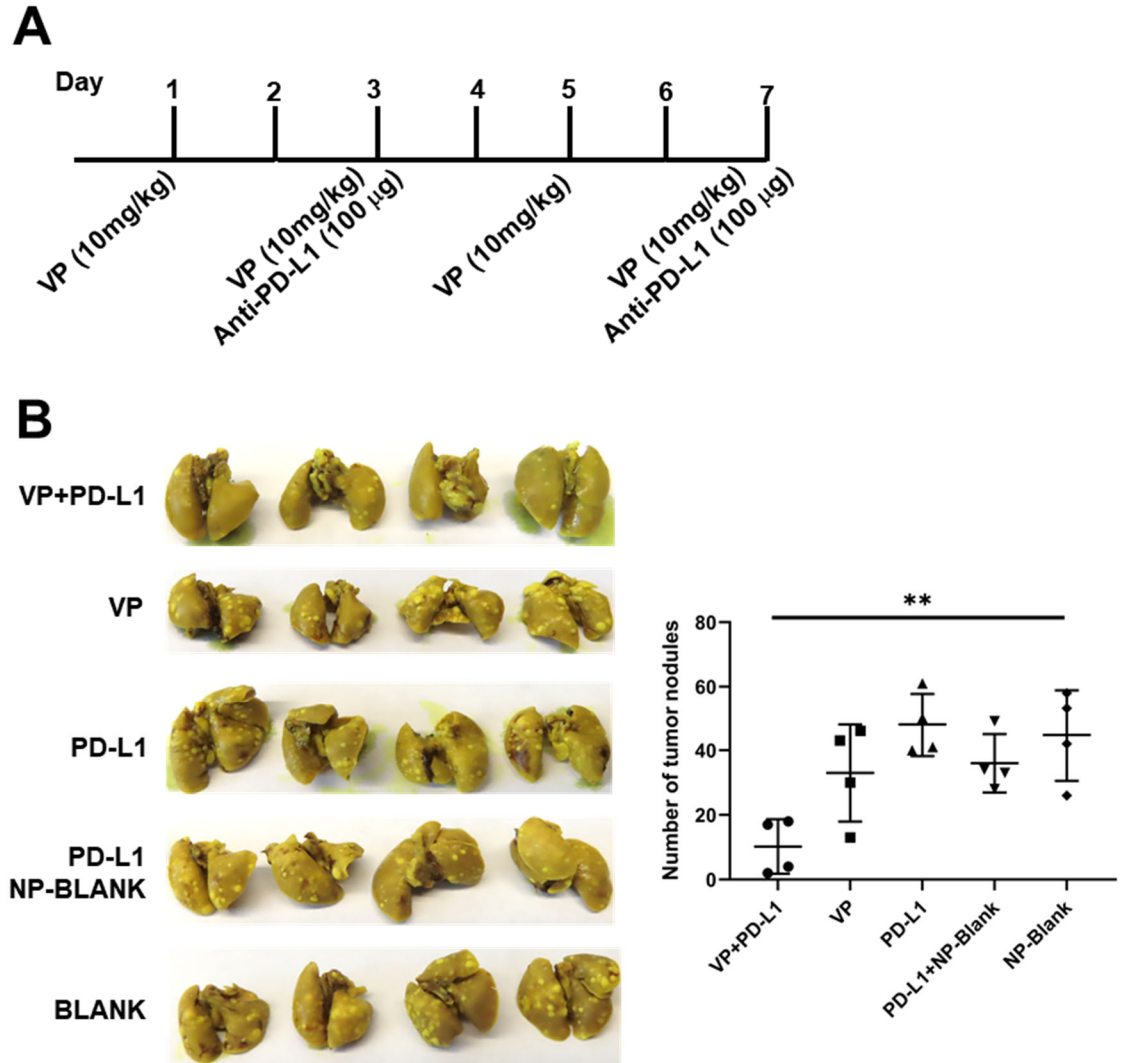
**Figure 4.13** Targeting YAP and its downstream signaling decreases tumor formation. (A) Therapeutic regimen for the EGFR$^{mut}$ mice with lung cancer development in progress. The mice were randomly distributed to the following five groups: verteporfin encapsulated in GRD-nanoparticles (VP-NP) alone, anti-PD-L1 antibody (PD-L1) alone, combination of VP-NP and PD-L1, combination of blank GRD-nanoparticles (NP-blank) and PD-L1, and PBS (blank). VP-NP, NP-blank, and blank were administered 3 times a week through tail vein injection, and PD-L1 was administered twice a week through intraperitoneal injection. (B) Images

of the Bouin's stained lungs of the EGFR$^{mut}$ mice from each group. The tumor

nodules were counted and presented as means ± SD (n=4), ** $p < 0.01$.
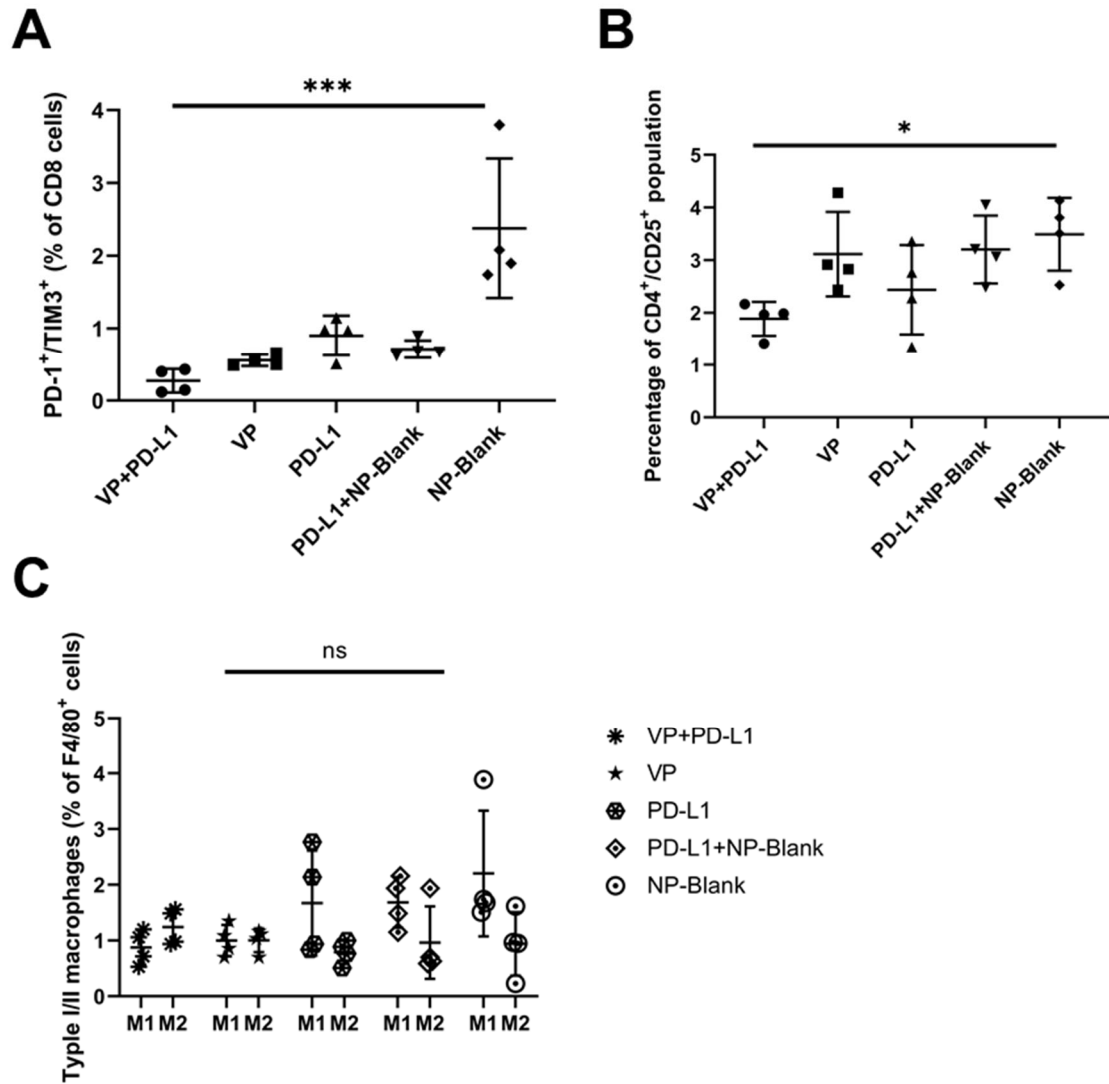
**Figure 4.14** Targeting YAP and its downstream signaling decreases tumor formation. The results of flow cytometry analysis for the cell populations within the lungs of the EGFR$^{mut}$ mice from each therapeutic group. The cell populations of the interests are expressed as the percentage of CD8$^+$ cells (A), CD4$^+$ cells (B), and F4/80$^+$ cells (C) (means ± SD, n=4), * $p < 0.05$, *** $p < 0.001$.
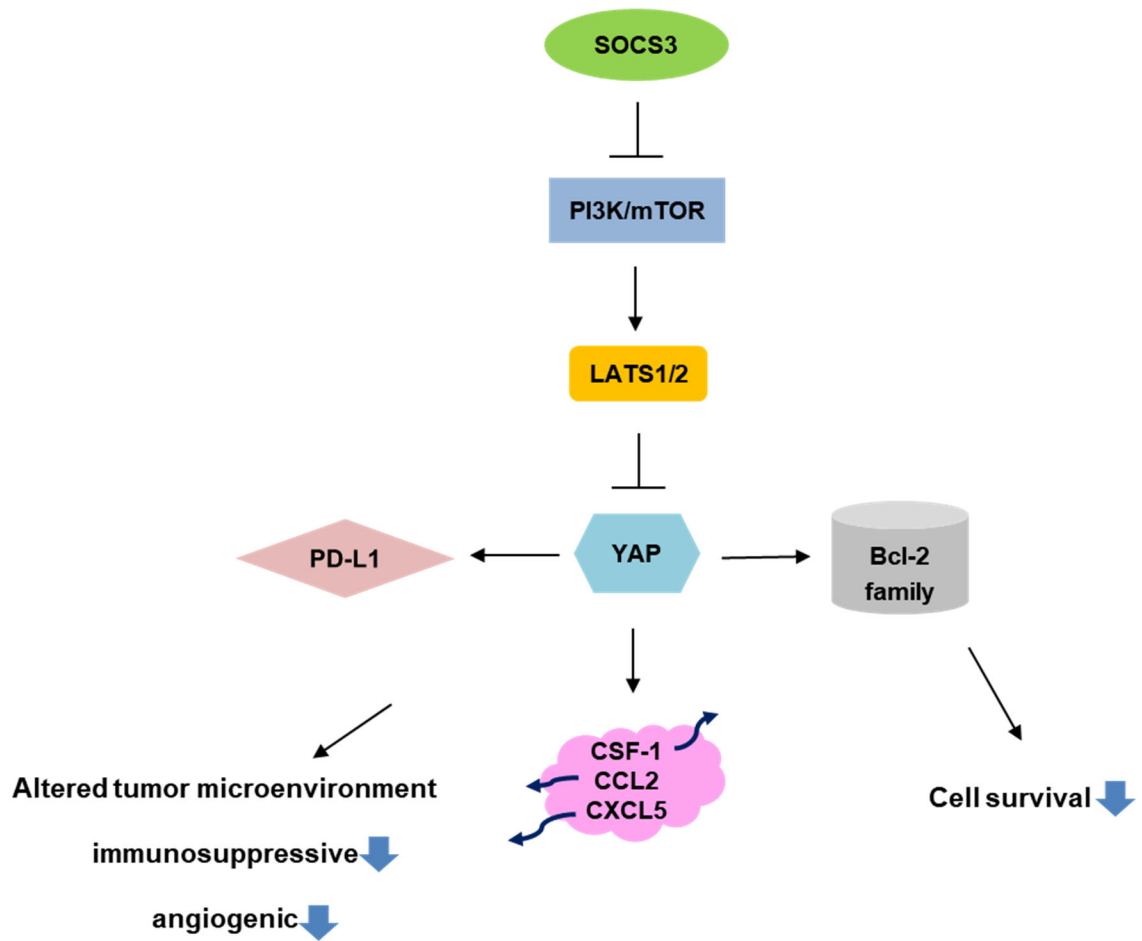
**Figure 4.15** A schematic summary of the mechanism of SOCS3 inhibiting cancer cell survival and reversing oncolytic immune environment through YAP downregulation.

# REFERENCES

1.3 References

Aquino NB, Sevigny MB, Sabangan J, Louie MC. The role of cadmium and nickel in estrogen receptor signaling and breast cancer: metalloestrogens or not? J Environ Sci Health C Environ Carcinog Ecotoxicol Rev. 2012;30(3):189-224. doi: 10.1080/10590501.2012.705159. PMID: 22970719; PMCID: PMC3476837.

Awadalla A, Mortada WI, Abol-Enein H, Shokeir AA. Correlation between blood levels of cadmium and lead and the expression of microRNA-21 in Egyptian bladder cancer patients. Heliyon. 2020 Dec 5;6(12):e05642. doi: 10.1016/j.heliyon.2020.e05642. PMID: 33313435; PMCID: PMC7721616.

Benbrahim-Tallaa L, Waterland RA, Dill AL, Webber MM, Waalkes MP. Tumor suppressor gene inactivation during cadmium-induced malignant transformation of human prostate cells correlates with overexpression of de novo DNA methyltransferase. Environ Health Perspect. 2007 Oct;115(10):1454-9. doi: 10.1289/ehp.10207. PMID: 17938735; PMCID: PMC2022656.

Bethune G, Bethune D, Ridgway N, Xu Z. Epidermal growth factor receptor (EGFR) in lung cancer: an overview and update. J Thorac Dis. 2010 Mar;2(1):48-51. PMID: 22263017; PMCID: PMC3256436.

Birchmeier C, Birchmeier W, Gherardi E, Vande Woude GF. Met, metastasis, motility and more. Nat Rev Mol Cell Biol. 2003 Dec;4(12):915-25. doi: 10.1038/nrm1261. PMID: 14685170.

Bizoń A, Jędryczko K, Milnerowicz H. The role of metallothionein in oncogenesis and cancer treatment. Postepy Hig Med Dosw (Online). 2017 Feb 14;71(0):98-109. doi: 10.5604/01.3001.0010.3794. PMID: 28258670.

Cao X, Fu M, Bi R, Zheng X, Fu B, Tian S, Liu C, Li Q, Liu J. Cadmium induced BEAS-2B cells apoptosis and mitochondria damage via MAPK signaling pathway. Chemosphere. 2021 Jan;263:128346. doi: 10.1016/j.chemosphere.2020.128346. Epub 2020 Sep 17. PMID: 33297271.

Castellanos E, Feld E, Horn L. Driven by Mutations: The Predictive Value of Mutation Subtype in EGFR-Mutated Non-Small Cell Lung Cancer. J Thorac Oncol. 2017 Apr;12(4):612-623. doi: 10.1016/j.jtho.2016.12.014. Epub 2016 Dec 23. PMID: 28017789.

Chakraborty PK, Scharner B, Jurasovic J, Messner B, Bernhard D, Thévenod F. Chronic cadmium exposure induces transcriptional activation of the Wnt pathway and upregulation of epithelial-to-mesenchymal transition markers in mouse kidney. Toxicol Lett. 2010 Sep 15;198(1):69-76. doi: 10.1016/j.toxlet.2010.05.007. Epub 2010 May 15. PMID: 20478370.

Chen C, Xun P, Nishijo M, He K. Cadmium exposure and risk of lung cancer: a meta-analysis of cohort and case-control studies among general and occupational populations. J Expo Sci Environ Epidemiol. 2016 Sep;26(5):437-44. doi: 10.1038/jes.2016.6. Epub 2016 Mar 9. PMID: 26956937.

Cherian MG, Jayasurya A, Bay BH. Metallothioneins in human tumors and potential roles in carcinogenesis. Mutat Res. 2003 Dec 10;533(1-2):201-9. doi: 10.1016/j.mrfmmm.2003.07.013. PMID: 14643421.

Choi YW, Jeon SY, Jeong GS, Lee HW, Jeong SH, Kang SY, Park JS, Choi JH, Koh YW, Han JH, Sheen SS. EGFR Exon 19 Deletion is Associated With Favorable Overall Survival After First-line Gefitinib Therapy in Advanced Non-Small Cell Lung Cancer Patients. Am J Clin Oncol. 2018 Apr;41(4):385-390. doi: 10.1097/COC.0000000000000282. PMID: 26967328.

da Cunha Santos G, Shepherd FA, Tsao MS. EGFR mutations and lung cancer. Annu Rev Pathol. 2011;6:49-69. doi: 10.1146/annurev-pathol-011110-130206. PMID: 20887192.

Dasgupta P, Kulkarni P, Bhat NS, Majid S, Shiina M, Shahryari V, Yamamura S, Tanaka Y, Gupta RK, Dahiya R, Hashimoto Y. Activation of the Erk/MAPK signaling pathway is a driver for cadmium induced prostate cancer. Toxicol Appl Pharmacol. 2020 Aug 15;401:115102. doi: 10.1016/j.taap.2020.115102. Epub 2020 Jun 6. PMID: 32512071; PMCID: PMC7425797.

de Sousa VML, Carvalho L. Heterogeneity in Lung Cancer. Pathobiology. 2018;85(1-2):96-107. doi: 10.1159/000487440. Epub 2018 Apr 10. PMID: 29635240.

Djordjevic VR, Wallace DR, Schweitzer A, Boricic N, Knezevic D, Matic S, Grubor N, Kerkez M, Radenkovic D, Bulat Z, Antonijevic B, Matovic V, Buha A. Environmental cadmium exposure and pancreatic cancer: Evidence from case control, animal and in vitro studies. Environ Int. 2019 Jul;128:353-361. doi: 10.1016/j.envint.2019.04.048. Epub 2019 May 8. PMID: 31078004.

Fisher OS, Boggon TJ. Signaling pathways and the cerebral cavernous malformations proteins: lessons from structural biology. Cell Mol Life Sci. 2014 May;71(10):1881-92. doi: 10.1007/s00018-013-1532-9. Epub 2013 Nov 29. PMID: 24287896; PMCID: PMC3999170.

Gao M, Li C, Xu M, Liu Y, Cong M, Liu S. LncRNA MT1DP Aggravates Cadmium-Induced Oxidative Stress by Repressing the Function of Nrf2 and is Dependent on Interaction with miR-365. Adv Sci (Weinh). 2018 Apr 24;5(7):1800087. doi: 10.1002/advs.201800087. PMID: 30027041; PMCID: PMC6051394.

Garcia-Morales P, Saceda M, Kenney N, Kim N, Salomon DS, Gottardis MM, Solomon HB, Sholler PF, Jordan VC, Martin MB. Effect of cadmium on estrogen receptor levels and estrogen-induced responses in human breast cancer cells. J Biol Chem. 1994 Jun 17;269(24):16896-901. PMID: 8207012.

Ghosh K, Chatterjee B, Behera P, Kanade SR. The carcinogen cadmium elevates CpG-demethylation and enrichment of NFYA and E2F1 in the promoter of oncogenic PRMT5 and EZH2 methyltransferases resulting in their elevated expression in vitro. Chemosphere. 2020 Mar;242:125186. doi: 10.1016/j.chemosphere.2019.125186. Epub 2019 Oct 23. PMID: 31675590.

Go H, Jeon YK, Park HJ, Sung SW, Seo JW, Chung DH. High MET gene copy number leads to shorter survival in patients with non-small cell lung cancer. J Thorac Oncol. 2010 Mar;5(3):305-13. doi: 10.1097/JTO.0b013e3181ce3d1d. PMID: 20107422.

Harrison PT, Vyse S, Huang PH. Rare epidermal growth factor receptor (EGFR) mutations in non-small cell lung cancer. Semin Cancer Biol. 2020 Apr;61:167-179. doi: 10.1016/j.semcancer.2019.09.015. Epub 2019 Sep 25. PMID: 31562956; PMCID: PMC7083237.

He RZ, Jiang J, Luo DX. The functions of N6-methyladenosine modification in lncRNAs. Genes Dis. 2020 Mar 19;7(4):598-605. doi: 10.1016/j.gendis.2020.03.005. PMID: 33335959; PMCID: PMC7729116.

He X, Chen MG, Ma Q. Activation of Nrf2 in defense against cadmium-induced oxidative stress. Chem Res Toxicol. 2008 Jul;21(7):1375-83. doi: 10.1021/tx800019a. Epub 2008 May 31. PMID: 18512965.

Heuberger DM, Schuepbach RA. Protease-activated receptors (PARs): mechanisms of action and potential therapeutic modulators in PAR-driven inflammatory diseases. Thromb J. 2019 Mar 29;17:4. doi: 10.1186/s12959-

019-0194-8. Erratum in: Thromb J. 2019 Nov 6;17:22. PMID: 30976204; PMCID: PMC6440139.

Hong W, Wu Q, Zhang J, Zhou Y. Prognostic value of EGFR 19-del and 21-L858R mutations in patients with non-small cell lung cancer. Oncol Lett. 2019 Oct;18(4):3887-3895. doi: 10.3892/ol.2019.10715. Epub 2019 Aug 6. PMID: 31516600; PMCID: PMC6732961.

Hsu JM, Chen CT, Chou CK, Kuo HP, Li LY, Lin CY, Lee HJ, Wang YN, Liu M, Liao HW, Shi B, Lai CC, Bedford MT, Tsai CH, Hung MC. Crosstalk between Arg 1175 methylation and Tyr 1173 phosphorylation negatively modulates EGFR-mediated ERK activation. Nat Cell Biol. 2011 Feb;13(2):174-81. doi: 10.1038/ncb2158. Epub 2011 Jan 23. PMID: 21258366; PMCID: PMC3048027.

Hu K, Li K, Lv J, Feng J, Chen J, Wu H, Cheng F, Jiang W, Wang J, Pei H, Chiao PJ, Cai Z, Chen Y, Liu M, Pang X. Suppression of the SLC7A11/glutathione axis causes synthetic lethality in KRAS-mutant lung adenocarcinoma. J Clin Invest. 2020 Apr 1;130(4):1752-1766. doi: 10.1172/JCI124049. PMID: 31874110; PMCID: PMC7108883.

Huang Q, Lu Q, Chen B, Shen H, Liu Q, Zhou Z, Lei Y. LncRNA-MALAT1 as a novel biomarker of cadmium toxicity regulates cell proliferation and apoptosis. Toxicol Res (Camb). 2017 Mar 17;6(3):361-371. doi: 10.1039/c6tx00433d. PMID: 30090505; PMCID: PMC6062301.

Huff MO, Todd SL, Smith AL, Elpers JT, Smith AP, Murphy RD, Bleser-Shartzer AS, Hoerter JE, Radde BN, Klinge CM. Arsenite and Cadmium Activate MAPK/ERK via Membrane Estrogen Receptors and G-Protein Coupled Estrogen Receptor Signaling in Human Lung Adenocarcinoma Cells. Toxicol Sci. 2016 Jul;152(1):62-71. doi: 10.1093/toxsci/kfw064. Epub 2016 Apr 12. PMID: 27071941.

Ikediobi CO, Badisa VL, Ayuk-Takem LT, Latinwo LM, West J. Response of antioxidant enzymes and redox metabolites to cadmium-induced oxidative stress in CRL-1439 normal rat liver cells. Int J Mol Med. 2004 Jul;14(1):87-92. PMID: 15202021.

Jackman DM, Yeap BY, Sequist LV, Lindeman N, Holmes AJ, Joshi VA, Bell DW, Huberman MS, Halmos B, Rabin MS, Haber DA, Lynch TJ, Meyerson M, Johnson BE, Jänne PA. Exon 19 deletion mutations of epidermal growth factor receptor are associated with prolonged survival in non-small cell lung

cancer patients treated with gefitinib or erlotinib. Clin Cancer Res. 2006 Jul 1;12(13):3908-14. doi: 10.1158/1078-0432.CCR-06-0462. PMID: 16818686.

Ju H, Arumugam P, Lee J, Song JM. Impact of Environmental Pollutant Cadmium on the Establishment of a Cancer Stem Cell Population in Breast and Hepatic Cancer. ACS Omega. 2017 Feb 28;2(2):563-572. doi: 10.1021/acsomega.6b00181. Epub 2017 Feb 15. PMID: 30023612; PMCID: PMC6044754.

Ju YS, Lee WC, Shin JY, Lee S, Bleazard T, Won JK, Kim YT, Kim JI, Kang JH, Seo JS. A transforming KIF5B and RET gene fusion in lung adenocarcinoma revealed from whole-genome and transcriptome sequencing. Genome Res. 2012 Mar;22(3):436-45. doi: 10.1101/gr.133645.111. Epub 2011 Dec 22. PMID: 22194472; PMCID: PMC3290779.

Kaarbø M, Mikkelsen OL, Malerød L, Qu S, Lobert VH, Akgul G, Halvorsen T, Maelandsmo GM, Saatcioglu F. PI3K-AKT-mTOR pathway is dominant over androgen receptor signaling in prostate cancer cells. Cell Oncol. 2010;32(1-2):11-27. doi: 10.3233/CLO-2009-0487. PMID: 20203370; PMCID: PMC4619056.

Kacew S, Merali Z, Singhal RL. Cadmium: sequential changes in nucleic acid synthesis as well as polyamines and cyclic AMP levels of rat pancreas. Gen Pharmacol. 1976 Dec;7(6):433-5. doi: 10.1016/0306-3623(76)90011-2. PMID: 190083.

Kim HG, Hwang YP, Jeong HG. Metallothionein-III induces HIF-1alpha-mediated VEGF expression in brain endothelial cells. Biochem Biophys Res Commun. 2008 May 2;369(2):666-71. doi: 10.1016/j.bbrc.2008.02.059. Epub 2008 Feb 22. PMID: 18295594.

Kobayashi Y, Mitsudomi T. Not all epidermal growth factor receptor mutations in lung cancer are created equal: Perspectives for individualized treatment strategy. Cancer Sci. 2016 Sep;107(9):1179-86. doi: 10.1111/cas.12996. Epub 2016 Aug 9. PMID: 27323238; PMCID: PMC5021039.

Kojima I, Tanaka T, Inagi R, Nishi H, Aburatani H, Kato H, Miyata T, Fujita T, Nangaku M. Metallothionein is upregulated by hypoxia and stabilizes hypoxia-inducible factor in the kidney. Kidney Int. 2009 Feb;75(3):268-77. doi: 10.1038/ki.2008.488. Epub 2008 Oct 1. PMID: 19148152.

Kolluru V, Pal D, Papu John AMS, Ankem MK, Freedman JH, Damodaran C. Induction of Plac8 promotes pro-survival function of autophagy in cadmium-induced prostate carcinogenesis. Cancer Lett. 2017 Nov 1;408:121-129. doi: 10.1016/j.canlet.2017.08.023. Epub 2017 Aug 24. PMID: 28844710; PMCID: PMC7521630.

Kolluru V, Tyagi A, Chandrasekaran B, Damodaran C. Profiling of differentially expressed genes in cadmium-induced prostate carcinogenesis. Toxicol Appl Pharmacol. 2019 Jul 15;375:57-63. doi: 10.1016/j.taap.2019.05.008. Epub 2019 May 11. PMID: 31082426; PMCID: PMC6554726.

Kulkarni P, Dasgupta P, Bhat NS, Hashimoto Y, Saini S, Shahryari V, Yamamura S, Shiina M, Tanaka Y, Dahiya R, Majid S. Role of the PI3K/Akt pathway in cadmium induced malignant transformation of normal prostate epithelial cells. Toxicol Appl Pharmacol. 2020 Dec 15;409:115308. doi: 10.1016/j.taap.2020.115308. Epub 2020 Oct 29. PMID: 33129824; PMCID: PMC7726053.

Kumarswamy R, Volkmann I, Thum T. Regulation and function of miRNA-21 in health and disease. RNA Biol. 2011 Sep-Oct;8(5):706-13. doi: 10.4161/rna.8.5.16154. Epub 2011 Jul 7. PMID: 21712654; PMCID: PMC3256347.

Kundu S, Sengupta S, Bhattacharyya A. EGFR upregulates inflammatory and proliferative responses in human lung adenocarcinoma cell line (A549), induced by lower dose of cadmium chloride. Inhal Toxicol. 2011 May;23(6):339-48. doi: 10.3109/08958378.2011.572931. PMID: 21605009.

Lamb LE, Zarif JC, Miranti CK. The androgen receptor induces integrin α6β1 to promote prostate tumor cell survival via NF-κB and Bcl-xL Independently of PI3K signaling. Cancer Res. 2011 Apr 1;71(7):2739-49. doi: 10.1158/0008-5472.CAN-10-2745. Epub 2011 Feb 10. PMID: 21310825; PMCID: PMC6878780.

Lawal AO, Marnewick JL, Ellis EM. Heme oxygenase-1 attenuates cadmium-induced mitochondrial-caspase 3- dependent apoptosis in human hepatoma cell line. BMC Pharmacol Toxicol. 2015 Dec 15;16:41. doi: 10.1186/s40360-015-0040-y. PMID: 26670903; PMCID: PMC4681021.

Leonetti A, Facchinetti F, Rossi G, Minari R, Conti A, Friboulet L, Tiseo M, Planchard D. BRAF in non-small cell lung cancer (NSCLC): Pickaxing another brick in the wall. Cancer Treat Rev. 2018 May;66:82-94. doi: 10.1016/j.ctrv.2018.04.006. Epub 2018 Apr 24. PMID: 29729495.

Leonetti A, Sharma S, Minari R, Perego P, Giovannetti E, Tiseo M. Resistance mechanisms to osimertinib in EGFR-mutated non-small cell lung cancer. Br J Cancer. 2019 Oct;121(9):725-737. doi: 10.1038/s41416-019-0573-8. Epub 2019 Sep 30. PMID: 31564718; PMCID: PMC6889286.

Liang Y, Pi H, Liao L, Tan M, Deng P, Yue Y, Xi Y, Tian L, Xie J, Chen M, Luo Y, Chen M, Wang L, Yu Z, Zhou Z. Cadmium promotes breast cancer cell proliferation, migration and invasion by inhibiting ACSS2/ATG5-mediated autophagy. Environ Pollut. 2021 Jan 15;273:116504. doi: 10.1016/j.envpol.2021.116504. Epub ahead of print. PMID: 33486244.

Liu Q, Zheng C, Shen H, Zhou Z, Lei Y. MicroRNAs-mRNAs Expression Profile and Their Potential Role in Malignant Transformation of Human Bronchial Epithelial Cells Induced by Cadmium. Biomed Res Int. 2015;2015:902025. doi: 10.1155/2015/902025. Epub 2015 Oct 4. PMID: 26504844; PMCID: PMC4609416.

Macdonald-Obermann JL, Pike LJ. Different epidermal growth factor (EGF) receptor ligands show distinct kinetics and biased or partial agonism for homodimer and heterodimer formation. J Biol Chem. 2014 Sep 19;289(38):26178-26188. doi: 10.1074/jbc.M114.586826. Epub 2014 Aug 1. PMID: 25086039; PMCID: PMC4176247.

Malhotra J, Malvezzi M, Negri E, La Vecchia C, Boffetta P. Risk factors for lung cancer worldwide. Eur Respir J. 2016 Sep;48(3):889-902. doi: 10.1183/13993003.00359-2016. Epub 2016 May 12. PMID: 27174888.

McEvoy SH, Halpenny DF, Viteri-Jusué A, Hayes SA, Plodkowski AJ, Riely GJ, Ginsberg MS. Investigation of patterns of nodal metastases in BRAF mutant lung cancer. Lung Cancer. 2017 Jun;108:62-65. doi: 10.1016/j.lungcan.2017.02.024. Epub 2017 Mar 1. PMID: 28625649; PMCID: PMC5538145.

Nagasaka M, Gadgeel SM. Role of chemotherapy and targeted therapy in early-stage non-small cell lung cancer. Expert Rev Anticancer Ther. 2018 Jan;18(1):63-70. doi: 10.1080/14737140.2018.1409624. Epub 2017 Nov 26. PMID: 29168933; PMCID: PMC6863145.

Nguyen LK, Kolch W, Kholodenko BN. When ubiquitination meets phosphorylation: a systems biology perspective of EGFR/MAPK signalling. Cell Commun Signal. 2013 Jul 31;11:52. doi: 10.1186/1478-811X-11-52. PMID: 23902637; PMCID: PMC3734146.

Pal D, Suman S, Kolluru V, Sears S, Das TP, Alatassi H, Ankem MK, Freedman JH, Damodaran C. Inhibition of autophagy prevents cadmium-induced prostate carcinogenesis. Br J Cancer. 2017 Jun 27;117(1):56-64. doi: 10.1038/bjc.2017.143. Epub 2017 Jun 6. PMID: 28588318; PMCID: PMC5520206.

Palazon A, Tyrakis PA, Macias D, Veliça P, Rundqvist H, Fitzpatrick S, Vojnovic N, Phan AT, Loman N, Hedenfalk I, Hatschek T, Lövrot J, Foukakis T, Goldrath AW, Bergh J, Johnson RS. An HIF-1α/VEGF-A Axis in Cytotoxic T Cells Regulates Tumor Progression. Cancer Cell. 2017 Nov 13;32(5):669-683.e5. doi: 10.1016/j.ccell.2017.10.003. PMID: 29136509; PMCID: PMC5691891.

Peng S, Wang R, Zhang X, Ma Y, Zhong L, Li K, Nishiyama A, Arai S, Yano S, Wang W. EGFR-TKI resistance promotes immune escape in lung cancer via increased PD-L1 expression. Mol Cancer. 2019 Nov 20;18(1):165. doi: 10.1186/s12943-019-1073-4. PMID: 31747941; PMCID: PMC6864970.

Person RJ, Tokar EJ, Xu Y, Orihuela R, Ngalame NN, Waalkes MP. Chronic cadmium exposure in vitro induces cancer cell characteristics in human lung cells. Toxicol Appl Pharmacol. 2013 Dec 1;273(2):281-8. doi: 10.1016/j.taap.2013.06.013. Epub 2013 Jun 26. PMID: 23811327; PMCID: PMC3863781.

Prajapati A, Chauhan G, Shah H, Gupta S. Oncogenic transformation of human benign prostate hyperplasia with chronic cadmium exposure. J Trace Elem Med Biol. 2020 Dec;62:126633. doi: 10.1016/j.jtemb.2020.126633. Epub 2020 Aug 7. PMID: 32818862.

Qu T, Mou Y, Dai J, Zhang X, Li M, Gu S, He Z. Changes and relationship of $N^6$-methyladenosine modification and long non-coding RNAs in oxidative damage induced by cadmium in pancreatic β-cells. Toxicol Lett. 2021 Jun 1;343:56-66. doi: 10.1016/j.toxlet.2021.02.014. Epub 2021 Feb 24. PMID: 33639196.

Qu W, Diwan BA, Reece JM, Bortner CD, Pi J, Liu J, Waalkes MP. Cadmium-induced malignant transformation in rat liver cells: role of aberrant oncogene expression and minimal role of oxidative stress. Int J Cancer. 2005 Apr 10;114(3):346-55. doi: 10.1002/ijc.20736. PMID: 15551354.

Ren C, Ren L, Yan J, Bai Z, Zhang L, Zhang H, Xie Y, Li X. Cadmium causes hepatopathy by changing the status of DNA methylation in the metabolic

pathway. Toxicol Lett. 2021 Apr 1;340:101-113. doi: 10.1016/j.toxlet.2020.12.009. Epub 2020 Dec 15. PMID: 33338565.

Rivera GA, Wakelee H. Lung Cancer in Never Smokers. Adv Exp Med Biol. 2016;893:43-57. doi: 10.1007/978-3-319-24223-1_3. PMID: 26667338.

Rossi A, Di Maio M. Platinum-based chemotherapy in advanced non-small-cell lung cancer: optimal number of treatment cycles. Expert Rev Anticancer Ther. 2016 Jun;16(6):653-60. doi: 10.1586/14737140.2016.1170596. Epub 2016 Apr 8. PMID: 27010977.

Schwartz GG, Reis IM. Is cadmium a cause of human pancreatic cancer? Cancer Epidemiol Biomarkers Prev. 2000 Feb;9(2):139-45. PMID: 10698473.

Shi H, Sun X, Kong A, Ma H, Xie Y, Cheng D, Wong CKC, Zhou Y, Gu J. Cadmium induces epithelial-mesenchymal transition and migration of renal cancer cells by increasing PGE2 through a cAMP/PKA-COX2 dependent mechanism. Ecotoxicol Environ Saf. 2021 Jan 1;207:111480. doi: 10.1016/j.ecoenv.2020.111480. Epub 2020 Oct 30. PMID: 33254385.

Singh B, Carpenter G, Coffey RJ. EGF receptor ligands: recent advances. F1000Res. 2016 Sep 8;5:F1000 Faculty Rev-2270. doi: 10.12688/f1000research.9025.1. PMID: 27635238; PMCID: PMC5017282.

Skipper A, Sims JN, Yedjou CG, Tchounwou PB. Cadmium Chloride Induces DNA Damage and Apoptosis of Human Liver Carcinoma Cells via Oxidative Stress. Int J Environ Res Public Health. 2016 Jan 2;13(1):88. doi: 10.3390/ijerph13010088. PMID: 26729151; PMCID: PMC4730479.

Somerville RP, Jungers KA, Apte SS. Discovery and characterization of a novel, widely expressed metalloprotease, ADAMTS10, and its proteolytic activation. J Biol Chem. 2004 Dec 3;279(49):51208-17. doi: 10.1074/jbc.M409036200. Epub 2004 Sep 7. PMID: 15355968.

Sone T, Koizumi S, Kimura M. Cadmium-induced synthesis of metallothioneins in human lymphocytes and monocytes. Chem Biol Interact. 1988;66(1-2):61-70. doi: 10.1016/0009-2797(88)90041-5. PMID: 3383288.

Suda K, Onozato R, Yatabe Y, Mitsudomi T. EGFR T790M mutation: a double role in lung cancer cell survival? J Thorac Oncol. 2009 Jan;4(1):1-4. doi: 10.1097/JTO.0b013e3181913c9f. PMID: 19096299.

Sun JM, Won YW, Kim ST, Kim JH, Choi YL, Lee J, Park YH, Ahn JS, Park K, Ahn MJ. The different efficacy of gefitinib or erlotinib according to epidermal growth factor receptor exon 19 and exon 21 mutations in Korean non-small cell lung cancer patients. J Cancer Res Clin Oncol. 2011 Apr;137(4):687-94. doi: 10.1007/s00432-010-0928-2. Epub 2010 Jun 16. PMID: 20552223.

Sun X, Fontaine JM, Bartl I, Behnam B, Welsh MJ, Benndorf R. Induction of Hsp22 (HspB8) by estrogen and the metalloestrogen cadmium in estrogen receptor-positive breast cancer cells. Cell Stress Chaperones. 2007 Winter;12(4):307-19. doi: 10.1379/csc-276.1. PMID: 18229450; PMCID: PMC2134793.

Sun Y, Zong C, Liu J, Zeng L, Li Q, Liu Z, Li Y, Zhu J, Li L, Zhang C, Zhang W. C-myc promotes miR-92a-2-5p transcription in rat ovarian granulosa cells after cadmium exposure. Toxicol Appl Pharmacol. 2021 Jun 15;421:115536. doi: 10.1016/j.taap.2021.115536. Epub 2021 Apr 15. PMID: 33865896.

't Mannetje A, Bencko V, Brennan P, Zaridze D, Szeszenia-Dabrowska N, Rudnai P, Lissowska J, Fabiánová E, Cassidy A, Mates D, Foretova L, Janout V, Fevotte J, Fletcher T, Boffetta P. Occupational exposure to metal compounds and lung cancer. Results from a multi-center case-control study in Central/Eastern Europe and UK. Cancer Causes Control. 2011 Dec;22(12):1669-80. doi: 10.1007/s10552-011-9843-3. Epub 2011 Sep 30. PMID: 21960145.

Takiguchi M, Achanzar WE, Qu W, Li G, Waalkes MP. Effects of cadmium on DNA-(Cytosine-5) methyltransferase activity and DNA methylation status during cadmium-induced cellular transformation. Exp Cell Res. 2003 Jun 10;286(2):355-65. doi: 10.1016/s0014-4827(03)00062-4. PMID: 12749863.

Tanwar VS, Zhang X, Jagannathan L, Jose CC, Cuddapah S. Cadmium exposure upregulates SNAIL through miR-30 repression in human lung epithelial cells. Toxicol Appl Pharmacol. 2019 Jun 15;373:1-9. doi: 10.1016/j.taap.2019.04.011. Epub 2019 Apr 16. PMID: 30998937; PMCID: PMC6547378.

Turley AE, Zagorski JW, Kennedy RC, Freeborn RA, Bursley JK, Edwards JR, Rockwell CE. Chronic low-level cadmium exposure in rats affects cytokine production by activated T cells. Toxicol Res (Camb). 2019 Jan 4;8(2):227-237. doi: 10.1039/c8tx00194d. PMID: 30997022; PMCID: PMC6425995.

Venza M, Visalli M, Biondo C, Oteri R, Agliano F, Morabito S, Teti D, Venza I. Epigenetic marks responsible for cadmium-induced melanoma cell

overgrowth. Toxicol In Vitro. 2015 Feb;29(1):242-50. doi: 10.1016/j.tiv.2014.10.020. PMID: 25448810.

Wallace DR, Spandidos DA, Tsatsakis A, Schweitzer A, Djordjevic V, Djordjevic AB. Potential interaction of cadmium chloride with pancreatic mitochondria: Implications for pancreatic cancer. Int J Mol Med. 2019 Jul;44(1):145-156. doi: 10.3892/ijmm.2019.4204. Epub 2019 May 21. PMID: 31115542; PMCID: PMC6559323.

Wang Y, Mandal AK, Son YO, Pratheeshkumar P, Wise JTF, Wang L, Zhang Z, Shi X, Chen Z. Roles of ROS, Nrf2, and autophagy in cadmium-carcinogenesis and its prevention by sulforaphane. Toxicol Appl Pharmacol. 2018 Aug 15;353:23-30. doi: 10.1016/j.taap.2018.06.003. Epub 2018 Jun 6. PMID: 29885333; PMCID: PMC6281793.

[1]Wang Y, Shi L, Li J, Li L, Wang H, Yang H. Long-term cadmium exposure promoted breast cancer cell migration and invasion by up-regulating TGIF. Ecotoxicol Environ Saf. 2019 Jul 15;175:110-117. doi: 10.1016/j.ecoenv.2019.03.046. Epub 2019 Mar 18. PMID: 30897409.

[2]Wang Y, Shi L, Li J, Wang H, Yang H. The roles of TG-interacting factor in cadmium exposure-promoted invasion and migration of lung cancer cells. Toxicol In Vitro. 2019 Dec;61:104630. doi: 10.1016/j.tiv.2019.104630. Epub 2019 Aug 19. PMID: 31437537.

Warren GW, Cummings KM. Tobacco and lung cancer: risks, trends, and outcomes in patients with cancer. Am Soc Clin Oncol Educ Book. 2013:359-64. doi: 10.14694/EdBook_AM.2013.33.359. PMID: 23714547.

Wei Z, Shaikh ZA. Cadmium stimulates metastasis-associated phenotype in triple-negative breast cancer cells through integrin and β-catenin signaling. Toxicol Appl Pharmacol. 2017 Aug 1;328:70-80. doi: 10.1016/j.taap.2017.05.017. Epub 2017 May 17. PMID: 28527916; PMCID: PMC5547749.

Wells A. EGF receptor. Int J Biochem Cell Biol. 1999 Jun;31(6):637-43. doi: 10.1016/s1357-2725(99)00015-1. PMID: 10404636.

Wierzowiecka B, Gomulkiewicz A, Cwynar-Zajac L, Olbromski M, Grzegrzolka J, Kobierzycki C, Podhorska-Okolow M, Dziegiel P. Expression of Metallothionein and Vascular Endothelial Growth Factor Isoforms in Breast Cancer Cells. In Vivo. 2016 May-Jun;30(3):271-8. PMID: 27107086.

Xiao C, Liu Y, Xie C, Tu W, Xia Y, Costa M, Zhou X. Cadmium induces histone H3 lysine methylation by inhibiting histone demethylase activity. Toxicol Sci. 2015 May;145(1):80-9. doi: 10.1093/toxsci/kfv019. Epub 2015 Feb 10. PMID: 25673502; PMCID: PMC4833035.

[1]Yang S, Zhang Z, Wang Q. Emerging therapies for small cell lung cancer. J Hematol Oncol. 2019 May 2;12(1):47. doi: 10.1186/s13045-019-0736-3. PMID: 31046803; PMCID: PMC6498593.

[2]Yang X, Chen J, Liao Y, Huang L, Wen C, Lin M, Li W, Zhu Y, Wu X, Iwamoto A, Wang Z, Liu H. MiR-27b-3p promotes migration and invasion in colorectal cancer cells by targeting HOXA10. Biosci Rep. 2019 Dec 20;39(12):BSR20191087. doi: 10.1042/BSR20191087. PMID: 31763673; PMCID: PMC6900470.

Yarden Y, Sliwkowski MX. Untangling the ErbB signalling network. Nat Rev Mol Cell Biol. 2001 Feb;2(2):127-37. doi: 10.1038/35052073. PMID: 11252954.

Yuan D, Ye S, Pan Y, Bao Y, Chen H, Shao C. Long-term cadmium exposure leads to the enhancement of lymphocyte proliferation via down-regulating p16 by DNA hypermethylation. Mutat Res. 2013 Oct 9;757(2):125-31. doi: 10.1016/j.mrgentox.2013.07.007. Epub 2013 Aug 12. PMID: 23948183.

Yun CH, Mengwasser KE, Toms AV, Woo MS, Greulich H, Wong KK, Meyerson M, Eck MJ. The T790M mutation in EGFR kinase causes drug resistance by increasing the affinity for ATP. Proc Natl Acad Sci U S A. 2008 Feb 12;105(6):2070-5. doi: 10.1073/pnas.0709662105. Epub 2008 Jan 28. PMID: 18227510; PMCID: PMC2538882.

Zhai H, Pan T, Yang H, Wang H, Wang Y. Cadmium induces A549 cell migration and invasion by activating ERK. Exp Ther Med. 2019 Sep;18(3):1793-1799. doi: 10.3892/etm.2019.7750. Epub 2019 Jul 8. PMID: 31410139; PMCID: PMC6676085.

Zhang Y, Guo S, Wang S, Li X, Hou D, Li H, Wang L, Xu Y, Ma B, Wang H, Jiang X. LncRNA OIP5-AS1 inhibits ferroptosis in prostate cancer with long-term cadmium exposure through miR-128-3p/SLC7A11 signaling. Ecotoxicol Environ Saf. 2021 Sep 1;220:112376. doi: 10.1016/j.ecoenv.2021.112376. Epub 2021 May 26. PMID: 34051661.

Zhong P, Liu J, Li H, Lin S, Zeng L, Luo L, Wu M, Zhang W. MicroRNA-204-5p regulates apoptosis by targeting Bcl2 in rat ovarian granulosa cells exposed

to cadmium†. Biol Reprod. 2020 Aug 21;103(3):608-619. doi: 10.1093/biolre/ioaa091. PMID: 32500147.

Zhou Z, Huang Z, Chen B, Lu Q, Cao L, Chen W. LncRNA-ENST00000446135 is a novel biomarker of cadmium toxicity in 16HBE cells, rats, and Cd-exposed workers and regulates DNA damage and repair. Toxicol Res (Camb). 2020 Dec 10;9(6):823-834. doi: 10.1093/toxres/tfaa088. PMID: 33447366; PMCID: PMC7786176.

## 2.6 REFERENCES

Achanzar WE, Diwan BA, Liu J, Quader ST, Webber MM, Waalkes MP. Cadmium-induced malignant transformation of human prostate epithelial cells. Cancer Research. 61: 455-458.

Akerstrom M, Barregard L, Lundh T, Sallsten G. 2013. The relationship between cadmium in kidney and cadmium in urine and blood in an environmentally exposed population. Toxicology and Applied Pharmacology. 268 (3): 286-293.

Alama A, Gangemi R, Ferrini S, Barisione G, Orengo AM, Truini M, Bello MG, Grossi F. CD133-Positive Cells from Non-Small Cell Lung Cancer Show Distinct Sensitivity to Cisplatin and Afatinib. Arch Immunol Ther Exp (Warsz). 2015 Jun;63(3):207-14. doi: 10.1007/s00005-015-0330-5. Epub 2015 Feb 13. PMID: 25678473.

Ali I, Damdimopoulou P, Stenius U, Halldin K. 2015. Cadmium at nanomolar concentrations activates Raf-MEK-ERK1/2 MAPKs signaling via EGFR in human cancer cell line. Chemico-Biological Interactions. 231 (2015):44-52.

Baloch S, Kazi TG, Baig JA, Afridi HI, Arain MB. 2020. Occupational exposure of lead and cadmium on adolescent and adult workers of battery recycling and welding workshops: adverse impact on health. Science of the Total Environment. 720: 137549.

Bertolini G, Roz L, Perego P, Tortoreto M, Fontanella E, Gatti L, Pratesi G, Fabbri A, Andriani F, Tinelli S, Roz E, Caserini R, Lo Vullo S, Camerini T, Mariani L, Delia D, Calabrò E, Pastorino U, Sozzi G. Highly tumorigenic lung cancer CD133+ cells display stem-like features and are spared by cisplatin treatment. Proc Natl Acad Sci U S A. 2009 Sep 22;106(38):16281-6. doi: 10.1073/pnas.0905653106. Epub 2009 Sep 10. PMID: 19805294; PMCID: PMC2741477.

Chen J, Wang X-F, Qin Y-C, Gong Y-B, Wang L, Li N-C. 2020. Downregulation of long non-coding RNA *DUXAP10* inhibits proliferation, migration, and invasion of renal cell carcinoma. European Review for Medical and Pharmacological Sciences. 24 (21): 11041-11051.

Cheng W-C, Chang C-Y, Lo C-C, Hsieh C-Y, Kuo T-T, Tseng G-C, Wong S-C, Chiang S-F, Kuang K C-Y, Lai L-C, Lu T-P, Chao KSC, Sher Y-P. 2021.

Identification of theranostic factors for patients developing metastasis after surgery for early-stage lung adenocarcinoma. Theranostics. 11 (8): 3661-3675.

Chi Y, Wang D, Wang J, Yu W, Yang J. Long Non-Coding RNA in the Pathogenesis of Cancers. Cells. 2019 Sep 1;8(9):1015. doi: 10.3390/cells8091015. PMID: 31480503; PMCID: PMC6770362.

Clementino M, Xie J, Yang P, Li Y, Lin H-P, Fenske WK, Tao H, Kondo K, Yang C, Wang Z. 2020. A positive feedback loop between c-Myc upregulation, glycolytic shift, and histone acetylation enhances cancer stem cell-like property and tumorigenicity of Cr(VI)-transformed cells. Toxicological Sciences. 177 (1): 71-83.

Cui Y, Wang W, Yao S, Qiu Z, Cong L. 2021. Relationship between circulating lung-specific X protein messenger ribonucleic acid expression and micrometastasis and prognosis in patients with early-stage nonsmall cell lung cancer. Journal of Cancer Research and Therapeutics. DOI: 10.4103/jcrt.JCRT_1007_20.

Dai J, Ji Y, Wang W, Kim D, Fai LY, Wang L, Luo J, Zhang Z. 2017. Loss of fructose-1,6-bisphosphatase induces glycolysis and promotes apoptosis resistance of cancer-stem like cells: an important role in hexavalent chromium-induced carcinogenesis. Toxicology and Applied Pharmacology.331 (2017):164-173.

Dasgupta P, Kulkani P, Bhat N, Majid S, Shiina M, Shahryari V, Yamamura S, Tanaka Y, Gupta R, Dahiya R, Hashimoto Y. 2020. Activation of the Erk/MAPK signaling pathway is a driver for cadmium induced prostate cancer. Toxicology and Applied Pharmacology. 401 (2020) 115120.

Dontu G, Abdallah WM, Foley JM, Jackson KW, Clarke MF, Kawamura MJ, Wicha MS. 2003. In vitro propagation and transcriptional profiling of human mammary stem/progenitor cells. Genes & Development. 17: 1253-1270.

Dykes IM, Emanueli C. Transcriptional and Post-transcriptional Gene Regulation by Long Non-coding RNA. Genomics Proteomics Bioinformatics. 2017 Jun;15(3):177-186. doi: 10.1016/j.gpb.2016.12.005. Epub 2017 May 19. PMID: 28529100; PMCID: PMC5487525.

Feng Yi, Hu X, Zhang Y, Zhang D, Li C, Zhang L. 2014. Methods for the study of long noncoding RNA in cancer cell signaling. Methods in Molecular Biology. 1165: 115-143.

Gao N, Li Y, Li J, Gao Z, Yang Z, Li Y, Liu H, Fan T. 2020. Long non-coding RNAs: the regulatory mechanisms, research strategies, and future directions in cancers. Frontiers in Oncology. 10: 598817.

Gao Y-S, Liu X-Z, Zhang Y-G, Liu X-J, Li L-Z. 2018. knockdown of long noncoding RNA LUCAT1 inhibits cell viability and invasion by regulating miR-375 in Glioma. Oncology Research. 26: 307-313.

Golovine K, Makov P, Uzzo RG, Kutikov A, Kaplan DJ, Fox E, Kolenko VM. 2010. Cadmium down-regulates expression of XIAP at the post-transcriptional level in prostate cancer cells through an NF-kB-independent, proteome-mediated mechanism. Molecular Cancer. 9:183.

Han K, Li C, Zhang X, Shang L. 2019. *DUXAP10* inhibition attenuates the proliferation and metastasis of hepatocellular carcinoma cells by regulation of the Wnt/β-catenin and PI3K/AKT signaling pathways. Bioscience Reports. 39 (5): BSR20181457.

Han P-B, Ji X-J, Zhang M, Gao L-Y. 2018. Upregulation of lncRNA LINC00473 promotes radioresistance of HNSCC cells through activating Wnt/β-catenin signaling pathway. European Review for Medical and Pharmacological Sciences. 22 (21): 7305-7313.

Hu N, Chen L, Li Q, Zhao H. 2019. LncRNA HOTAIRM1 is involved in the progression of acute myeloid leukemia through targeting miR0148b. RSC Advances. 9: 10352-10359.

Huang Q, Lu Q, Chen B, Shen H, Liu Q, Zhou Z, Lei Y. 2017. LncRNA-MALAT as a novel biomarker of cadmium toxicity regulates cell proliferation and apoptosis. Toxicological Research. 6: 361-371.

Huff J, Lunn R, Waalkes M, Tomatis L, Infante P. 2007. Cadmium-induced cancers in animals and in humans. International Journal of Occupational and Environmental Health. 13 (2): 202-212.

Huntzicker EG, Estay IS, Zhen H, Lokteva LA, Jackson PK, Oro AE. 2005. Dual degradation signals control Gli protein stability and tumor formation. Genes & Development. 20: 276-281.

Incardona JP, Gaffield W, Kapur RP, Roelink H. 1998. The teratogenic Veratrum alkaloid cyclopamine inhibits sonic hedgehog signal transduction. Development. 125: 3553-3562.

Jiang Q, Xing W, Cheng J, Yu Y. 2020. Knockdown of lncRNA XIST suppresses cell tumorigenicity in human non-small cell lung cancer by regulating miR-142-5p/Pax6 axis. OncoTragets and Therapy. 13: 4919-4929.

Jinag N, Zhang X, Gu X, Li X, Shang L. 2021. Progress in understanding the role of lncRNA in programmed cell death. Cell Death Discovery. (2021) 7: 30.

Jing Y, Liu L-Z, Jiang Y, Zhu Y, Guo NL, Barnett J, Rojanasakul Y, Agani F, Jiang B-H. 2012. Cadmium increases HIF-1 and VEGF expression through ROS, ERK, and AKT signaling pathways and induces malignant transformation of human bronchial epithelial cells. Toxicological Sciences. 125 (1): 10-19.

Kiselev Y, Anderson S, Johannessen C, Fjukstad B, Olsen KS, Stenvold H, Al-Saad S, Donnem T, Richardsen E, Bremnes RM, Busund L-T R. 2018. Transcription factor Pax6 as a novel prognostic factor and putative tumor suppressor in non small cell lung cancer. Scientific Reports. 8: 5059.

Li C, Chen X, Liu T, Chen G. 2021. LncRNA HOTAIRM1 regulates cell proliferation and the metastasis of thyroid cancer by targeting Wnt10b. Oncology Reports. 45: 1083-1093.

Li J, Jiang L, Liu Z, Li Y, Xu Y, Liu H. 2020. Oncogenic pseudogene *DUXAP10* knockdown suppresses proliferation and invasion and induces apoptosis of papillary thyroid carcinoma cells by inhibition of Akt/mTOR

pathway. Clinical and Experimental Pharmacology and Physiology. 47 (8): 1473-1483.

Li J, Meng H, Bai Y, Wang K. Regulation of lncRNA and Its Role in Cancer Metastasis. Oncol Res. 2016;23(5):205-17. doi: 10.3727/096504016X14549667334007. PMID: 27098144; PMCID: PMC7838649.

Li P, Zhang X, Murphy AJ, Costa M, Zhao X, Sun H. 2021. Downregulation of hedgehog-interacting protein (HHIP) contributes to hexavalent chromium-induced malignant transformation of human bronchial epithelial cells. Carcinogenesis. 42 (1):136-147.

Li Q, Dong C, Cui J, Wang Y, Hong X. 2018. Over-expressed lncRNA OTAIRM1 promotes tumor growth and invasion through up-regulating HOXA1 and sequestering G9a/EZH2/Dnmts away from the HOXA1 gene in glioblastoma multiforme. Journal of Experimental & Clinical Cancer Research. 37: 265.

Lian Y, Xu Y, Xiao C, Xia R, Gong H, Yang P, Chen T, Wu D, Cai Z, Zhang J, Wang K. 2017. The pseudogene derived from long non-coding RNA *DUXAP10* promotes colorectal cancer cell growth through epigenetically silencing of p21 and PTEN. Scientific Reports. 7 (1): 7312.

Liang Y, Pi H, Liao L, Tan M, Deng P, Yue Y, Xi Y, Tian L, Xie J, Chen M, Luo Y, Wang L, Yu Z, Zhou Z. 2021. Cadmium promotes breast cancer cell proliferation, migration and invasion by inhibiting ACSS2/ATG5-mediated autophagy. Environmental Pollution. DOI:10.1016/j.envpol.2021.116504.

Liang Z, Zhu R, Li Y, Jiang H, Li R, Tang L, Wang Q, Ren Z. 2020. Differential epigenetic and transcriptional profile in MCF-7 breast cancer cells exposed to cadmium. Chemosphere. DOI: 10.1016/j.chemosphere.2020.128148.

Liu Z, Han L, Yu H, Gao N, Xin H. 2020. LINC01619 promotes non-small cell lung cancer development via regulating Pax6 by suppressing microRNA-129-5p. American Journal of Translational Research. 12 (6): 2538-2553.

Luzon-Toro B, Fernandez RM, Martos-Martinez JM, Rubio-Manzanares-Dorado M, Antinolo G, Borrego S. 2019. LncRNA LUCAT1 as a novel prognostic biomarker for patients with papillary thyroid cancer. Scientific Reports. 9: 14374.

Mercer TR, Mattick JS. Structure and function of long noncoding RNAs in epigenetic regulation. Nat Struct Mol Biol. 2013 Mar;20(3):300-7. doi: 10.1038/nsmb.2480. PMID: 23463315.

Ming H, Li B, Zhou L, Goel A, Huang G. 2021. Long non-coding RNAs and cancer metastasis: molecular basis and therapeutic implications. BBA-Reviews on Cancer. 1875 (2021): 188519.

Misra RR, Smith GT, Waalkes MP. 1998. Evaluation of the direct genotoxic potential of cadmium in four different rodent cell lines. Toxicology. 126 (1998): 103-114.

Miyata T, Oyama T, Yoshimatsu T, Higa H, Kawano D, Sekimura A, Yamashita N, So T, Gotoh A. 2017. The clinical significance of cancer stem cell markers ALDH1A1 and CD133 in lung adenocarcinoma. Anticancer Research. 37: 2541-2547.

Ooki A, Dinalankara W, Marchionni L, Tsay J-C, Goparaju C, Maleki Z, Rom WN, Pass HI, Hoque MO. 2018. Epigenetically regulated Pax6 drives cancer cells toward a stem-like state via GLI-SOX2 signaling axis in lung adenocarcinoma. Oncogene. 37 (45): 5967-5981.

Perona R, Lopez-Ayllon BD, de Castro Carpeno J, Belda-Iniesta C. 2011. A role for cancer stem cells in drug resistance and metastasis in non-small-cell lung cancer. Clinical Translational Oncology. 13: 289-293.

P M MM, Shahi MH, Tayyab M, Farheen S, Khanam N, Tabassum S, Ali A. Cadmium-induced neurodegeneration and activation of noncanonical sonic hedgehog pathway in rat cerebellum. J Biochem Mol Toxicol. 2019 Apr;33(4):e22274. doi: 10.1002/jbt.22274. Epub 2018 Dec 1. PMID: 30506660.

Qian Z, Zhang Q, Hu Y, Zhang T, Li J, Liu Z, Zheng H, Gao Y, Jia W, Hu A, Li B, Hao J. 2018. Investigating the mechanism by which SMAD3 induces Pax6 transcription to promote the development of non-small cell lung cancer. Respiratory Research. 19: 262.

Rudin CM, Brambilla E, Faivre-Finn C, Sage J. 2021. Small-cell lung cancer. Nature Review Disease Primer. (2012) 7: 3.

Shi X, Wang X. 2019. LINC00473 mediates cyclin D1 expression through a balance between activation and repression signals in breast cancer cells. FEBS Letters. 593: 751-759.

Siegel RL, Miller KD, Fuchs HE, Jemal A. 2021. Cancer statistics, 2021. CA CANCER J CLIN. 71: 7-33.

Siegel RL, Miller KD, Jemal A. 2020. Cancer statistics, 2020. CA CANCER J CLIN. 70: 7-30.

Song X, Wei Z, Shaikh Z. 2015. Requirement of Era and basal activities of EGFR and Src kinase in Cd-induced activation of MAPK/ERK pathway in human breast cancer MCF-7 cells. Toxicology and Applied Pharmacology. 287 (2015): 26-34.

Sun L, Wang L, Chen T, Yao B, Wang Y, Li Q, Yang W, Liu Z. 2019. MicroRNA-1914, which is regulated by lncRNA *DUXAP10*, inhibits cell proliferation by targeting the GPR39-mediated PI3K/AKT/mTOR pathway in HCC. Journal of Cellular and Molecular Medicine. 23 (12): 8292-8304.

Venza M, Visalli M, Biondo C, Oteri R, Agliano F, Morabito S, Teti D, Venza I. 2014. Epigenetic marks responsible for cadmium-induced melanoma cell overgrowth. Toxicology in Vitro. 29 (2015):242-250.

Waalkes MP. 2020. Cadmium carcinogenesis in review. Journal of Inorganic Chemistry. 79 (2000): 241-244.

Wang PS, Wang Z, Yang C. Dysregulations of long non-coding RNAs - The emerging "lnc" in environmental carcinogenesis. Semin Cancer Biol. 2021

Apr 3:S1044-579X(21)00079-1. doi: 10.1016/j.semcancer.2021.03.029. Epub ahead of print. PMID: 33823237.

Wang Z and Yang C. 2019. Metal carcinogen exposure induces cancer stem cell-like property through epigenetic reprograming: A novel mechanism of metal carcinogenesis. Seminars in Cancer Biology. 57: 95-104.

Wang X, Li XD, Fu Z, Zhou Y, Huang X, Jiang X. 2019. Long non-coding RNA LINC00473/miR-195-5p promotes glioma progression via YAP1-TEAD1-Hippo signaling. International Journal of Oncology. 56: 508-521.

Wang Z, Lin H-P, Li Y, Tao H, Yang P, Xie J, Maddy D, Kondo K, Yang C. 2019. Chronic hexavalent chromium exposure induces cancer stem cell-like property and tumorigenesis by increasing c-Myc expression. Toxicological Sciences. 172 (2): 252-264.

Wang Z, Ren B, Huang J, Yin R, Jiang F, Zhang Q. 2018. LncRNA *DUXAP10* modulates cell proliferation in esophageal squamous cell carcinoma through epigenetically silencing p21. Cancer Biology & Therapy. 19 (11): 998-1005.

Wang Z, Wu J, Humphries B, Kondo K, Jiang Y, Shi X, Yang C. 2018. Upregulation of histone-lysine methyltransferases plays a causal role in hexavalent chromium-induced cancer stem cell like property and cell transformation. Toxicology and Applied Pharmacology. 342 (2018): 22-30.

Wang Z, Humphries B, Xiao H, Jiang Y, Yang C. 2014. MicroRNA-200b suppresses arsenic-transformed cell migration by targeting protein kinase C$\alpha$ and Wnt5b-protein kinase C$\alpha$ positive feedback loop and inhibiting Rac1 activation. The Journal of Biological Chemistry. 289 (26): 18373-18386.

Wang Z, Zhao Y, Smith E, Goodall GJ, Drew PA, Brabletz T, Yang C. 2011. Reversal and prevention of arsenic-induced human bronchial epithelial cell malignant transformation by microRNA-200b. Toxicological Sciences. 121 (1): 110-122.

Wei C-C, Nie F-Q, Jiang L-L, Chen Q-N, Chen Z-Y, Chen X, Pan X, Liu Z-L, Lu B-B, Wang Z-X. 2017. The pseudogene *DUXAP10* promotes and aggressive phenotype through binding with LSD1 and repressing LATS2 and RRAD in non small cell lung cancer. Oncotarget. 8 (3); 5233-5246.

Wei Z, Shan Z, Shaikh Z. 2018. Epithelial-mesenchymal transition in breast epithelial cells treated with cadmium and the role of Snail. Toxicology and Applied Pharmacology. 344 (2018): 46-55.

Wei Z, Song X, Shaikh Z. 2015. Cadmium promotes the proliferation of triple-negative breast cancer cells through EGFR-mediated cell cycle regulation. Toxicology and Applied Pharmacology. 289 (2015): 98-108.

Wu H, Qi XW, Yan GN, Zhang QB, Xu C, Bian XW. Is CD133 expression a prognostic biomarker of non-small-cell lung cancer? A systematic review and meta-analysis. PLoS One. 2014 Jun 18;9(6):e100168. doi: 10.1371/journal.pone.0100168. PMID: 24940615; PMCID: PMC4062503.

Xiao C, Liu Y, Xie C, Tu W, Xia Y, Costa M, Zhou X. 2015. Cadmium induces histone H3 lysine methylation by inhibiting demethylase activity. Toxicological Sciences. 145 (1): 80-89.

Xu, Y, Yu X, Wei C, Nie F, Huang M, Sun M. 2018. Over-expression of oncogenic pseudogene *DUXAP10* promotes cell proliferation and invasion by regulating LATS1 and b-catenin in gastric cancer. Journal of Experimental & Clinical Cancer Research. 37: 13.

Xu Y, Jiang E, Shao Z, Shang Z. 2021. Long noncoding RNAs in the metastasis of oral squamous cell carcinoma. Frontiers in Oncology. 10: 616717.

Yang C, Liu Y, Lemmon MA, Kazanietz MG. 2006. Essential role for Rac in Heregulin β1 mitogenic signaling: a mechanism that involves epidermal growth factor receptor and is independent of ErbB4. Molecular and Cellular Biology. 26 (3): 831-842.

Yang C, Wu J, Zhang R, Zhang P, Eckard J, Yusuf R, Huang X, Rossman TG, Frenkel K. 2005. Caffeic acid phenethyl ester (CAPE) prevents transformation of human cells by arsenic (As) and suppresses growth of As-transformed cells. Toxicology. 213 (2005): 81-96.

Yao R, Feng W-T, Xu L-J, Zong X-M, Liu H, Zhou L-L. 2018. *DUXAP10* regulates proliferation and apoptosis of chronic myeloid leukemia via PTEN pathway. European Review for Medical and Pharmacological Sciences. 22 (15): 4934-4940.

Yuan D, Ye S, Pan Y, Bao Y, Chen H, Shao C. 2013. Long-term cadmium exposure leads to the enhancement of lymphocyte proliferation via down-regulating p16 by DNA hypermethylation. Mutaion Research/Genetic Toxicology and Environmental Mutagenesis. 757 (2013):125-131.

Yue C, Liang C, Ge H, Yan L, Xu Y, Li G, Li P, Wei Z, Wu J. 2019. Pseudogene *DUXAP10* acts as a diagnostic and prognostic marker and promotes cell proliferation by activating PI3K/AKT pathway in hepatocellular carcinoma. Onco Targets and Therapy. 12: 4555-4566.

Zhang L, Mi L, Xuan Y, Gao C, Wang Y-H, Ming H-X, Liu J. 2018. LncRNA HOTAIRM1 inhibits the progression of hepatocellular carcinoma by inhibiting the Wnt signaling pathway. European Review for Medical and Pharmacological Sciences. 22 (15): 4861-4868.

Zhang Q, Wang G, Xu L, Yao Z, Song L. 2019. Long non-coding RNA LIN00473 promotes glioma cells proliferation and invasion by impairing miR-637/CDK6 axis. Artificial Cells, Nanomedicine, and Biotechnology. 47 (1): 3896-3903.

Zhang W, Song Y. 2018. LINC00473 predicts poor prognosis and regulates cell migration and invasion in gastric cancer. Biomedicine & Pharmacotherapy. 107: 1-6.

Zhang X, Yang X, Wang J, Liang T, Gu Y, Yang D. 2015. Down-regulation of Pax6 by promoter methylation is associated with poor prognosis in non

small cell lung cancer. International Journal of Clinical Experimental Pathology. 8 (9): 11452-11457.

Zhang X, Wang W, Zhu W, Dong J, Cheng Y, Yin Z, Shen F. Mechanisms and Functions of Long Non-Coding RNAs at Multiple Regulatory Levels. Int J Mol Sci. 2019 Nov 8;20(22):5573. doi: 10.3390/ijms20225573. PMID: 31717266; PMCID: PMC6888083.

Zhou Q, Hou Z, Zuo S, Zhou X, Feng Y, Sun Y, Yuan X. 2019. LUCAT1 promotes colorectal cancer tumorigenesis by targeting the ribosomal protein L40-MDM2-p53 pathway through binding with UBA52. Cancer Science. 110: 1194-1207.

Zhou Z, Huang Z, Chen B, Lu Q, Cao L, Chen W. 2020. LncRNA-ENST00000446135 is a novel biomarker of cadmium toxicity in 16HBE cells, rats, and Cd-exposed workers and regulates DNA damage and repair. Toxicological Research. 6: 823-834.

## 3.6 REFERENCES

Al Olayan EM, Aloufi AS, AlAmri OD, El-Habit OH, Abdel Moneim AE. Protocatechuic acid mitigates cadmium-induced neurotoxicity in rats: Role of oxidative stress, inflammation and apoptosis. Sci Total Environ. 2020 Jun 25;723:137969. doi: 10.1016/j.scitotenv.2020.137969. Epub 2020 Mar 16. PMID: 32392679.

Benbrahim-Tallaa L, Waterland RA, Dill AL, Webber MM, Waalkes MP. Tumor suppressor gene inactivation during cadmium-induced malignant transformation of human prostate cells correlates with overexpression of de novo DNA methyltransferase. Environ Health Perspect. 2007 Oct;115(10):1454-9. doi: 10.1289/ehp.10207. PMID: 17938735; PMCID: PMC2022656.

Benetatos L, Dasoula A, Hatzimichael E, Georgiou I, Syrrou M, Bourantas KL. Promoter hypermethylation of the *MEG3* (DLK1/*MEG3*) imprinted gene in multiple myeloma. Clin Lymphoma Myeloma. 2008 Jun;8(3):171-5. doi: 10.3816/CLM.2008.n.021. PMID: 18650181.

Broude, E., Swift, M., Vivo, C. et al. p21[Waf1/Cip1/Sdi1] mediates retinoblastoma protein degradation. Oncogene, 2007 26, 6954–6958. https://doi.org/10.1038/sj.onc.1210516

Budkova Z, Sigurdardottir AK, Briem E, Bergthorsson JT, Sigurdsson S, Magnusson MK, Traustadottir GA, Gudjonsson T, Hilmarsdottir B. Expression of ncRNAs on the DLK1-DIO3 Locus Is Associated With Basal

and Mesenchymal Phenotype in Breast Epithelial Progenitor Cells. Front Cell Dev Biol. 2020 Jun 16;8:461. doi: 10.3389/fcell.2020.00461. PMID: 32612992; PMCID: PMC7308478.

Campanero MR, Flemington EK. Regulation of E2F through ubiquitin-proteasome-dependent degradation: stabilization by the pRB tumor suppressor protein. Proc Natl Acad Sci U S A. 1997 Mar 18;94(6):2221-6. doi: 10.1073/pnas.94.6.2221. PMID: 9122175; PMCID: PMC20068.

Chak WP, Lung RW, Tong JH, Chan SY, Lun SW, Tsao SW, Lo KW, To KF. Downregulation of long non-coding RNA *MEG3* in nasopharyngeal carcinoma. Mol Carcinog. 2017 Mar;56(3):1041-1054. doi: 10.1002/mc.22569. Epub 2016 Oct 20. PMID: 27597634.

Chial, H. (2008) Tumor suppressor (TS) genes and the two-hit hypothesis. Nature Education 1(1):177

Costa C, Santos M, Martínez-Fernández M, Dueñas M, Lorz C, García-Escudero R, Paramio JM. E2F1 loss induces spontaneous tumour development in Rb-deficient epidermis. Oncogene. 2013 Jun 13;32(24):2937-51. doi: 10.1038/onc.2012.316. Epub 2012 Aug 13. PMID: 22890321.

Dan J, Wang J, Wang Y, Zhu M, Yang X, Peng Z, Jiang H, Chen L. LncRNA-*MEG3* inhibits proliferation and metastasis by regulating miRNA-21 in gastric cancer. Biomed Pharmacother. 2018 Mar;99:931-938. doi: 10.1016/j.biopha.2018.01.164. Epub 2018 Feb 20. PMID: 29710493.

Deng C, Zhang P, Harper JW, Elledge SJ, Leder P. Mice lacking p21CIP1/WAF1 undergo normal development, but are defective in G1 checkpoint control. Cell. 1995 Aug 25;82(4):675-84. doi: 10.1016/0092-8674(95)90039-x. PMID: 7664346.

Ding L, Tian Y, Wang L, Bi M, Teng D, Hong S. 2019. Hypermethylated long noncoding RNA *MEG3* promotes the progression of gastric cancer. Aging (Albany NY). 11 (19): 8139-8155.

Doi T, Puri P, McCann A, Bannigan J, Thompson J. Epigenetic effect of cadmium on global de novo DNA hypomethylation in the cadmium-induced ventral body wall defect (VBWD) in the chick model. Toxicol Sci. 2011 Apr;120(2):475-80. doi: 10.1093/toxsci/kfr022. Epub 2011 Jan 27. PMID: 21278052.

Dong Z, Zhang A, Liu S, Lu F, Guo Y, Zhang G, Xu F, Shi Y, Shen S, Liang J, Guo W. 2017. Aberrant methylation-mediated silencing of lncRNA *MEG3*

functions as a ceRNA in esophageal cancer. Molecular Cancer Research. 15 (7): 800-810.

Dontu G, Abdallah WM, Foley JM, Jackson KW, Clarke MF, Kawamura MJ, Wicha MS. In vitro propagation and transcriptional profiling of human mammary stem/progenitor cells. Genes Dev. 2003 May 15;17(10):1253-70. doi: 10.1101/gad.1061803. PMID: 12756227; PMCID: PMC196056.

Gadepalli VS, Deb SP, Deb S, Rao RR. Lung cancer stem cells, p53 mutations and MDM2. Subcell Biochem. 2014;85:359-70. doi: 10.1007/978-94-017-9211-0_19. PMID: 25201204.

Gao Y, Huang P, Zhang J. Hypermethylation of *MEG3* promoter correlates with inactivation of *MEG3* and poor prognosis in patients with retinoblastoma. J Transl Med. 2017 Dec 29;15(1):268. doi: 10.1186/s12967-017-1372-8. PMID: 29287592; PMCID: PMC5747938.

Gartel AL, Radhakrishnan SK. Lost in transcription: p21 repression, mechanisms, and consequences. Cancer Res. 2005 May 15;65(10):3980-5. doi: 10.1158/0008-5472.CAN-04-3995. PMID: 15899785.

Ghosh K, Chatterjee B, Behera P, Kanade SR. The carcinogen cadmium elevates CpG-demethylation and enrichment of NFYA and E2F1 in the promoter of oncogenic PRMT5 and EZH2 methyltransferases resulting in their elevated expression in vitro. Chemosphere. 2020 Mar;242:125186. doi: 10.1016/j.chemosphere.2019.125186. Epub 2019 Oct 23. PMID: 31675590.

Guo W, Dong Z, Liu S, Qiao Y, Kuang G, Guo Y, Shen S, Liang J. 2017. Promoter hypermethylation-mediated downregulation of miR-770 and its host gene *MEG3*, a long non-coding RNA, in the development of gastric cardia adenocarcinoma. Molecular Carcinogenesis. 56 (8): 1924-1934.

Han T, Zhuo M, Yuan C, Xiao X, Cui J, Qin G, Wang L, Jiao F. Coordinated silencing of the Sp1-mediated long noncoding RNA *MEG3* by EZH2 and HDAC3 as a prognostic factor in pancreatic ductal adenocarcinoma. Cancer Biol Med. 2020 Nov 15;17(4):953-969. doi: 10.20892/j.issn.2095-3941.2019.0427. Epub 2020 Dec 15. PMID: 33299646; PMCID: PMC7721101.

Han Z, Yu C, Tian Y, Zeng T, Cui W, Mager J, Wu Q. Expression patterns of long noncoding RNAs from Dlk1-Dio3 imprinted region and the potential mechanisms of Gtl2 activation during blastocyst development. Biochem

Biophys Res Commun. 2015 Jul 31;463(3):167-73. doi: 10.1016/j.bbrc.2015.04.126. Epub 2015 May 22. PMID: 26005002.

Hsieh PF, Yu CC, Chu PM, Hsieh PL. Long Non-Coding RNA *MEG3* in Cellular Stemness. Int J Mol Sci. 2021 May 19;22(10):5348. doi: 10.3390/ijms22105348. PMID: 34069546; PMCID: PMC8161278.

Humphries B, Wang Z, Li Y, Jhan JR, Jiang Y, Yang C. ARHGAP18 Downregulation by miR-200b Suppresses Metastasis of Triple-Negative Breast Cancer by Enhancing Activation of RhoA. Cancer Res. 2017 Aug 1;77(15):4051-4064. doi: 10.1158/0008-5472.CAN-16-3141. Epub 2017 Jun 15. PMID: 28619708.

Iftode A, Drăghici GA, Macașoi I, Marcovici I, Coricovac DE, Dragoi R, Tischer A, Kovatsi L, Tsatsakis AM, Cretu O, Dehelean C. Exposure to cadmium and copper triggers cytotoxic effects and epigenetic changes in human colorectal carcinoma HT-29 cells. Exp Ther Med. 2021 Jan;21(1):100. doi: 10.3892/etm.2020.9532. Epub 2020 Nov 26. PMID: 33363611; PMCID: PMC7725023.

Johnson DG. The paradox of E2F1: oncogene and tumor suppressor gene. Mol Carcinog. 2000 Mar;27(3):151-7. doi: 10.1002/(sici)1098-2744(200003)27:3<151::aid-mc1>3.0.co;2-c. PMID: 10708476.

Kleinjans JC, van Maanen JM, van Schooten FJ. Human respiratory disease: environmental carcinogens and lung cancer risk. Ciba Found Symp. 1993;175:171-8; discussion 178-81. doi: 10.1002/9780470514436.ch10. PMID: 8222989.

Kiran Kumar KM, Naveen Kumar M, Patil RH, Nagesh R, Hegde SM, Kavya K, Babu RL, Ramesh GT, Sharma SC. Cadmium induces oxidative stress and apoptosis in lung epithelial cells. Toxicol Mech Methods. 2016 Nov;26(9):658-666. doi: 10.1080/15376516.2016.1223240. Epub 2016 Nov 6. PMID: 27687512.

Kosaka T, Yatabe Y, Endoh H, Kuwano H, Takahashi T, Mitsudomi T. Mutations of the epidermal growth factor receptor gene in lung cancer: biological and clinical implications. Cancer Res. 2004 Dec 15;64(24):8919-23. doi: 10.1158/0008-5472.CAN-04-2818. PMID: 15604253.

Kruyt FA, Schuringa JJ. Apoptosis and cancer stem cells: Implications for apoptosis targeted therapy. Biochem Pharmacol. 2010 Aug 15;80(4):423-30. doi: 10.1016/j.bcp.2010.04.010. Epub 2010 Apr 13. PMID: 20394737.

166

Küster MM, Schneider MA, Richter AM, Richtmann S, Winter H, Kriegsmann M, Pullamsetti SS, Stiewe T, Savai R, Muley T, Dammann RH. Epigenetic Inactivation of the Tumor Suppressor *IRX1* Occurs Frequently in Lung Adenocarcinoma and Its Silencing Is Associated with Impaired Prognosis. Cancers (Basel). 2020 Nov 26;12(12):3528. doi: 10.3390/cancers12123528. PMID: 33256112; PMCID: PMC7760495.

Lagadinou ED, Sach A, Callahan K, Rossi RM, Neering SJ, Minhajuddin M, Ashton JM, Pei S, Grose V, O'Dwyer KM, Liesveld JL, Brookes PS, Becker MW, Jordan CT. BCL-2 inhibition targets oxidative phosphorylation and selectively eradicates quiescent human leukemia stem cells. Cell Stem Cell. 2013 Mar 7;12(3):329-41. doi: 10.1016/j.stem.2012.12.013. Epub 2013 Jan 17. PMID: 23333149; PMCID: PMC3595363.

Liu X, Zhang Y, Wang Y, Yan Y, Wang J, Gu J, Chun B, Liu Z. Investigation of cadmium-induced apoptosis and the protective effect of N-acetylcysteine in BRL 3A cells. Mol Med Rep. 2016 Jul;14(1):373-9. doi: 10.3892/mmr.2016.5218. Epub 2016 May 6. PMID: 27175572.

Liu Z, Lin H, Gan Y, Cui C, Zhang B, Gu L, Zhou J, Zhu G, Deng D. *P16* Methylation Leads to Paclitaxel Resistance of Advanced Non-Small Cell Lung Cancer. J Cancer. 2019 Apr 5;10(7):1726-1733. doi: 10.7150/jca.26482. PMID: 31205528; PMCID: PMC6547999.

Luo J, Hendryx M. Environmental carcinogen releases and lung cancer mortality in rural-urban areas of the United States. J Rural Health. 2011 Winter;27(4):342-9. doi: 10.1111/j.1748-0361.2010.00357.x. Epub 2011 Jan 11. PMID: 21967377.

Misra RR, Smith GT, Waalkes MP. 1998. Evaluation of the direct genotoxic potential of cadmium in four different rodent cell lines. Toxicology. 126 (1998): 103-114.

Ou L, Wang H, Wu Z, Wang P, Yang L, Li X, Sun K, Zhu X, Zhang R. Effects of cadmium on osteoblast cell line: Exportin 1 accumulation, p-JNK activation, DNA damage and cell apoptosis. Ecotoxicol Environ Saf. 2021 Jan 15;208:111668. doi: 10.1016/j.ecoenv.2020.111668. Epub 2020 Nov 27. PMID: 33396178.

Qin WX, Shi Y, Zhu D, Li YP, Chen YH, Cui J, Cui GY, Pan JX, Ren ZY. EZH2-mediated H3K27me3 enrichment on the lncRNA *MEG3* promoter regulates the growth and metastasis of glioma cells by regulating miR-21-

3p. Eur Rev Med Pharmacol Sci. 2020 Mar;24(6):3204-3214. doi: 10.26355/eurrev_202003_20687. PMID: 32271438.

Qiu B, Wang Y, Tao J, Wang Y. Expression and correlation of Bcl-2 with pathological grades in human glioma stem cells. Oncol Rep. 2012 Jul;28(1):155-60. doi: 10.3892/or.2012.1800. Epub 2012 May 4. PMID: 22562364.

Román M, Baraibar I, López I, Nadal E, Rolfo C, Vicent S, Gil-Bazo I. KRAS oncogene in non-small cell lung cancer: clinical perspectives on the treatment of an old target. Mol Cancer. 2018 Feb 19;17(1):33. doi: 10.1186/s12943-018-0789-x. PMID: 29455666; PMCID: PMC5817724.

Safa AR. Resistance to Cell Death and Its Modulation in Cancer Stem Cells. Crit Rev Oncog. 2016;21(3-4):203-219. doi: 10.1615/CritRevOncog.2016016976. PMID: 27915972; PMCID: PMC5356509.

Shats I, Deng M, Davidovich A, Zhang C, Kwon JS, Manandhar D, Gordân R, Yao G, You L. Expression level is a key determinant of E2F1-mediated cell fate. Cell Death Differ. 2017 Apr;24(4):626-637. doi: 10.1038/cdd.2017.12. Epub 2017 Feb 17. PMID: 28211871; PMCID: PMC5384025.

Sommerkamp P, Renders S, Ladel L, Hotz-Wagenblatt A, Schönberger K, Zeisberger P, Przybylla A, Sohn M, Zhou Y, Klibanski A, Cabezas-Wallscheid N, Trumpp A. The long non-coding RNA *MEG3* is dispensable for hematopoietic stem cells. Sci Rep. 2019 Feb 14;9(1):2110. doi: 10.1038/s41598-019-38605-8. PMID: 30765776; PMCID: PMC6375991.

Tao Y, Yue P, Miao Y, Gao S, Wang B, Leng SX, Meng X, Zhang H. The lncRNA *MEG3*/miR-16-5p/VGLL4 regulatory axis is involved in etoposide-induced senescence of tumor cells. J Gene Med. 2021 Feb;23(2):e3291. doi: 10.1002/jgm.3291. Epub 2020 Dec 22. PMID: 33141998.

Vuillier C, Lohard S, Fétiveau A, Allègre J, Kayaci C, King LE, Braun F, Barillé-Nion S, Gautier F, Dubrez L, Gilmore AP, Juin PP, Maillet L. E2F1 interacts with BCL-xL and regulates its subcellular localization dynamics to trigger cell death. EMBO Rep. 2018 Feb;19(2):234-243. doi: 10.15252/embr.201744046. Epub 2017 Dec 12. PMID: 29233828; PMCID: PMC5797968.

Waalkes MP. 2020. Cadmium carcinogenesis in review. Journal of Inorganic Chemistry. 79 (2000): 241-244.

Wang Z, Humphries B, Xiao H, Jiang Y, Yang C. MicroRNA-200b suppresses arsenic-transformed cell migration by targeting protein kinase Cα and Wnt5b-protein kinase Cα positive feedback loop and inhibiting Rac1 activation. J Biol Chem. 2014 Jun 27;289(26):18373-86. doi: 10.1074/jbc.M114.554246. Epub 2014 May 19. PMID: 24841200; PMCID: PMC4140296.

Wang Z, Zhao Y, Smith E, Goodall GJ, Drew PA, Brabletz T, Yang C. Reversal and prevention of arsenic-induced human bronchial epithelial cell malignant transformation by microRNA-200b. Toxicol Sci. 2011 May;121(1):110-22. doi: 10.1093/toxsci/kfr029. Epub 2011 Feb 2. PMID: 21292642; PMCID: PMC3080188.

Wu Q, Ni X. ROS-mediated DNA methylation pattern alterations in carcinogenesis. Curr Drug Targets. 2015;16(1):13-9. doi: 10.2174/1389450116666150113121054. PMID: 25585126.

Wu X, Li J, Ren Y, Zuo Z, Ni S, Cai J. *MEG3* can affect the proliferation and migration of colorectal cancer cells through regulating miR-376/PRKD1 axis. Am J Transl Res. 2019 Sep 15;11(9):5740-5751. PMID: 31632544; PMCID: PMC6789261.

Wu Z, Yu Q. E2F1-mediated apoptosis as a target of cancer therapy. Curr Mol Pharmacol. 2009 Jun;2(2):149-60. doi: 10.2174/1874467210902020149. PMID: 20021455.

Xu P, Wu Z, Xi Y, Wang L. Epigenetic regulation of placental glucose transporters mediates maternal cadmium-induced fetal growth restriction. Toxicology. 2016 Nov 30;372:34-41. doi: 10.1016/j.tox.2016.10.011. Epub 2016 Oct 27. PMID: 27931521.

Yang C, Liu Y, Lemmon MA, Kazanietz MG. Essential role for Rac in heregulin beta1 mitogenic signaling: a mechanism that involves epidermal growth factor receptor and is independent of ErbB4. Mol Cell Biol. 2006 Feb;26(3):831-42. doi: 10.1128/MCB.26.3.831-842.2006. PMID: 16428439; PMCID: PMC1347034.

Yang C, Wu J, Zhang R, Zhang P, Eckard J, Yusuf R, Huang X, Rossman TG, Frenkel K. Caffeic acid phenethyl ester (CAPE) prevents transformation of human cells by arsenite (As) and suppresses growth of As-transformed

cells. Toxicology. 2005 Sep 15;213(1-2):81-96. doi:
10.1016/j.tox.2005.05.011. PMID: 16085347.

Yang P, Xie J, Li Y, Lin HP, Fenske W, Clementino M, Jiang Y, Yang C, Wang Z.
Deubiquitinase USP7-mediated MCL-1 up-regulation enhances Arsenic
and Benzo(a)pyrene co-exposure-induced Cancer Stem Cell-like property
and Tumorigenesis. Theranostics. 2020 Jul 11;10(20):9050-9065. doi:
10.7150/thno.47897. PMID: 32802178; PMCID: PMC7415806.

Yew TL, Chiu FY, Tsai CC, Chen HL, Lee WP, Chen YJ, Chang MC, Hung SC.
Knockdown of p21(Cip1/Waf1) enhances proliferation, the expression of
stemness markers, and osteogenic potential in human mesenchymal stem
cells. Aging Cell. 2011 Apr;10(2):349-61. doi: 10.1111/j.1474-
9726.2011.00676.x. Epub 2011 Feb 23. PMID: 21342417.

Yuan D, Ye S, Pan Y, Bao Y, Chen H, Shao C. Long-term cadmium exposure
leads to the enhancement of lymphocyte proliferation via down-regulating
p16 by DNA hypermethylation. Mutat Res. 2013 Oct 9;757(2):125-31. doi:
10.1016/j.mrgentox.2013.07.007. Epub 2013 Aug 12. PMID: 23948183.

Zeuner A, Francescangeli F, Contavalli P, Zapparelli G, Apuzzo T, Eramo A,
Baiocchi M, De Angelis ML, Biffoni M, Sette G, Todaro M, Stassi G, De
Maria R. Elimination of quiescent/slow-proliferating cancer stem cells by
Bcl-XL inhibition in non-small cell lung cancer. Cell Death Differ. 2014
Dec;21(12):1877-88. doi: 10.1038/cdd.2014.105. Epub 2014 Jul 18. PMID:
25034785; PMCID: PMC4227145.

Zhang X, Wu N, Wang J, Li Z. LncRNA *MEG3* inhibits cell proliferation and
induces apoptosis in laryngeal cancer via miR-23a/APAF-1 axis. J Cell
Mol Med. 2019 Oct;23(10):6708-6719. doi: 10.1111/jcmm.14549. Epub
2019 Jul 21. PMID: 31328388; PMCID: PMC6787452.

Zhao H, Liu W, Wang Y, Dai N, Gu J, Yuan Y, Liu X, Bian J, Liu ZP. Cadmium
induces apoptosis in primary rat osteoblasts through caspase and
mitogen-activated protein kinase pathways. J Vet Sci. 2015;16(3):297-306.
doi: 10.4142/jvs.2015.16.3.297. Epub 2015 Sep 21. PMID: 26425111;
PMCID: PMC4588015.

Zhou C, Huang C, Wang J, Huang H, Li J, Xie Q, Liu Y, Zhu J, Li Y, Zhang D,
Zhu Q, Huang C. LncRNA *MEG3* downregulation mediated by DNMT3b
contributes to nickel malignant transformation of human bronchial
epithelial cells via modulating PHLPP1 transcription and HIF-1α translation.

Oncogene. 2017 Jul 6;36(27):3878-3889. doi: 10.1038/onc.2017.14. Epub 2017 Mar 6. PMID: 28263966; PMCID: PMC5525547.

## 4.6 REFERENCES

Ando Y, Ohuchida K, Otsubo Y, Kibe S, Takesue S, Abe T, Iwamoto C, Shindo K, Moriyama T, Nakata K, Miyasaka Y, Ohtsuka T, Oda Y, Nakamura M. Necroptosis in pancreatic cancer promotes cancer cell migration and invasion by release of CXCL5. PLoS One. 2020 Jan 30;15(1):e0228015. doi: 10.1371/journal.pone.0228015. PMID: 31999765; PMCID: PMC6991976.

Azad T, Janse van Rensburg HJ, Lightbody ED, Neveu B, Champagne A, Ghaffari A, Kay VR, Hao Y, Shen H, Yeung B, Croy BA, Guan KL, Pouliot F, Zhang J, Nicol CJB, Yang X. A LATS biosensor screen identifies VEGFR as a regulator of the Hippo pathway in angiogenesis. Nat Commun. 2018 Mar 13;9(1):1061. doi: 10.1038/s41467-018-03278-w. PMID: 29535383; PMCID: PMC5849716.

Babon JJ, Varghese LN, Nicola NA. Inhibition of IL-6 family cytokines by SOCS3. Semin Immunol. 2014 Feb;26(1):13-9. doi: 10.1016/j.smim.2013.12.004. Epub 2014 Jan 10. PMID: 24418198; PMCID: PMC3970923.

Barclay JL, Anderson ST, Waters MJ, Curlewis JD. SOCS3 as a tumor suppressor in breast cancer cells, and its regulation by PRL. Int J Cancer. 2009 Apr 15;124(8):1756-66. doi: 10.1002/ijc.24172. PMID: 19115200.

Billing U, Jetka T, Nortmann L, Wundrack N, Komorowski M, Waldherr S, Schaper F, Dittrich A. Robustness and Information Transfer within IL-6-induced JAK/STAT Signalling. Commun Biol. 2019 Jan 18;2:27. doi: 10.1038/s42003-018-0259-4. PMID: 30675525; PMCID: PMC6338669.

Blandin Knight S, Crosbie PA, Balata H, Chudziak J, Hussell T, Dive C. Progress and prospects of early detection in lung cancer. Open Biol. 2017 Sep;7(9):170070. doi: 10.1098/rsob.170070. PMID: 28878044; PMCID: PMC5627048.

Boopathy GTK, Hong W. Role of Hippo Pathway-YAP/TAZ Signaling in Angiogenesis. Front Cell Dev Biol. 2019 Apr 10;7:49. doi: 10.3389/fcell.2019.00049. PMID: 31024911; PMCID: PMC6468149.

Chang AL, Miska J, Wainwright DA, Dey M, Rivetta CV, Yu D, Kanojia D, Pituch KC, Qiao J, Pytel P, Han Y, Wu M, Zhang L, Horbinski CM, Ahmed AU, Lesniak MS. CCL2 Produced by the Glioma Microenvironment Is Essential for the Recruitment of Regulatory T Cells and Myeloid-Derived Suppressor Cells. Cancer Res. 2016 Oct 1;76(19):5671-5682. doi: 10.1158/0008-5472.CAN-16-0144. Epub 2016 Aug 16. PMID: 27530322; PMCID: PMC5050119.

Chang YC, Wu JW, Wang CW, Jang AC. Hippo Signaling-Mediated Mechanotransduction in Cell Movement and Cancer Metastasis. Front Mol Biosci. 2020 Jan 31;6:157. doi: 10.3389/fmolb.2019.00157. PMID: 32118029; PMCID: PMC7025494.

Chen X, Sievers E, Hou Y, Park R, Tohme M, Bart R, Bremner R, Bading JR, Conti PS. Integrin alpha v beta 3-targeted imaging of lung cancer. Neoplasia. 2005 Mar;7(3):271-9. doi: 10.1593/neo.04538. PMID: 15799827; PMCID: PMC1501139.

Cheng X, Chen H. Tumor heterogeneity and resistance to EGFR-targeted therapy in advanced nonsmall cell lung cancer: challenges and perspectives. Onco Targets Ther. 2014 Sep 23;7:1689-704. doi: 10.2147/OTT.S66502. PMID: 25285017; PMCID: PMC4181629.

Chi X, Ding B, Zhang L, Zhang J, Wang J, Zhang W. lncRNA GAS5 promotes M1 macrophage polarization via miR-455-5p/SOCS3 pathway in childhood pneumonia. J Cell Physiol. 2019 Aug;234(8):13242-13251. doi: 10.1002/jcp.27996. Epub 2018 Dec 24. PMID: 30584669.

Chu Q, Shen D, He L, Wang H, Liu C, Zhang W. Prognostic significance of SOCS3 and its biological function in colorectal cancer. Gene. 2017 Sep 5;627:114-122. doi: 10.1016/j.gene.2017.06.013. Epub 2017 Jun 8. PMID: 28603075.

Croker BA, Kiu H, Pellegrini M, Toe J, Preston S, Metcalf D, O'Donnell JA, Cengia LH, McArthur K, Nicola NA, Alexander WS, Roberts AW. IL-6 promotes acute and chronic inflammatory disease in the absence of SOCS3. Immunol Cell Biol. 2012 Jan;90(1):124-9. doi: 10.1038/icb.2011.29. Epub 2011 Apr 26. PMID: 21519345; PMCID: PMC3146962.

Dees C, Pötter S, Zhang Y, Bergmann C, Zhou X, Luber M, Wohlfahrt T, Karouzakis E, Ramming A, Gelse K, Yoshimura A, Jaenisch R, Distler O, Schett G, Distler JH. TGF-β-induced epigenetic deregulation of SOCS3 facilitates STAT3 signaling to promote fibrosis. J Clin Invest. 2020 May

1;130(5):2347-2363. doi: 10.1172/JCI122462. PMID: 31990678; PMCID: PMC7190914.

Dhar K, Rakesh K, Pankajakshan D, Agrawal DK. SOCS3 promotor hypermethylation and STAT3-NF-κB interaction downregulate SOCS3 expression in human coronary artery smooth muscle cells. Am J Physiol Heart Circ Physiol. 2013 Mar 15;304(6):H776-85. doi: 10.1152/ajpheart.00570.2012. Epub 2013 Jan 18. PMID: 23335796; PMCID: PMC3602771.

Dong ZY, Zhang JT, Liu SY, Su J, Zhang C, Xie Z, Zhou Q, Tu HY, Xu CR, Yan LX, Li YF, Zhong WZ, Wu YL. EGFR mutation correlates with uninflamed phenotype and weak immunogenicity, causing impaired response to PD-1 blockade in non-small cell lung cancer. Oncoimmunology. 2017 Jul 26;6(11):e1356145. doi: 10.1080/2162402X.2017.1356145. PMID: 29147605; PMCID: PMC5674946.

Dontu G, Abdallah WM, Foley JM, Jackson KW, Clarke MF, Kawamura MJ, Wicha MS. In vitro propagation and transcriptional profiling of human mammary stem/progenitor cells. Genes Dev. 2003 May 15;17(10):1253-70. doi: 10.1101/gad.1061803. PMID: 12756227; PMCID: PMC196056.

Fisher ML, Grun D, Adhikary G, Xu W, Eckert RL. Inhibition of YAP function overcomes BRAF inhibitor resistance in melanoma cancer stem cells. Oncotarget. 2017 Nov 22;8(66):110257-110272. doi: 10.18632/oncotarget.22628. PMID: 29299145; PMCID: PMC5746380.

Forsthuber A, Lipp K, Andersen L, Ebersberger S, Graña-Castro ', Ellmeier W, Petzelbauer P, Lichtenberger BM, Loewe R. CXCL5 as Regulator of Neutrophil Function in Cutaneous Melanoma. J Invest Dermatol. 2019 Jan;139(1):186-194. doi: 10.1016/j.jid.2018.07.006. Epub 2018 Oct 4. PMID: 30009831.

Freudlsperger C, Burnett JR, Friedman JA, Kannabiran VR, Chen Z, Van Waes C. EGFR-PI3K-AKT-mTOR signaling in head and neck squamous cell carcinomas: attractive targets for molecular-oriented therapy. Expert Opin Ther Targets. 2011 Jan;15(1):63-74. doi: 10.1517/14728222.2011.541440. Epub 2010 Nov 26. PMID: 21110697; PMCID: PMC3399735.

Fu Y, Zhang Y, Lei Z, Liu T, Cai T, Wang A, Du W, Zeng Y, Zhu J, Liu Z, Huang JA. Abnormally activated OPN/integrin αVβ3/FAK signalling is responsible for EGFR-TKI resistance in EGFR mutant non-small-cell lung cancer. J

Hematol Oncol. 2020 Dec 7;13(1):169. doi: 10.1186/s13045-020-01009-7. PMID: 33287873; PMCID: PMC7720454.

Godin-Heymann N, Bryant I, Rivera MN, Ulkus L, Bell DW, Riese DJ 2nd, Settleman J, Haber DA. Oncogenic activity of epidermal growth factor receptor kinase mutant alleles is enhanced by the T790M drug resistance mutation. Cancer Res. 2007 Aug 1;67(15):7319-26. doi: 10.1158/0008-5472.CAN-06-4625. PMID: 17671201; PMCID: PMC2882853.

Gong J, Chehrazi-Raffle A, Reddi S, Salgia R. Development of PD-1 and PD-L1 inhibitors as a form of cancer immunotherapy: a comprehensive review of registration trials and future considerations. J Immunother Cancer. 2018 Jan 23;6(1):8. doi: 10.1186/s40425-018-0316-z. PMID: 29357948; PMCID: PMC5778665.

Gregorieff A, Liu Y, Inanlou MR, Khomchuk Y, Wrana JL. Yap-dependent reprogramming of Lgr5(+) stem cells drives intestinal regeneration and cancer. Nature. 2015 Oct 29;526(7575):715-8. doi: 10.1038/nature15382. Epub 2015 Oct 21. PMID: 26503053.

Hamanishi J, Mandai M, Matsumura N, Abiko K, Baba T, Konishi I. PD-1/PD-L1 blockade in cancer treatment: perspectives and issues. Int J Clin Oncol. 2016 Jun;21(3):462-73. doi: 10.1007/s10147-016-0959-z. Epub 2016 Feb 22. PMID: 26899259; PMCID: PMC4901122.

Hata A, Katakami N, Nanjo S, Okuda C, Kaji R, Masago K, Fujita S, Yoshida H, Zama K, Imai Y, Hirata Y. Programmed death-ligand 1 expression and T790M status in EGFR-mutant non-small cell lung cancer. Lung Cancer. 2017 Sep;111:182-189. doi: 10.1016/j.lungcan.2017.07.022. Epub 2017 Jul 20. PMID: 28838391.

He B, You L, Uematsu K, Zang K, Xu Z, Lee AY, Costello JF, McCormick F, Jablons DM. SOCS-3 is frequently silenced by hypermethylation and suppresses cell growth in human lung cancer. Proc Natl Acad Sci U S A. 2003 Nov 25;100(24):14133-8. doi: 10.1073/pnas.2232790100. Epub 2003 Nov 14. PMID: 14617776; PMCID: PMC283558.

Hou P, Kapoor A, Zhang Q, Li J, Wu CJ, Li J, Lan Z, Tang M, Ma X, Ackroyd JJ, Kalluri R, Zhang J, Jiang S, Spring DJ, Wang YA, DePinho RA. Tumor Microenvironment Remodeling Enables Bypass of Oncogenic KRAS Dependency in Pancreatic Cancer. Cancer Discov. 2020 Jul;10(7):1058-1077. doi: 10.1158/2159-8290.CD-19-0597. Epub 2020 Apr 27. PMID: 32341020; PMCID: PMC7334087.

Hsu PC, Jablons DM, Yang CT, You L. Epidermal Growth Factor Receptor (EGFR) Pathway, Yes-Associated Protein (YAP) and the Regulation of Programmed Death-Ligand 1 (PD-L1) in Non-Small Cell Lung Cancer (NSCLC). Int J Mol Sci. 2019 Aug 5;20(15):3821. doi: 10.3390/ijms20153821. PMID: 31387256; PMCID: PMC6695603.

Hsu PC, Yang CT, Jablons DM, You L. The Role of Yes-Associated Protein (YAP) in Regulating Programmed Death-Ligand 1 (PD-L1) in Thoracic Cancer. Biomedicines. 2018 Dec 7;6(4):114. doi: 10.3390/biomedicines6040114. PMID: 30544524; PMCID: PMC6315659.

Huang L, Fu L. Mechanisms of resistance to EGFR tyrosine kinase inhibitors. Acta Pharm Sin B. 2015 Sep;5(5):390-401. doi: 10.1016/j.apsb.2015.07.001. Epub 2015 Jul 26. PMID: 26579470; PMCID: PMC4629442.

Huang L, Hu B, Ni J, Wu J, Jiang W, Chen C, Yang L, Zeng Y, Wan R, Hu G, Wang X. Transcriptional repression of SOCS3 mediated by IL-6/STAT3 signaling via DNMT1 promotes pancreatic cancer growth and metastasis. J Exp Clin Cancer Res. 2016 Feb 4;35:27. doi: 10.1186/s13046-016-0301-7. PMID: 26847351; PMCID: PMC4743194.

Huang YH, Hsu KH, Tseng JS, Chen KC, Hsu CH, Su KY, Chen JJW, Chen HW, Yu SL, Yang TY, Chang GC. The Association of Acquired T790M Mutation with Clinical Characteristics after Resistance to First-Line Epidermal Growth Factor Receptor Tyrosine Kinase Inhibitor in Lung Adenocarcinoma. Cancer Res Treat. 2018 Oct;50(4):1294-1303. doi: 10.4143/crt.2017.512. Epub 2018 Jan 4. PMID: 29334606; PMCID: PMC6192936.

Huang Z, Wang SL, Chen H, Shen RK, Li XD, Huang QS, Wu CY, Weng DF, Lin JH. Clinicopathological and prognostic values of ErbB receptor family amplification in primary osteosarcoma. Scand J Clin Lab Invest. 2019 Dec;79(8):601-612. doi: 10.1080/00365513.2019.1683764. Epub 2019 Oct 30. PMID: 31663373.

Hynes NE, MacDonald G. ErbB receptors and signaling pathways in cancer. Curr Opin Cell Biol. 2009 Apr;21(2):177-84. doi: 10.1016/j.ceb.2008.12.010. Epub 2009 Feb 7. PMID: 19208461.

Inomata M, Azechi K, Takata N, Hayashi K, Tokui K, Taka C, Okazawa S, Kambara K, Imanishi S, Miwa T, Hayashi R, Matsui S, Tobe K. Association of Tumor PD-L1 Expression with the T790M Mutation and Progression-Free Survival in Patients with EGFR-Mutant Non-Small Cell Lung Cancer Receiving EGFR-TKI Therapy. Diagnostics (Basel). 2020 Nov

25;10(12):1006. doi: 10.3390/diagnostics10121006. PMID: 33255696; PMCID: PMC7759886.

Iwai Y, Ishida M, Tanaka Y, Okazaki T, Honjo T, Minato N. Involvement of PD-L1 on tumor cells in the escape from host immune system and tumor immunotherapy by PD-L1 blockade. Proc Natl Acad Sci U S A. 2002 Sep 17;99(19):12293-7. doi: 10.1073/pnas.192461099. Epub 2002 Sep 6. PMID: 12218188; PMCID: PMC129438.

Ji XC, Shi YJ, Zhang Y, Chang MZ, Zhao G. Reducing Suppressors of Cytokine Signaling-3 (SOCS3) Expression Promotes M2 Macrophage Polarization and Functional Recovery After Intracerebral Hemorrhage. Front Neurol. 2020 Nov 12;11:586905. doi: 10.3389/fneur.2020.586905. PMID: 33281724; PMCID: PMC7688919.

Jiang Y, Chen M, Nie H, Yuan Y. PD-1 and PD-L1 in cancer immunotherapy: clinical implications and future considerations. Hum Vaccin Immunother. 2019;15(5):1111-1122. doi: 10.1080/21645515.2019.1571892. Epub 2019 Mar 19. PMID: 30888929; PMCID: PMC6605868.

Kanematsu T, Yano S, Uehara H, Bando Y, Sone S. Phosphorylation, but not overexpression, of epidermal growth factor receptor is associated with poor prognosis of non-small cell lung cancer patients. Oncol Res. 2003;13(5):289-98. doi: 10.3727/096504003108748348. PMID: 12688680.

Kauffmann-Guerrero D, Syunyaeva Z, Kahnert K, Tufman A. Excellent platinum dependent response to chemotherapy after relapse under TKI treatment in NSCLC with sensitizing EGFR mutations and no detectable resistance mutations: three case studies. AME Case Rep. 2019 Oct 4;3:36. doi: 10.21037/acr.2019.09.02. PMID: 31728434; PMCID: PMC6851420.

Kim EH, Sohn BH, Eun YG, Lee DJ, Yim SY, Kang SG, Lee JS. Silence of Hippo Pathway Associates with Pro-Tumoral Immunosuppression: Potential Therapeutic Target of Glioblastomas. Cells. 2020 Jul 23;9(8):1761. doi: 10.3390/cells9081761. PMID: 32717825; PMCID: PMC7464204.

Kim MH, Kim CG, Kim SK, Shin SJ, Choe EA, Park SH, Shin EC, Kim J. YAP-Induced PD-L1 Expression Drives Immune Evasion in BRAFi-Resistant Melanoma. Cancer Immunol Res. 2018 Mar;6(3):255-266. doi: 10.1158/2326-6066.CIR-17-0320. Epub 2018 Jan 30. PMID: 29382670.

Kleinsteuber K, Heesch K, Schattling S, Sander-Juelch C, Mock U, Riecken K, Fehse B, Fleischer B, Jacobsen M. SOCS3 promotes interleukin-17

expression of human T cells. Blood. 2012 Nov 22;120(22):4374-82. doi: 10.1182/blood-2011-11-392738. Epub 2012 Oct 1. PMID: 23033269.

Kobayashi Y, Fujino T, Nishino M, Koga T, Chiba M, Sesumi Y, Ohara S, Shimoji M, Tomizawa K, Takemoto T, Mitsudomi T. EGFR T790M and C797S Mutations as Mechanisms of Acquired Resistance to Dacomitinib. J Thorac Oncol. 2018 May;13(5):727-731. doi: 10.1016/j.jtho.2018.01.009. Epub 2018 Feb 2. PMID: 29410323.

Lee HJ, Seo AN, Kim EJ, Jang MH, Kim YJ, Kim JH, Kim SW, Ryu HS, Park IA, Im SA, Gong G, Jung KH, Kim HJ, Park SY. Prognostic and predictive values of EGFR overexpression and EGFR copy number alteration in HER2-positive breast cancer. Br J Cancer. 2015 Jan 6;112(1):103-11. doi: 10.1038/bjc.2014.556. Epub 2014 Oct 28. PMID: 25349977; PMCID: PMC4453607.

[1]Li Y, Xiao Y, Lin HP, Reichel D, Bae Y, Lee EY, Jiang Y, Huang X, Yang C, Wang Z. In vivo β-catenin attenuation by the integrin α5-targeting nano-delivery strategy suppresses triple negative breast cancer stemness and metastasis. Biomaterials. 2019 Jan;188:160-172. doi: 10.1016/j.biomaterials.2018.10.019. Epub 2018 Oct 18. PMID: 30352320.

Li Z, Liu S, Cai Y. EGFR/MAPK signaling regulates the proliferation of Drosophila renal and nephric stem cells. J Genet Genomics. 2015 Jan 20;42(1):9-20. doi: 10.1016/j.jgg.2014.11.007. Epub 2014 Dec 9. PMID: 25619598.

[2]Li Z, Zhou J, Zhang J, Li S, Wang H, Du J. Cancer-associated fibroblasts promote PD-L1 expression in mice cancer cells via secreting CXCL5. Int J Cancer. 2019 Oct 1;145(7):1946-1957. doi: 10.1002/ijc.32278. Epub 2019 Apr 6. PMID: 30873585; PMCID: PMC6767568.

Lim ZF, Ma PC. Emerging insights of tumor heterogeneity and drug resistance mechanisms in lung cancer targeted therapy. J Hematol Oncol. 2019 Dec 9;12(1):134. doi: 10.1186/s13045-019-0818-2. PMID: 31815659; PMCID: PMC6902404.

Lindemann C, Hackmann O, Delic S, Schmidt N, Reifenberger G, Riemenschneider MJ. SOCS3 promoter methylation is mutually exclusive to EGFR amplification in gliomas and promotes glioma cell invasion through STAT3 and FAK activation. Acta Neuropathol. 2011 Aug;122(2):241-51. doi: 10.1007/s00401-011-0832-0. Epub 2011 May 18. PMID: 21590492.

Liu B, Wu S, Ma J, Yan S, Xiao Z, Wan L, Zhang F, Shang M, Mao A. lncRNA
GAS5 Reverses EMT and Tumor Stem Cell-Mediated Gemcitabine
Resistance and Metastasis by Targeting miR-221/SOCS3 in Pancreatic
Cancer. Mol Ther Nucleic Acids. 2018 Dec 7;13:472-482. doi:
10.1016/j.omtn.2018.09.026. Epub 2018 Oct 6. PMID: 30388621; PMCID:
PMC6205337.

Liu H, Zhang B, Sun Z. Spectrum of EGFR aberrations and potential clinical
implications: insights from integrative pan-cancer analysis. Cancer Commun
(Lond). 2020 Jan;40(1):43-59. doi: 10.1002/cac2.12005. Epub 2020 Feb 18.
PMID: 32067422; PMCID: PMC7163653.

Luckey MA, Kim TH, Prakhar P, Keller HR, Crossman A, Choi S, Love PE, Walsh
STR, Park JH. SOCS3 is a suppressor of γc cytokine signaling and
constrains generation of murine Foxp3+ regulatory T cells. Eur J Immunol.
2020 Jul;50(7):986-999. doi: 10.1002/eji.201948307. Epub 2020 Mar 19.
PMID: 32144749; PMCID: PMC7335320.

Maugeri-Saccà M, Barba M, Pizzuti L, Vici P, Di Lauro L, Dattilo R, Vitale I,
Bartucci M, Mottolese M, De Maria R. The Hippo transducers TAZ and YAP
in breast cancer: oncogenic activities and clinical implications. Expert Rev
Mol Med. 2015 Jul 2;17:e14. doi: 10.1017/erm.2015.12. PMID: 26136233.

Mayrhofer M, Gourain V, Reischl M, Affaticati P, Jenett A, Joly JS, Benelli M,
Demichelis F, Poliani PL, Sieger D, Mione M. A novel brain tumour model in
zebrafish reveals the role of YAP activation in MAPK- and PI3K-induced
malignant growth. Dis Model Mech. 2017 Jan 1;10(1):15-28. doi:
10.1242/dmm.026500. Epub 2016 Nov 24. PMID: 27935819; PMCID:
PMC5278524.

Mazzarella L, Guida A, Curigliano G. Cetuximab for treating non-small cell lung
cancer. Expert Opin Biol Ther. 2018 Apr;18(4):483-493. doi:
10.1080/14712598.2018.1452906. PMID: 29534625.

Miao J, Hsu PC, Yang YL, Xu Z, Dai Y, Wang Y, Chan G, Huang Z, Hu B, Li H,
Jablons DM, You L. YAP regulates PD-L1 expression in human NSCLC
cells. Oncotarget. 2017 Dec 9;8(70):114576-114587. doi:
10.18632/oncotarget.23051. PMID: 29383103; PMCID: PMC5777715.

Molavi O, Wang P, Zak Z, Gelebart P, Belch A, Lai R. Gene methylation and
silencing of SOCS3 in mantle cell lymphoma. Br J Haematol. 2013
May;161(3):348-56. doi: 10.1111/bjh.12262. Epub 2013 Feb 22. PMID:
23432547.

Nagano T, Tachihara M, Nishimura Y. Mechanism of Resistance to Epidermal Growth Factor Receptor-Tyrosine Kinase Inhibitors and a Potential Treatment Strategy. Cells. 2018 Nov 15;7(11):212. doi: 10.3390/cells7110212. PMID: 30445769; PMCID: PMC6262543.

O'Kane GM, Bradbury PA, Feld R, Leighl NB, Liu G, Pisters KM, Kamel-Reid S, Tsao MS, Shepherd FA. Uncommon EGFR mutations in advanced non-small cell lung cancer. Lung Cancer. 2017 Jul;109:137-144. doi: 10.1016/j.lungcan.2017.04.016. Epub 2017 Apr 27. PMID: 28577943.

Passarelli A, Aieta M, Sgambato A, Gridelli C. Targeting Immunometabolism Mediated by CD73 Pathway in *EGFR*-Mutated Non-small Cell Lung Cancer: A New Hope for Overcoming Immune Resistance. Front Immunol. 2020 Jul 14;11:1479. doi: 10.3389/fimmu.2020.01479. PMID: 32760402; PMCID: PMC7371983.

Passaro A, Malapelle U, Del Re M, Attili I, Russo A, Guerini-Rocco E, Fumagalli C, Pisapia P, Pepe F, De Luca C, Cucchiara F, Troncone G, Danesi R, Spaggiari L, De Marinis F, Rolfo C. Understanding EGFR heterogeneity in lung cancer. ESMO Open. 2020 Oct;5(5):e000919. doi: 10.1136/esmoopen-2020-000919. PMID: 33067323; PMCID: PMC7569934.

Pierconti F, Martini M, Pinto F, Cenci T, Capodimonti S, Calarco A, Bassi PF, Larocca LM. Epigenetic silencing of SOCS3 identifies a subset of prostate cancer with an aggressive behavior. Prostate. 2011 Feb 15;71(3):318-25. doi: 10.1002/pros.21245. Epub 2010 Aug 17. PMID: 20717995.

Puhr M, Santer FR, Neuwirt H, Marcias G, Hobisch A, Culig Z. SOCS-3 antagonises the proliferative and migratory effects of fibroblast growth factor-2 in prostate cancer by inhibition of p44/p42 MAPK signalling. Endocr Relat Cancer. 2010 May 18;17(2):525-38. doi: 10.1677/ERC-10-0007. PMID: 20335309.

Ruppert AM, Beau-Faller M, Neuville A, Guerin E, Voegeli AC, Mennecier B, Legrain M, Molard A, Jeung MY, Gaub MP, Oudet P, Quoix E. EGFR-TKI and lung adenocarcinoma with CNS relapse: interest of molecular follow-up. Eur Respir J. 2009 Feb;33(2):436-40. doi: 10.1183/09031936.00162307. PMID: 19181917.

Schabath MB, Cote ML. Cancer Progress and Priorities: Lung Cancer. Cancer Epidemiol Biomarkers Prev. 2019 Oct;28(10):1563-1579. doi: 10.1158/1055-9965.EPI-19-0221. PMID: 31575553; PMCID: PMC6777859.

Soo RA, Lim SM, Syn NL, Teng R, Soong R, Mok TSK, Cho BC. Immune checkpoint inhibitors in epidermal growth factor receptor mutant non-small cell lung cancer: Current controversies and future directions. Lung Cancer. 2018 Jan;115:12-20. doi: 10.1016/j.lungcan.2017.11.009. Epub 2017 Nov 13. PMID: 29290252.

Suda K, Murakami I, Yu H, Kim J, Ellison K, Rivard CJ, Mitsudomi T, Hirsch FR. Heterogeneity in Immune Marker Expression after Acquisition of Resistance to EGFR Kinase Inhibitors: Analysis of a Case with Small Cell Lung Cancer Transformation. J Thorac Oncol. 2017 Jun;12(6):1015-1020. doi: 10.1016/j.jtho.2017.02.002. Epub 2017 Feb 11. PMID: 28193529.

Tan CS, Kumarakulasinghe NB, Huang YQ, Ang YLE, Choo JR, Goh BC, Soo RA. Third generation EGFR TKIs: current data and future directions. Mol Cancer. 2018 Feb 19;17(1):29. doi: 10.1186/s12943-018-0778-0. PMID: 29455654; PMCID: PMC5817792.

Tao H, Shi P, Zhao XD, Xuan HY, Gong WH, Ding XS. DNMT1 deregulation of SOCS3 axis drives cardiac fibroblast activation in diabetic cardiac fibrosis. J Cell Physiol. 2021 May;236(5):3481-3494. doi: 10.1002/jcp.30078. Epub 2020 Sep 28. PMID: 32989761.

Turenchalk GS, St John MA, Tao W, Xu T. The role of lats in cell cycle regulation and tumorigenesis. Biochim Biophys Acta. 1999 Oct 29;1424(2-3):M9-M16. doi: 10.1016/s0304-419x(99)00021-9. PMID: 10528150.

Wan J, Che Y, Kang N, Wu W. SOCS3 blocks HIF-1α expression to inhibit proliferation and angiogenesis of human small cell lung cancer by downregulating activation of Akt, but not STAT3. Mol Med Rep. 2015 Jul;12(1):83-92. doi: 10.3892/mmr.2015.3368. Epub 2015 Feb 17. PMID: 25695729; PMCID: PMC4438922.

[2]Wang J, Zhou H, Han Y, Liu X, Wang M, Wang X, Yin G, Li X, Xiang M. SOCS3 methylation in synergy with Reg3A overexpression promotes cell growth in pancreatic cancer. J Mol Med (Berl). 2014 Dec;92(12):1257-69. doi: 10.1007/s00109-014-1184-8. Epub 2014 Jul 5. PMID: 24996521.

[3]Wang L, Ma Q, Yao R, Liu J. Current status and development of anti-PD-1/PD-L1 immunotherapy for lung cancer. Int Immunopharmacol. 2020 Feb;79:106088. doi: 10.1016/j.intimp.2019.106088. Epub 2019 Dec 31. PMID: 31896512.

Wang L, Shi L, Gu J, Zhan C, Xi J, Ding J, Ge D. CXCL5 regulation of proliferation and migration in human non-small cell lung cancer cells. J Physiol Biochem. 2018 May;74(2):313-324. doi: 10.1007/s13105-018-0619-z. Epub 2018 Mar 10. PMID: 29526026.

[1]Wang Z, Humphries B, Xiao H, Jiang Y, Yang C. MicroRNA-200b suppresses arsenic-transformed cell migration by targeting protein kinase Cα and Wnt5b-protein kinase Cα positive feedback loop and inhibiting Rac1 activation. J Biol Chem. 2014 Jun 27;289(26):18373-86. doi: 10.1074/jbc.M114.554246. Epub 2014 May 19. PMID: 24841200; PMCID: PMC4140296.

Wang Z, Li Y, Xiao Y, Lin HP, Yang P, Humphries B, Gao T, Yang C. Integrin α9 depletion promotes β-catenin degradation to suppress triple-negative breast cancer tumor growth and metastasis. Int J Cancer. 2019 Nov 15;145(10):2767-2780. doi: 10.1002/ijc.32359. Epub 2019 May 3. PMID: 31008533; PMCID: PMC6750961.

[4]Wang Z, Yang P, Xie J, Lin HP, Kumagai K, Harkema J, Yang C. Arsenic and benzo[a]pyrene co-exposure acts synergistically in inducing cancer stem cell-like property and tumorigenesis by epigenetically down-regulating SOCS3 expression. Environ Int. 2020 Apr;137:105560. doi: 10.1016/j.envint.2020.105560. Epub 2020 Feb 18. PMID: 32062438; PMCID: PMC7099608.

Weber A, Hengge UR, Bardenheuer W, Tischoff I, Sommerer F, Markwarth A, Dietz A, Wittekind C, Tannapfel A. SOCS-3 is frequently methylated in head and neck squamous cell carcinoma and its precursor lesions and causes growth inhibition. Oncogene. 2005 Oct 6;24(44):6699-708. doi: 10.1038/sj.onc.1208818. PMID: 16007169.

Xia H, Dai X, Yu H, Zhou S, Fan Z, Wei G, Tang Q, Gong Q, Bi F. EGFR-PI3K-PDK1 pathway regulates YAP signaling in hepatocellular carcinoma: the mechanism and its implications in targeted therapy. Cell Death Dis. 2018 Feb 15;9(3):269. doi: 10.1038/s41419-018-0302-x. PMID: 29449645; PMCID: PMC5833379.

Xia H, Qi H, Li Y, Pei J, Barton J, Blackstad M, Xu T, Tao W. LATS1 tumor suppressor regulates G2/M transition and apoptosis. Oncogene. 2002 Feb 14;21(8):1233-41. doi: 10.1038/sj.onc.1205174. PMID: 11850843.

Yeh P, Chen H, Andrews J, Naser R, Pao W, Horn L. DNA-Mutation Inventory to Refine and Enhance Cancer Treatment (DIRECT): a catalog of clinically

relevant cancer mutations to enable genome-directed anticancer therapy. Clin Cancer Res. 2013 Apr 1;19(7):1894-901. doi: 10.1158/1078-0432.CCR-12-1894. Epub 2013 Jan 23. PMID: 23344264; PMCID: PMC4121886.

Yu S, Liu D, Shen B, Shi M, Feng J. Immunotherapy strategy of EGFR mutant lung cancer. Am J Cancer Res. 2018 Oct 1;8(10):2106-2115. PMID: 30416860; PMCID: PMC6220136.

Yun CH, Mengwasser KE, Toms AV, Woo MS, Greulich H, Wong KK, Meyerson M, Eck MJ. The T790M mutation in EGFR kinase causes drug resistance by increasing the affinity for ATP. Proc Natl Acad Sci U S A. 2008 Feb 12;105(6):2070-5. doi: 10.1073/pnas.0709662105. Epub 2008 Jan 28. PMID: 18227510; PMCID: PMC2538882.

[1]Zhang W, Jiang M, Chen J, Zhang R, Ye Y, Liu P, Yu W, Yu J. SOCS3 Suppression Promoted the Recruitment of CD11b+Gr-1-F4/80-MHCII- Early-Stage Myeloid-Derived Suppressor Cells and Accelerated Interleukin-6-Related Tumor Invasion *via* Affecting Myeloid Differentiation in Breast Cancer. Front Immunol. 2018 Jul 23;9:1699. doi: 10.3389/fimmu.2018.01699. PMID: 30083161; PMCID: PMC6064721.

[2]Zhang X, Wang Y, Yuan J, Li N, Pei S, Xu J, Luo X, Mao C, Liu J, Yu T, Gan S, Zheng Q, Liang Y, Guo W, Qiu J, Constantin G, Jin J, Qin J, Xiao Y. Macrophage/microglial Ezh2 facilitates autoimmune inflammation through inhibition of Socs3. J Exp Med. 2018 May 7;215(5):1365-1382. doi: 10.1084/jem.20171417. Epub 2018 Apr 6. PMID: 29626115; PMCID: PMC5940261.

Zhao J, Ou B, Han D, Wang P, Zong Y, Zhu C, Liu D, Zheng M, Sun J, Feng H, Lu A. Tumor-derived CXCL5 promotes human colorectal cancer metastasis through activation of the ERK/Elk-1/Snail and AKT/GSK3β/β-catenin pathways. Mol Cancer. 2017 Mar 29;16(1):70. doi: 10.1186/s12943-017-0629-4. PMID: 28356111; PMCID: PMC5372323.

Zhao Y, Tan YS, Haslam SZ, Yang C. Perfluorooctanoic acid effects on steroid hormone and growth factor levels mediate stimulation of peripubertal mammary gland development in C57BL/6 mice. Toxicol Sci. 2010 May;115(1):214-24. doi: 10.1093/toxsci/kfq030. Epub 2010 Jan 29. PMID: 20118188; PMCID: PMC2855353.

Zhu Y, Knolhoff BL, Meyer MA, Nywening TM, West BL, Luo J, Wang-Gillam A, Goedegebuure SP, Linehan DC, DeNardo DG. CSF1/CSF1R blockade reprograms tumor-infiltrating macrophages and improves response to T-cell

checkpoint immunotherapy in pancreatic cancer models. Cancer Res. 2014 Sep 15;74(18):5057-69. doi: 10.1158/0008-5472.CAN-13-3723. Epub 2014 Jul 31. PMID: 25082815; PMCID: PMC4182950.

Zygulska AL, Krzemieniecki K, Pierzchalski P. Hippo pathway - brief overview of its relevance in cancer. J Physiol Pharmacol. 2017 Jun;68(3):311-335. PMID: 28820389.

Vita

<u>EDUCATION</u>

**Ph.D.** (2021)

    Toxicology and Cancer Biology

    University of Kentucky, Lexington, Kentucky, USA

**M.S.** (2011)

    Biochemistry and Molecular Biology,

    Georgetown University, Washington, D.C., USA

**M.S.** (2009)

    Life Sciences

    National Chung-Hsing University, Taichung, Taiwan

**B.A.** (2007)

    German

    Tamkang University, Taipei, Taiwan

<u>POSITIONS AND EXPERIENCES</u>

Graduate research assistant (2017-2021)

    *University of Kentucky, Lexington, KY, USA*

    Research project: (1) epigenetic mechanisms of heavy metal carcinogenesis; (2) nanomedicine for lung cancer with EGFR mutation

Graduate research assistant (2016-2017)

    *Augusta University, Augusta, GA, USA*

    Research project: Reprogramming glioblastoma cells by exosomes secreted from neural progenitor cells

Research assistant (2012-2016)

*Academia Sinica, Taipei, Taiwan*

Research project: Directed evolution of human lysosomal enzyme for cancer chemotherapy

Senior Technician (2011-2012)

*Columbia University Medical Center, New York, NY, USA*

Responsibilities: (1) molecular diagnostic tests, e.g. KRAS, EGFR mutations; (2) validation of newly developed tests

Graduate student (2010-2011)

*Center for Drug Discovery, Georgetown University, Washington, D.C., USA*

Research project: Therapeutic effect of a small molecule for prostate cancer

Graduate student (2007-2009)

*Department of Life Sciences, National Chung-Hsing University, Taichung, Taiwan*

Research project: Molecular characteristics of multi-drug resistant bacteria isolated from nosocomial outbreak

Undergraduate study (2005-2006)

*Department of Chemistry, Tamkang University, Taipei, Taiwan*

Research project: expression, isolation, and hydrolysis reaction of thermophilic bacterial phosphatase


SCIENTIFIC MEMBERSHIP

2019 – present      American Association for the Advancement of Science

2019 – present      Society of Toxicology


HONOR

2020 Society of Toxicology Annual Meeting Travel Award

PUBLICATIONS

- HP Lin, M Rea, Z Wang, and C Yang.
  Down-regulation of lncRNA MEG3 promotes chronic low dose cadmium exposure-induced cell transformation and cancer stem cell-like property. (under review) 2021.

- HP Lin, Z Wang, and C Yang.
  LncRNA DUXAP10 activates the Hedgehog pathway to promote chronic cadmium exposure-induced cancer stem cell-like property and tumorigenesis. *Toxicological Sciences*, 2021.

- Y Li, D Qian, HP Lin, J Xie, P Yang, D Maddy, Y Xiao, X Huang, Z Wang, and C Yang.
  Nanoparticle-delivered miriplatin ultrasmall dots suppress triple negative breast cancer lung metastasis by targeting circulating tumor cells. *Journal of Controlled Release*, 2020.

- J Xie, P Yang, HP Lin, Y Li, M Clementino, WK Fenske, C Yang, C Wang, and Z Wang.
  Integrin $\alpha 4$ up-regulation activates the hedgehog pathway to promote arsenic and benzo [$\alpha$] pyrene co-exposure-induced cancer stem cell-like property and tumorigenesis. *Cancer Letters*, 2020.

- P Yang, J Xie, Y Li, HP Lin, WK Fenske, M Clementino, Y Jiang, C Yang, and Z Wang.
  Deubiquitinase USP7-mediated MCL-1 up-regulation enhances arsenic and benzo(a)pyrene co-exposure-induced cancer stem cell-like property and tumorigenesis. *Theranostics*, 2020.

- M Clementino, J Xie, P Yang, Y Li, HP Lin, WK Fenske, H Tao, K Kondo, C Yang, and Z Wang.
  A positive feedback loop between c-Myc up-regulation, glycolytic shift and histone acetylation enhances cancer stem cell-like property and tumorigenicity of Cr(VI)-transformed cells. *Toxicological Sciences*, 2020.

- Z Wang, P Yang, J Xie, HP Lin, K Kumagai, J Harkema, and C Yang.
  Arsenic and benzo[a]pyrene co-exposure acts synergistically in inducing cancer stem cell-like property and tumorigenesis by epigenetically down-regulating SOCS3 expression. *Environmental International*, 2020.

- Z Wang, HP Lin, Y Li, H Tao, P Yang, D Maddy, and C Yang.
  Chronic hexavalent chromium exposure induces cancer stem cell-like property and tumorigenesis by increasing c-Myc expression. *Toxicological Sciences*, 2019.

186

- Z Wang, Y Li, Y Xiao, <u>HP Lin</u>, P Yang, B Humphries, T Gao, and C Yang. Integrin α9 depletion promotes β-catenin degradation to suppress triple negative breast cancer tumor growth and metastasis. *International Journal of Cancer*, 2019.

- Y Li, Y Xiao, <u>HP Lin</u>, D Reichel, Y Bae, EY Lee, Y Jiang, X Huang, C Yang, and Z Wang.
  In vivo β-catenin attenuation by the integrin α5-targeting nano-delivery strategy suppresses triple negative breast cancer stemness and metastasis. *Biomaterials*, 2018.

- L Zong, JN Kong, MB Dinkins, S Leanhart, Z Zhu, SD Spassieva, H Qin, <u>HP Lin</u>, A Elsherbini, R Wang, X Jian, M Nikolova-Karakashian, G Wang, and E Bieberich.
  Increased liver tumor formation in neutral sphingomyelinase-2-deficient mice. *Journal of Lipid Research*, 2018.

- JN Kong, Z Zhu, Y Itokazu, G Wang, MB Dinkins, L Zhong, <u>HP Lin</u>, A Elsherbini, S Leanhart, X Jiang, H Qin, W Zhi, SD Spassieva, and E Bieberich.
  Novel function of ceramide for regulation of mitochondrial ATP release in astrocytes. *Journal of Lipid Research*, 2018.

- YT Hsieh, <u>HP Lin</u>, BM Chen, PT Huang, and SR Roffler.
  Effect of Cellular Location of Human Carboxylesterase 2 on CPT-11 Hydrolysis and Anticancer activity. *PLOS ONE*, 2015.

## CONFERENCE PUBLICATIONS & POSTER PRESENTATION

- Mechanism of Cadmium Carcinogenesis – Epigenetic Modification and the Induction of CSC-like Cells
  *Society of Toxicology Annual Meeting, Anaheim, CA, March 2020*

- Mechanism of Cadmium Carcinogenesis – Epigenetic Modification and the Induction of CSC-like Cells
  *Departmental Retreat, Lexington, KY, August 2019*

- Directed evolution of human beta-glucuronidase through ECSTASY, a high throughput screening system
  *Biophysics Annual Conference, Taipei, Taiwan, November 2015*

- Effect of Small Molecule KED-4-69 on Gene Expression Profile of Prostate Cancer Cell Line

*Department of Biochemistry & Molecular Biology, Georgetown University, Washington, D.C., December 2010*

- Dominant Clinical *Acinetobacter baumannii* Strains in Central Taiwan
  *19th Annual Meeting Taiwan Society of Microbiology, Taipei, Taiwan, November 2008*

- The Study of Hydrolysis Reaction of Phosphate Group Catalyzed and Regulated by Thermophilic Bacterial Phophatase
  *2006 Annual Meeting of Chemical Society, Taipei, Taiwan, November 2006*